Characterization of the Flexible Tail of the Prion Protein and Its Mimic Shadoo

DISSERTATION

zur
Erlangung der naturwissenschaftlichen Doktorwürde
(Dr. sc. nat.)

vorgelegt der
Mathematisch-naturwissenschaftlichen Fakultät

der
Universität Zürich

von
Paolo Dametto
aus
Italien

Promotionskomitee

Prof. Dr. med. Dr. sc. Adriano Aguzzi (Vorsitz)

Prof. Dr. Rudolf Aebersold

Prof. Dr. Mathias Heikenwalder

Prof. Dr. Peter Sonderegger

Zürich, 2014

TABLE OF CONTENTS

SUMMARY

The cellular prion protein (PrP^C) is an extracellular and glycosylphosphatidyl-inositol (GPI)-linked protein, that is enriched in detergent-resistant membranes (lipid rafts), and ubiquitously expressed and highly abundant in the nervous system. It is highly conserved among species, with a long, unstructured and flexible tail (FT, residues 23-128), and a globular domain (GD, residues 129-231).

Transmissible spongiform encephalopathies (TSE) are neurodegenerative diseases characterized by spongiform changes, neuronal death, astrocytosis, and accumulation of the pathological protein PrP^{Sc} – an abnormally folded, insoluble and partially protease-resistant isoform of the endogenous protein PrP^C.

Whereas it is well established that PrP^C is required for PrP^{Sc}-mediated toxicity in prion infections, suggesting a crucial interaction between PrP^{Sc} and PrP^C, the mechanisms by which aggregated prions are lethal to neurons remain a mystery. Only recently, Mallucci and coworkers showed that accumulation of PrP^{Sc} causes chronic endoplasmic reticulum (ER) stress, in particular persistent translational repression of global protein synthesis by phosphorylation of eIF2α, associated with synaptic failure and neuronal loss in prion-infected mice. Furthermore, our group uncovered a critical role for the FT of PrP^C as the effector domain of PrP^C-mediated neuronal death. Ligands targeting the α1 and α3 helices of the PrP^C GD induced rapid neurotoxicity in cerebellar organotypic cultured slices (COCS). However, toxicity was prevented when a mutated version of PrP^C, harboring deletions within the FT, was expressed in COCS, suggesting that the FT has neurotoxic properties and is required to transmit the toxic signals originating from the GD. The FT domain contains several different motifs and it has been reported to interact with a broad range of proteins, endowing a number of potential, yet poorly understood, attributes to the FT, ranging from neurotrophic to neurotoxic properties. Clearly, a unifying view of the true function of FT is yet to be determined.

The work presented in this thesis focuses on characterizing the properties of the FT of PrP^C *in vivo,* in order to contribute to the understanding of the role of this domain.

In light of the aforementioned data describing the FT-mediated neurotoxicity, a mouse line expressing a membrane-anchored version of the FT of PrP^C (FTgpi) was generated and we found this protein to be a potent neurotoxin. Mice expressing FTgpi develope severe ataxia and die within a few weeks. On histological examination, these mice experienced massive loss of cerebellar granule neurons (CGNs) and widespread astrocytosis. The unstructured

nature of the protein led us to speculate that FTgpi may trigger ER stress. Indeed, mouse cerebelli exhibited a comprehensive ER stress response with significantly increased levels of several stress-response markers (spliced XPB1, BiP, CHOP and HSP40). Moreover, we demonstrated that FTgpi interacts with BiP, a key chaperone responsible in protein folding within the ER. This binding could sequester the availability of BiP to other essential proteins, altering the physiological homeostasis of the ER.

The requirement of an intact FT for the toxicity of anti-GD antibodies, and the similarities between the signaling pathways evoked by prions and FTgpi, suggests that the FT may be the effector of neurotoxicity in most prion-related conditions. In addition, FTgpi mice may represent a safer model, versus working directly with infectious prions, for further investigations into the mechanisms of toxicity underlying human prion diseases.

Shadoo (Sho) is a GPI-anchored protein encoded by the *Sprn* gene. It exhibits homology and domain organization similar to the FT of PrP^C and is highly conserved among species. A recent publication claims that Sho has similar neurotrophic properties to the FT of PrP^C, suggesting a possible overlapping function.

$Prnp^{o/o}$ mice develop a chronic demyelinating polyneuropathy (CDP) in the peripheral nerve, but not in the central nervous system (CNS), suggesting that the presence of an alternative, substitute, protein may prevent the neuropathological phenotype in the CNS but not in peripheral nerves, possibly due to its lack of expression. Sho is expressed specifically in the CNS, whereas expression in the peripheral nerves is not documented.

I wished to test the hypothesis that Sho is functionally homologous to the neuroprotective function of the FT of PrP^C in the CNS, thereby rescuing the phenotype induced by the lack of PrP. Mice overexpressing transgenic Sho (by ~2.5 fold) driven by *Prnp* promoter (*Sprn* mice), which allows Sho expression in peripheral nerves, were kindly provided by Dr. David Westaway (University of Alberta, Centre for Research in Neurodegenerative Diseases). I crossed *Sprn* with $Prnp^{o/o}$ mice in order to obtain a mouse line over-expressing Sho under the *Prnp* promoter on a $Prnp^{o/o}$ background.

Histological examinations and behavioral experiments demonstrated that CPD still presented in the periphery of the *Sprn/*$Prnp^{0/0}$ mice, indicating that Sho does not influence the development of polyneuropathy in peripheral nerve and, therefore, is not the substitute protein for PrP^C in the CNS. Although the identity of the substitute protein remains unknown, this work provides further understanding to the role and function of Sho.

ZUSSAMENFASSUNG

Das zelluläre Prion Protein (PrP^C) ist ein ubiquitär exprimiertes Protein, das insbesondere im Nervensystem nachweisbar ist. Das extrazelluläre PrP^C ist durch einen glycosylphosphatidyl-inositol (GPI) Anker in Detergenzien-resistenten Membranen (DRM) eingebunden und liegt dort angereichert vor. Die Aminosäuresequenz des humanen PrP^C ist evolutionär hoch konserviert und in zwei Proteindomänen unterteilt: einen langestreckten und unstrukturierten flexiblen Part (flexible tail, FT, Aminosäuren 23 - 128) und eine C-terminalen globuläre Domäne (globular domain, GD; Aminosäuren 129 - 231). Die Akkumulation von pathologischem PrP^{Sc}, einer missgefalteten, unlöslichen und partiell protease-resistenten Isoform des endogenen Proteins PrP^C, begleitet von spongiformen Veränderungen, neuronalem Zelltod und Astrozytose kennzeichnet die Transmissible Spongiforme Enzephalopathien (TSE) als Untergruppe der Enzephalopathien.

Studien haben gezeigt, dass PrP^C für die PrP^{Sc} assoziierte Toxizität notwendig ist, was auf eine Interaktion zwischen PrP^C und PrP^{Sc} schließen lässt. Allerdingssind die Mechanismen durch die Prionen zum Absterben von Nervenzellen führen noch weitestgehend ungeklärt. Erst vor kurzem konnte die Arbeitsgruppe um Mallucci et al zeigen, dass die Akkumulation von PrP^{Sc} zu chronischem Stress im endoplasmatischen Retikulum (ER) und durch die Phosphorylierung von eif2α zur Repression der globalen Proteinsynthese in Prionen-infizierten Mäusen führt, einhergehend mit Fehlfunktion der Synapsen und neuronalem Zellverlust. Zudem entdeckte unsere Forschungsgruppe eine entscheidende Rolle des PrP^C FT als Effektor von PrP^C vermitteltem Zelltod. Die Bindung von Liganden an die α1 und α3 Helix der GD des PrP^C führt zu rapider Neurotoxizität in zerebellären organotypischen kultivierten Schnitten (COCS). Durch Expression einer mutierten PrP^C Version mit Deletionen im FT konnte die Toxizität im COCS-Modell unterbunden werden. Dies weist darauf hin, dass der FT neurotoxische Eigenschaften besitzt und notwendig ist, um die Signale von der PrP^C GD zu vermitteln. Die FT Domäne enthält verschiedene Motive, die Studien zufolge mit zahlreichen Proteinen interagieren können, was eine Vielzahl an potenziellen neurotrophen bzw. neurotoxischen Protein-Protein-Interaktionen ermöglicht Die reguläre Funktion der FT Domäne von PrP^C und ihr genauer Beitrag zur Pathogenese bleibt bisher ungeklärt.
Gegenstand dieser Dissertation ist die funktionelle Charakterisierung des FT von PrP^C in vivo, um seine Bedeutung bei der PrP^C vermittelten Toxizität zu verstehen.

Zur Beantwortung dieser Frage habe ich eine transgene Mauslinie mit einer in der Membran verankerten Version des FT (FTgpi) generiert. Die FTgpi exprimierenden Mäuse, entwickeln eine schwere Ataxie und sterben innerhalb von Wochen. Histologische Untersuchungen des Gehirns zeigten einen massiven Verlust von zerebellären Körnerzellen und eine weitverbreitete Astrozytose. Aufgrund der intrinsisch unstrukturierten Natur des transgenen Proteins vermuteten wir hinter der Neurotoxizität die Aktivierung der zellulären Stressanwort auf ungefaltete Proteine. Tatsächlich waren einige ERStress Marker in den Kleinhirnen betroffener Mäuse signifikant erhöht (spiced XPB1, BIP, CHOP, und HSP40).
Ich konnte zudem nachweisen, dass FTgpi mit BiP, einem für die Proteinfaltung im ER entscheidenden Chaperon, interagiert. Diese Bindung könnte die Verfügbarkeit von BiP für andere Proteine reduzieren und so die physiologische Homöostase im ER beeinflussen.
Die Notwendigkeit eines intakten FT für die Toxizität von Anti-PrP-Antikörpern und die Ähnlichkeit der durch Prionen und FTgpi-vermittelten Neurotoxizität lassen vermuten, dass der FT eine bedeutende Rolle bei der Vermittlung von Toxizität in denmeisten PrP-abhängien Erkrankungen einnimmt. Die beschriebenen FTgpi Mäuse stellen zudem im Gegensatz zu Prionen-infizierten Modellen aus biosicherheitstechnischen Überlegungen ein deutlich sichereres Modell zum Studium der pathophysiologischen Mechanismen dar.

Shadoo (Sho) ist ein GPI-verankertes Protein, das durch das Sprn Gen kodiert wird. Es hat eine Homologie und ähnliche Organisation von Domänen wie der FT von PrP^C und ist ebenfalls evolutionär hoch konserviert. Eine kürzlich veröffentliche Studie konnte zeigen, dass Sho ähnlich neurotrophe Eigenschaften wie die FT Domäne von PrP^C besitzt. Dies deutet auf sich überlappende Eigenschaften der Proteine hin.
Prnp$^{o/o}$ Mäuse entwickeln eine chronische demyeliniserende Polyneuropathie (CDP) des peripheren Nervensystems (PNS), nicht aber des zentralen Nervensystems (ZNS). Dies deutet auf einen alternativen Substituten für PrP^C hin, der den neuropathologischen Phänotyp im ZNS, nicht aber im PNS verhindern kann. Sho wird spezifisch im ZNS exprimiert, während Expression im peripheren Nervensystem nicht dokumentiert ist.
Ich wollte die Hypothese prüfen, ob Sho im ZNS als funktionelles Homolog der neuroprotektiven Funktion von FT PrP^C wirkt und damit den Verlust der Funktion von PrP^C kompensieren kann.
Transgene Mäuse, die Sho unter dem *Prnp* Promoter (Sprn Mäuse) überexprimieren (ca 2.5fach) erlauben die Expression auch im peripheren Nerven und wurden freundlicherweise

von Dr. David Westaway (University of Alberta) zur Verfügung gestellt. Ich kreuzte die Sprn-Mäuse mit *Prnp*$^{o/o}$ Mäusen, um eine Sho überexprimierende Mauslinie auf einem *Prnp*$^{o/o}$ Background zu erhalten. Histologische Untersuchungen und Verhaltensexperimente haben gezeigt, dass die CDP nach wie vor vorhanden ist und Sho keinen Einfluss auf die Entwicklung der Polyneuropathie der peripheren Nerven hat. Sho stellt somit keinen funktionellen Ersatz für PrP^{C} im ZNS dar. Obwohl die Identität des funktionellen Substituts für PrP^{C} unbekannt bleibt, erbrachte diese Versuchsreihe wichtige Einblicke in die Funktion von Sho.

ABBREVIATIONS

AA	amino acid
AKT	protein kinase B
Bcl-2	B-cell lymphoma 2
BSE	bovine spongiform encephalopathy
CC1	positively charged cluster 1 of PrP^C (residues 23-27)
CC2	positively charged cluster 2 of PrP^C (residues 94-110)
CDP	chronic demyelinating polyneuropathy
CGC	cerebellar granular cell
COCS	cerebellar organotypic cultured slices
CJD	Creutzfeldt-Jakob disease
fCJD	familial Creutzfeldt-Jakob disease
sCJD	sporadic Creutzfeldt-Jakob disease
vCJD	variant Creutzfeldt-Jakob disease
CNS	central nervous system
CWD	chronic wasting disease
DAPI	4,6-diamidino-2-phenylindole
DNA	deoxyribonucleic acid
DPL	doppel protein
DRG	dorsal root ganglia
ELISA	enzyme-linked immunoassay
ER	endoplasmic reticulum
ERK	extracellular-signal-regulated kinase
FFI	familial fatal insomnia
FT	N-proximal flexible tail of PrP^C (residues 23-124)
FTgpi	truncated version of PrP^C ($PrP_{\Delta 141-225}$)
GD	globular domain of PrP^C (residues 124-230)
GFAP	glial acidic fibrillary protein
GPI	glycosylphosphatidyl-inositol
GSS	Gerstmann-Sträussler-Scheinker disease
HC	hydrophobic core of PrP^C (residues 112-133)
H&E	hematoxylin and eosin
HRP	horseradish peroxidase

kD	kilo Dalton
NMR	nuclear magnetic resonance
OR	octapeptide repeats of PrP^C (residues 50-90)
ORF	open reading frame
PBS	phosphate-buffered saline
PK	protease K
PNGase F	peptide-N4-(N-acetyl-beta-glucosaminyl)asparagine amidase
POMs	set of 19 anti-PrP monoclonal antibodies [1]
Prnp	murine PrP^C gene locus
Prnd	murine Doppel gene locus
PRNP	human PrP^C gene
***Prnp*$^{o/o}$**	*Prnp* knock-out mouse
PrP^C	cellular prion protein
PrP^{Sc}	scrapie-associated prion protein
$PrP_{\Delta 32\text{-}134}$	truncated version of PrP^C (lacking residues 32-134)
$PrP_{\Delta 94\text{-}134}$	truncated version of PrP^C (lacking residues 94-134)
ROS	radical oxygen species
rt	room temperature
SD	standard deviation
SDS-PAGE	sodium dodecyl sulfate polyacrylamide gel electrophoresis
sFT	truncated version of PrP^C (lacking residues 141-254)
$sFT_{\Delta HC}$	truncated version of PrP^C (lacking residues 112-254)
Sho	shadoo protein
SP	signal peptide
Sprn	murine Shadoo gene locus
***Sprn*$^{-/-}$**	*Sprn* knock-out mouse
TUNEL	terminal deoxynucleotidyl transferase dUTP nick end labeling
$T_{1/2}$	half-life
UPR	unfolded protein response
wt	wild-type mouse
ΔPrP	mutants of PrP^C carrying various deletions in the HC domain (e.g. $PrP_{\Delta 32\text{-}121}$, $PrP_{\Delta 32\text{-}134}$) [2]

CHAPTER 1

INTRODUCTION

TRANSMISSIBLE SPONGIFORM ENCEPHALOPATHIES

Transmissible spongiform encephalopathies (TSEs) are inevitably fatal neurodegenerative conditions that affect both humans and animals. Human TSEs include Creutzfeldt-Jakob disease (CJD), kuru, fatal familial insomnia (FFI), and Gerstmann-Sträussler-Scheinker syndrome (GSS); in animals, they include scrapie in sheep, bovine spongiform encephalopathy (BSE) in cattle, and chronic wasting disease (CWD) in cervids [3].

Stanley B. Prusiner defined as 'prion' (generally indicated as PrP^{Sc}) the agent causing these disorders, thus TSEs are also termed prion diseases [4,5]. Prions stem from the anagram of "proteinaceous infectious particles", and consist solely of proteins which are capable of replicating and transmitting infections without the need for informational nucleic acids. The latter sets prions apart from conventional infection agents such as viruses and bacteria. Griffith was the first to suggest that the infectious agent is merely a protein and it is devoid of nucleic acids, but it was only accepted after the systematic work conducted by Prusiner [5,6]. In support of this conjecture, experimental evidence that prions are resistant to different enzymatic, chemical and physical procedures employed to destroy nucleic acids, but are sensitive to treatments that denature proteins, had accumulated [5-8]. Follow up experiments aiming at identifying the protein responsible for TSEs, pinpointed *PRNP* as the endogenous gene coding for a 37 kDa protein, designated as PrP^{C} [4,9,10]. At this point, an audacious hypothesis was proposed: prions consist of misfolded infectious proteins which propagate, and act as a template for the conversion of the endogenous cellular form of the protein, PrP^{c}, into misfolded prions, PrP^{Sc} [11,12].

Although many similarities to other neurodegenerative protein misfolding diseases such as Alzheimer's, Huntington's and Parkinson's disease have been described [13,14] prion diseases are unique in that they are transmissible. However, this concept is evolving and prion-like transmissibility has lately been characterized for other amyloidosis diseases as well [15-17]. For instance, only recently it has been shown that the intracerebral and intraperitoneal inoculation of β-amyloid–containing brain extracts can induce cerebral β-amyloidosis and associated pathologies in susceptible hosts [17], suggesting that, like prion disease, cerebral β-amyloidosis can be seeded in the brain by homologous protein aggregates delivered into the peritoneal cavity [17]. However, unlike mice infected with prions, those inoculated with amyloid-beta (Aβ) do not die. Hence, the transmission of Aβ and PrP differs conspicuously in

the neurological effects they induce in their hosts, the difference being no less than a matter of life and death [18].

PRION DISEASES IN ANIMALS

Animal TSEs include, among others, scrapie in sheep and goat, BSE in cattle, transmissible mink encephalopathy (TME), and CWD in deer and elk [19]. Scrapie was recognized as early as 1738, characterized by the affected animals scraping their fleeces, stumbling and behavioral changes [19]. Although the origin of scrapie remains completely obscure, the pathology and transmissibility of this disease are today clearly understood. CWD has been known of since the late 1960s and was first reported as fatal wasting disease in captive mule deer in Colorado [20]. To date, 10% of the wild deer population in Colorado and Wyoming is thought to be affected [21]. As for scrapie, the origin of CWD remains elusive. CWD is believed to be transmitted among cervids with high efficiency, but transmission to other species has not been demonstrated [22].

BSE was first reported in the United Kingdom in 1985; the pathologic changes in the brain tissue of the animals were similar to those described for TSEs. The emergence of BSE was possibly caused by transmission of sheep scrapie to cattle through infected feed prepared from rendered carcasses [23,24]. This new form of TSE, commonly referred to as 'mad-cow disease', rapidly developed into a major global epidemic that peaked in the first half of the 1990s. Since then, the incidence of BSE has decreased in all affected Western European countries due to regulations that prevent feeding ruminant meat and bone meal to ruminants, and stringent prion testing of slaughtered cattle. Although incidence is declining, cases have been documented in the US as well as in countries previously believed to be BSE-free. Additionally, scrapie outbreaks are constantly documented in Europe. The fact that, most likely, millions of people (primarily in the United Kingdom) have been in contact with BSE-contaminated meat, prion diseases still present a major challenge, and vigilance needs to be maintained to prevent future outbreaks [25].

PRION DISEASES IN HUMANS

Humans TSEs include Creutzfeldt-Jakob disease (CJD), kuru, fatal familial insomnia (FFI), and Gerstmann-Sträussler-Scheinker syndrome (GSS). Human prion diseases are classified as inherited, infectious or sporadic disorders, according to clinical signs, genetic and neuropathological findings [19]. Frequently, rapid cognitive decline and progressive dementia, myoclonus, cerebellar impairment and ataxia characterize prion diseases. Once

clinical symptoms appear, death follows very rapidly [19]. Prion diseases are influenced by an amino acid polymorphism resulting in a methione > valine substitution at PrP codon 129 [26], caused by the single nucleotide polymorphism (SNP) ATG-to-GTG. Individuals who carry this specific SNP have been found to be predisposed to contracting CJD.

CJD has a very low incidence (~ 1 person in one million per year) and it was initially described as a sporadic disease (sCJD) [3]. The cause of sCJD is not fully understood – somatic mutations in the *PRNP* gene have been suggested to underlie this disease; alternatively, some individuals may possess a genetic background with a propensity, albeit very low, for PrP^{C} to self-assemble into aggregates of PrP^{Sc} leading to spontaneous manifestation of this disease [25].

Acquired conditions may occur after exposure to infectious material, as seen in variant CJD (vCJD), kuru, and iatrogenic CJD [19]. When BSE arose, scientists had proposed that BSE could have been transmitted to humans as a new variant form of vCJD. A dramatic increase of human TSEs, epidemiological, biochemical and neuropathological evidence, although indirect, have suggested that this was the case [3,27-29]. The incidence of vCJD appears to be decreasing, but a ≥30-year incubation period for BSE/vCJD is not implausible [3], and another rise in the incidence of vCJD has been proposed [30]. Until the middle of the 20th century, Kuru was the primary cause of death in Papua New Guinea [31]. Kuru is caused by the ingestion of tissues of the central nervous system (CNS) during ritualistic anthropophagy by New Guinea tribes. The incidence has steadily fallen following the cessation of cannibalism in Papua New Guinea [30]. Iatrogenicity refers to the accidental transmission of a disease, in this case CJD, during the course of medical procedures [19,32,33]. Neurosurgical equipment in particular is a prime example of the route for transmission [34], underscoring the importance of sensitive diagnostic tools which could be used for screening units prior to transfusions or surgical operations.

Familial TSEs account for 10-20% of all TSE cases in humans and include genetic CJD (gCJD), GSS and FFI [19]. Several mutations in the *PRNP* gene have been identified in families with hereditary or genetic gCJD, and inheritance of these mutations is autosomally dominant with high penetrance [3]. GSS is another autosomal-dominantly inherited and transmissible TSE, caused by mutations in the prion protein open reading frame (ORF) [3,35,36]. GSS typically presents with progressive cerebellar ataxia or spastic parapesis and cognitive decline and was first reported in an Austrian family in 1928, and again in 1936 when another member of the same family was affected [37]. Fatal familial insomnia (FFI) was initially described in 1986 in an Italian family that was affected by insomnia and dysautonomia [38]. FFI was classified as a

TSE once transmission to mice had been demonstrated [39]. FFI predominantly affects the thalamus region of the brain, and clinical signs typically include deregulation of the sleep-wake cycle and attention deficit [40].

Interestingly, all inherited TSEs appear early in life, possibly due to the presence of abnormal PrP throughout development and postnatal life. In contrast, sporadic prion diseases may occur because of a stochastic event.

PRION CONVERSION REACTION

The prevailing hypothesis on the nature of the infectious prion is the 'protein-only' hypothesis. This proposes that the agent causing the infectious disease consists essentially of the abnormally folded PrP^{Sc} [41].

Prion diseases are associated with abundant accumulation of PrP^{Sc} in the CNS. PrP^{Sc} and PrP^{C} were found to share a similar amino acid structure, and no known covalent modifications have been found to differentiate the two proteins [42]. However, the resolution of the 3-dimensional (3D) structure of mouse, hamster and human PrP^{C} by nuclear magnetic resonance (NMR) [43-45] has provided some evidence for a possible conversion mechanism. It has therefore been proposed that PrP^{Sc} is a posttranslational derivative of PrP^{C}, having acquired a different 3D conformational structure, and that pathologic PrP^{Sc} operates as a seed promoting further conversion of PrP^{C} [46]. How PrP^{C} is converted to PrP^{Sc} remains unclear, but two likely conversion processes, the 'template-directed refolding' model and the 'seeded nucleation' model [47-49] have been proposed and are depicted in Figure 1.1. Indeed, it has been shown that PrP^{C} and PrP^{Sc} can be distinguished because of their different biochemical profiles: PrP^{C} is rich in α-helices (~ 45%) and has relatively few β-sheets; PrP^{C} is soluble, and sensitive to proteinase K (PK) digestion, whereas PrP^{Sc} is enriched in β-sheet content (~ 45%) and is therefore prone to aggregation; PrP^{Sc} is insoluble in detergents, and partially resistant to PK [3,50].

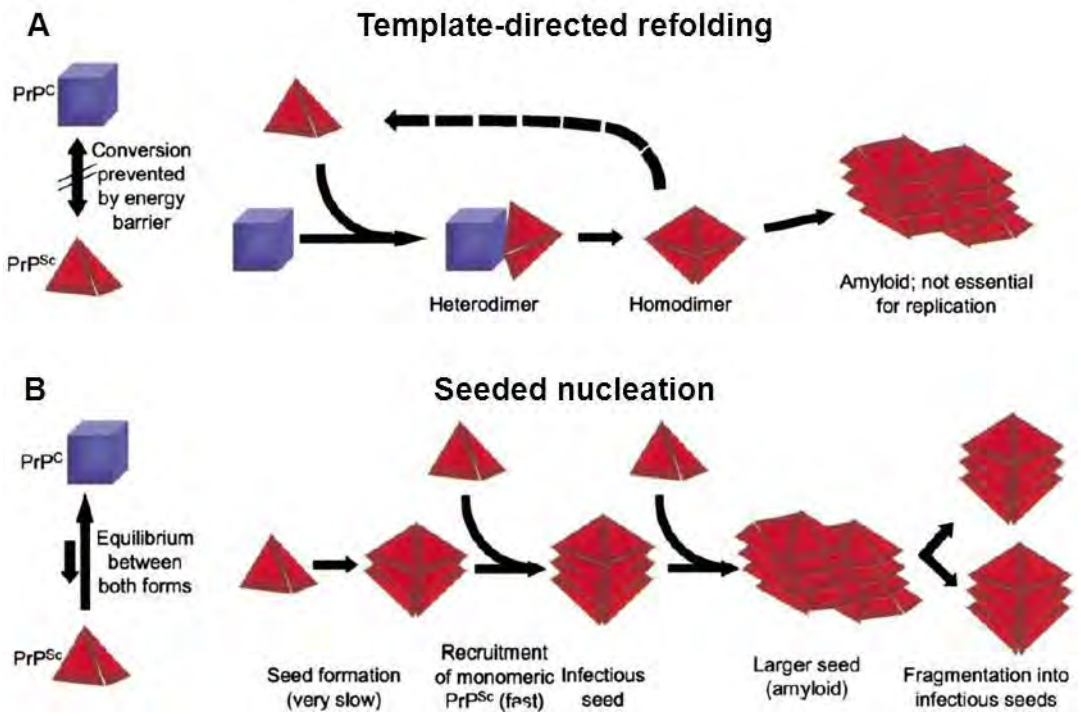

Figure 1.1 Proposed models for the conversion of PrP^C into PrP^{Sc}. *(**a**) The 'template-directed refolding model' posits an interaction between PrP^{Sc} and PrP^C. The latter is subsequently induced to transform itself into PrP^{Sc}. A high energy barrier may prevent spontaneous conversion of PrP^C into PrP^{Sc}. (**b**) The 'seeded nucleation model' proposes that PrP^C and PrP^{Sc} are in a thermodynamic equilibrium, strongly in favor of PrP^C. Only a highly ordered seed of several monomeric PrP^{Sc} molecules can further recruit monomeric PrP^{Sc} entities and eventually generate larger aggregates with an amyloid structure. Within such a crystal-like seed, PrP^{Sc} becomes stabilized. Fragmentation of PrP^{Sc} aggregates increases the number of seeds, which can then recruit further PrP^{Sc} and thus replicate the prion agent. Adapted from Aguzzi and Polymenidou, 2004 [23].*

A) The 'template-directed refolding' presumes that a high activation energy barrier prevents spontaneous conversion of PrP^C into PrP^{Sc}, and that the conformational change is kinetically controlled. Exogenous PrP^{Sc} exerts a catalytic action and lowers the energy barrier, hence promoting the misfolding process. In familial prion diseases, pathogenic mutations may lower the energy barrier favoring spontaneous conversion into PrP^{Sc} with no necessity of exogenous PrP^{Sc}.

B) The 'seeded nucleation' model assumes that PrP^C and PrP^{Sc} are in a thermodynamic equilibrium, strongly favoring PrP^C in a nondisease state. A highly ordered seed of PrP^{Sc} can be stabilized on contact with other seeds and, in turn, further recruits additional monomeric PrP^{Sc}, resulting in amyloid. Subsequent fragmentation of PrP^{Sc} aggregates increases the number of infectious seeds, which can recruit further PrP^{Sc} and thus results in apparent

replication of the agent. In this model, the formation of the seed is the rate limiting step. Aggregates need to be continuously fragmented, generating an increasing number of seeds to result in exponential accumulation of PrP^{Sc} [51].

In support of the 'protein-only' hypothesis, mice devoid of the prion protein PrP^{C} (*Prnp*$^{o/o}$ mice) have been shown to be completely resistant to prion infection [52]. In addition, in *Prnp*$^{o/o}$ mice previously inoculated with prions, the brain tissue does not harbor prion infectivity [53]. Reintroduction of *Prnp* by transgenesis restores susceptibility and prion replication in *Prnp*$^{o/o}$ mice [54-56]. These findings suggest that PrP^{C} acts as an essential substrate for the propagation of the infectious agent.

Currently, it is widely accepted that prions mainly consist of PrP^{Sc}. However, it remains to be formally proven whether the infectious unit consists exclusively of PrP^{Sc}.

PRION DISEASE HALLMARKS AND PATHOGENESIS

Although the clinical profiles differ among the distinct prion diseases, the histological hallmarks of brain damage are similar, and are represented by the presence of PrP^{Sc} aggregate deposits, synaptic alteration, extensive spongiform degeneration, astrogliosis, and neuronal loss [57]. These result in clinical symptoms which include cognitive and motor dysfunctions (Figure 1.2) [58].

Since neuronal loss and gliosis accompany many other conditions of the CNS, it is the spongiform change that is mostly specific to prion diseases [57]. Spongiform changes may be mild, moderate or severe and are characterized by diffuse or focally clustered, small, round or oval vacuoles in the neuropil of the deep cortical layers, cerebellar cortex or subcortical grey matter, which might become confluent [57]. Presence and distribution of spongiform change vary greatly between cases and disease subtypes. For instance, some prion diseases have equivocal, little, or no spongiform change, such as FFI, which is specifically characterized by prominent thalamic atrophy with profound astrogliosis [59].

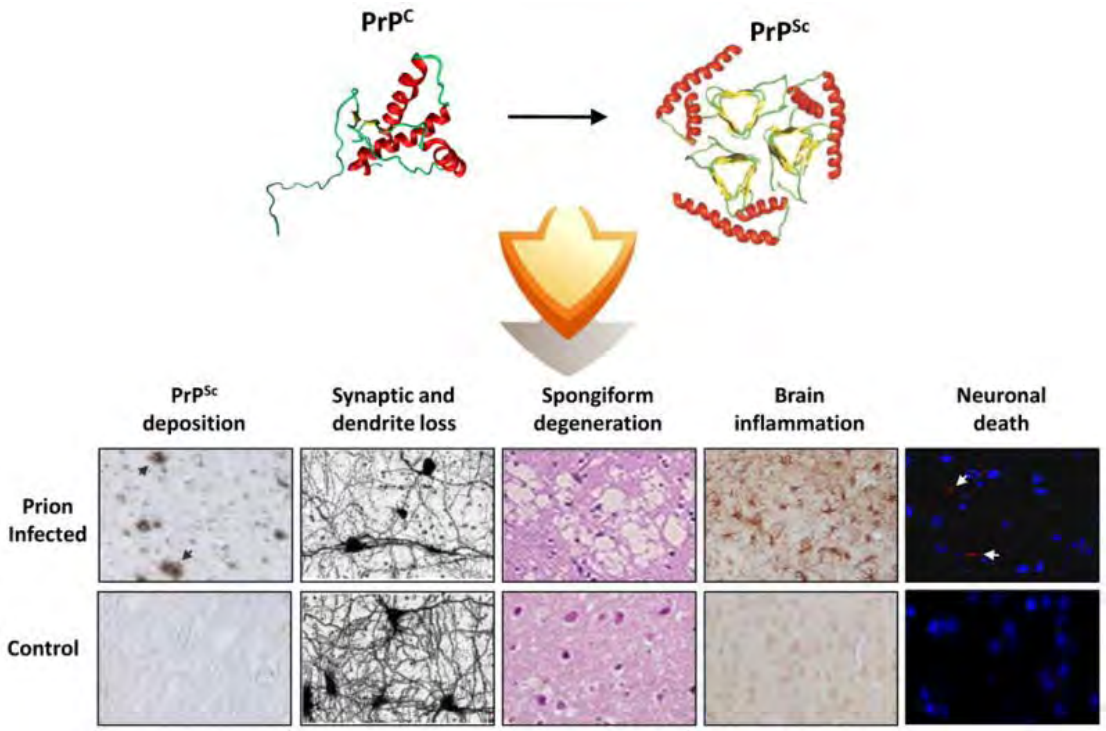

Figure 1.2. Histopathological hallmarks of prion diseases. *From left to right. PrP^{Sc} deposits, which are detected by anti-PrP antibody, are induced by the abnormal aggregated conformer of PrP^{C}, PrP^{Sc}; synaptic and dendritic loss (visualized by silver staining), vacuolization and spongiosis (H&E staining), astrogliosis and brain inflammation (shown by GFAP staining), neuronal death (TUNEL and caspase-3 staining). Adapted from Soto and Satani [58].*

Despite decades of intense research in prion diseases, the mechanisms and molecular determinants of prion pathogenesis leading to gliosis, spongiosis, and neuronal cell loss are not yet fully understood. *Prnp*$^{0/0}$ mice do not present with major abnormalities or neuronal loss, suggesting that prion diseases are not caused by PrP^{C} loss-of-function [60]. Furthermore, *Prnp*$^{0/0}$ mouse models do not support prion replication, nor do they show clinical signs of cognitive impairment and motor dysfunction after prion inoculation [52], indicating that PrP^{C} is necessary for PrP^{Sc} replication, which in turn leads to neurodegeneration, and that PrP^{Sc} might not be directly responsible for prion-dependent neuronal loss. In addition, prion infection after grafting PrP^{C}-overexpressing brain tissue onto *Prnp*$^{0/0}$ brains resulted in PrP^{Sc} propagation, with pathological changes restricted to the grafted area [61,62]. Further investigations have shown that transgenic mice expressing an anchorless form of PrP were still capable of replicating prions, but without signs of pathology, indicating that membrane-anchoring of PrP is also necessary to induce pathology [63]; and depletion of endogenous neuronal PrP^{c} in mice with established neuroinvasive prion infection reversed early spongiform change and prevented neuronal loss and progression to clinical disease [64].

These findings indicate that prion propagation and neurotoxicity may be distinct and independent events, and that neurotoxicity is somehow transduced through the expression of cellular PrP^{C} on target cells [64].

Charles Weissmann has proposed that toxicity could be mediated by PrP forms other than PrP^{Sc}, for instance a toxic intermediate generally denoted as PrP* (Weissmann, 1991a), offering an explanation for those cases when spongiform pathology is present with few PrP^{Sc} deposits [19]. In recent years, the concept that oligomeric and even smaller units, rather than larger aggregates, might be responsible for neurotoxicity in many neurodegenerative disorders that are accompanied by misfolded aggregates has been discussed [65]. Indeed, it has been proposed that larger aggregates may actually have a protective function [65]. When abnormal and aggregated proteins cannot be refolded or degraded by proteasomal degradation and autophagy, cells have an alternative line of defense whereby aggregates are sequestered by microtubule-mediated transport and collected at a single cytoplasmic site near the centriole. This process generates a large inclusion body called an 'aggresome' [65,66].

In 2012, Moreno et al showed for the first time that accumulation of PrP^{Sc} during prion infection causes persistent translational repression of global protein synthesis in mice, indicating an association between endoplasmic reticulum (ER) stress and neurodegeneration [67]. Moreover, ER stress has been detected in patients with Parkinson's disease [68], Alzheimer's disease [69], and amyotrophic lateral sclerosis (ALS) [70,71]. However, whether ER stress is a cause or consequence of neurodegenerative processes in such diseases is currently not known.

THE CELLULAR PRION PROTEIN

BIOSYNTHESIS AND EXPRESSION PATTERN OF PrP^C

PrP^C is a glycosylphosphatidyl inositol (GPI)-linked glycoprotein enriched in detergent-resistant membranes (lipid rafts), and synthesized in the rough ER [3]. PrP^C comprises 253 amino acids which undergo post-translational modifications such as removal of the signal peptide (1-22aa), addition of two glycosylation chains (highly branched glycosyl groups with sialic acid substitutions) at asparagine 181 and 197, formation of a disulfide bridge between cysteine 197 and 214, and attachment of a GPI anchor after replacement of a C-terminus peptide (Figure 1.3) [72].

The cellular prion protein is highly conserved among species. It has been identified in mammals, birds [73], amphibians [74], and fish [75], suggesting that PrP^C may play an important functional role, although *Prnp*$^{o/o}$ mice have no significant impairments and have a normal life span [52].

PrP^C is highly expressed in the central nervous system, predominantly within neurons, although it is also expressed by other neural cell lineages including astrocytes and oligodendrocytes [76], whereas expression on microglia is minimal [77]. It is also expressed at high levels in a broad range of peripheral tissues and cells including heart, skeletal muscle, kidney and lymphocytes [78,79]. In addition, ectopic PrP^C expression and prion replication competence can be induced by inflammatory conditions in organs that physiologically express very low amounts PrP^C [80].

THE PHYSIOLOGICAL FUNCTION OF PrP^C

Despite many efforts, and advances in the characterization of PrP^C, its physiological role is still unclear. To date, the study of *Prnp*$^{0/0}$ mice has failed to elucidate the molecular function of this highly conserved protein. It seems rather unlikely that a highly conserved protein has evolved solely to bestow susceptibility to prion diseases upon organisms [19]. Although *Prnp*$^{o/o}$ mice are viable, they show a chronic demyelinating polyneuropathy (CDP) in peripheral nerves [81]. Interestingly, CDP develops if PrP^C is solely ablated from neurons, but it is prevented when PrP^C is specifically ablated in Schwann cells [81]. This confers an important role for neuronal PrP^c in peripheral nerve myelin maintenance [81].

Many other functions have been proposed for PrP^C, such as modulation of cell signaling, maintenance of circadian rhythms and neuronal development [82]; however, their significance in these processes has not been confirmed. Furthermore, several dozen proteins

have been described to bind neuronal PrP^c in various cellular compartments [3,83] although, in most cases, there are no known associated biological functions for these interactions. One cannot exclude that PrP^C exerts diverse roles according to the cellular context, local environment and its interaction partners [84]. It has therefore been hypothesized that PrP^c acts as a scaffold protein and has the ability to drive the assembly of multi-component complexes at the cell surface [84].

STRUCTURE OF PrP^C

The structure of mature PrP^C is well-conserved comprising a long, unstructured and flexible tail (FT, residues 23-128), and a globular domain (GD, residues 129-231) of three α-helices and a two-stranded antiparallel β-sheet that flanks the first α-helix (Figure 1.3A) [85,86]. The FT contains several different domains: the signal peptide (SP), the small charge cluster one domain (CC1), the octarepeat region (OR) and the charge cluster two domain (CC2) (Figure 1.3A). The hydrophobic core (HC) is a stretch of 20 hydrophobic amino acids that separates the FT from the GD (Figure 1.3A) [45]. The HC is highly conserved among species which may reflect an important biological function [3]. Accordingly, a number of mice carrying different mutations involving the HC (generally defined as ΔPrP mice) have been created in order to clarify the role of this region; the loss of HC leads to very severe disorders in newborn mice, causing death within 8 days on a *Prnp*$^{0/0}$ background [2].

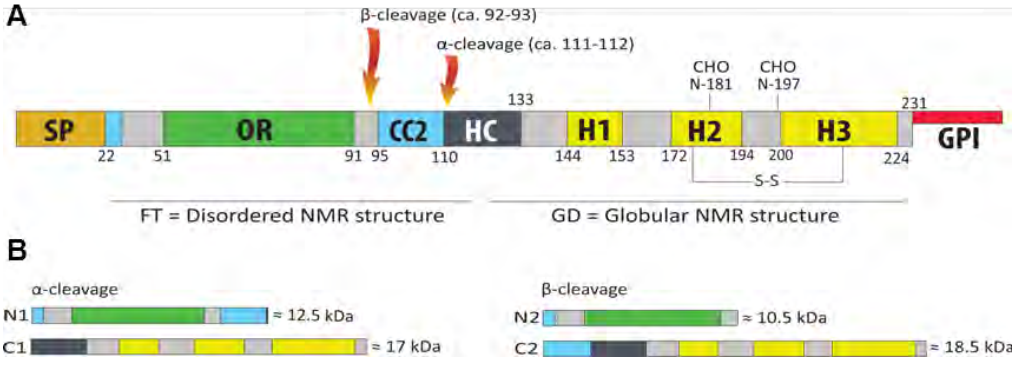

***Figure 1.3. The structure of PrP^C and the products of α- and β-cleavage**. (**A**) FT: flexible tail; GD: globular domain. PrP^C comprises signal peptide (SP; shown in orange), which is cleaved at the level of the endoplasmic reticulum, the octarepeat region (OR; shown in green), the charge cluster 1 and 2 domain (CC1 and CC2; pale blue), the hydrophobic core domain (HC; dark grey), three α-helices (H1, H2, H3; yellow) And a glycosylphosphatidyl inositol anchor (GPI; red). The two glycosylation sites are at N181 and N197. A disulfide bridge is also present, connecting C179 and C214. (**B**) Fragments generated by α- and β-cleavage.*

PrP^C undergoes proteolytic cleavage that generates an N-terminal fragment (N1) and a C-fragment (C1) (Figure 1.3B). Evidence suggests that ADAM9/ADAM10 or ADAM17 metallo-proteases are involved in this proteolytic process [87]. This α-cleavage occurs approximate to the 111/112 peptidyl bond; it can be either constitutive or regulated by protein kinase C (PKC), and has been hypothesized to be a key regulator of PrP function and/or malfunction [88]. Different roles have been attributed to C1, such as the regulation of p53-dependent staurosporine-induced caspase-3 activation in cell systems [89]; however its precise role remains elusive. A second cleavage site, the β-cleavage site, has been identified immediately before the CC2 domain, approximate to the 92/93 peptidyl bond (Figure 1.3B) [90]. Although attempts have been made, both *in vitro* and *in vivo,* to characterize and describe the functions of the products of these cleavages, their physiological roles remain unknown.

PrP^C DOUBLE AND SHADOW

Since it is well conserved amongst different species, PrP^C must possess some beneficial physiological attribute; however, results from *Prnp*$^{o/o}$ mice only partially untangled the physiological function of PrP^C. Another avenue of research into the biology of PrP^C has recently discovered two paralogs of PrP^C, Doppel and Shadoo, the 'double' and 'shadow' of PrP^C, respectively [91].

Doppel is predominantly expressed in the testis and it appears to have a crucial role in the proper functioning of the male reproductive system [92]. It is encoded by the *Prnd* gene in mice, which is located 16 kilobase (kb) downstream of the murine *Prnp* locus [93]. Doppel is processed similarly to PrP^C: it migrates through the secretory pathway to the plasma membrane, where it resides in lipid rafts in testis of wild type (wt) mice [94]. The tertiary structure of Doppel is very similar to the GD of PrP^C, sharing the same secondary structure elements, despite their primary sequence sharing only 25% homology [95]. Interestingly, overexpression of Doppel in the CNS of *Prnp*$^{o/o}$ mice correlates with ataxia and death of cerebellar neurons [96], although the mechanistic aspects of this deleterious effect are unknown.

Shadoo (Sho) is a CNS-expressed protein which has many similar properties with PrP^C and may possess overlapping activity [97]. Shadoo is encoded by the *Sprn* gene, and seems to be widely conserved in nature, from lower organisms (e.g. zebrafish) to rodents and primates [98]. In contrast to Doppel, the architecture of Shadoo is similar to that of the PrP^C FT,

although Shadoo lacks an OR region [91]. As previously mentioned, the HC is the most conserved region of PrP^C, suggesting functional homology across species [91].

Over the past 14 years, research efforts have focused on the biology of PrP^C and its family members in order to clarify their functional roles; as yet, the full picture is yet to be disclosed.

AIMS OF THIS THESIS

Prion diseases affect both humans and many species of animals, and no effective treatment is currently available. Although recent publications point to ER stress as a major culprit for synaptic impairments and neurodegeneration in prion-infected mice, the exact mechanisms and cellular processes by which prions kill neurons are not fully understood. Furthermore, our group recently showed that antibodies targeting the α1 and α3 helices of the GD are surprisingly neurotoxic, and their toxicity is strictly dependent on an intact FT of $PrP^{C,}$ uncovering a pivotal role of the FT domain in PrP-induced toxicity [99].
In light of this evidence, I wished to investigate:

- **the role of FT of PrP^{C} in triggering neuronal death *in vivo***, by means of a newly generated transgenic mouse line expressing a redacted version of the prion protein lacking the GD but retaining the GPI anchor signal ($PrP_{\Delta 141-225}$ or FTgpi). In particular, I focused on identifying:
    - FT structural determinants involved in toxicity
    - the signaling pathways evoked by FT
    - the temporal occurrence of these pathways

Prnp$^{o/o}$ mice show CDP in peripheral nerves [81]. Shadoo is a CNS-expressed protein which has structural homology with the FT of PrP^{C}, and it has been shown to share some of its FT neuroprotective properties [97]. Therefore, I wished to elucidate:

- **the predicted role of Shadoo in reversing the CDP observed in peripheral nerves in *Prnp*$^{o/o}$ mice**. Mice overexpressing transgenic Sho ~2.5-fold, driven by the *Prnp* promoter, were kindly provided by Dr. David Westaway *(University of Alberta, Centre for Research in Neurodegenerative Diseases)*. These mice were crossed with *Prnp*$^{o/o}$ mice in order to obtain mice over-expressing Sho on a *Prnp*$^{o/o}$ background. The severity of CDP was assessed at different time points by immunohistochemistry, ultrastructure analysis and behavioral experiments.

CHAPTER 2

MEMBRANE TETHERING OF THE FLEXIBLE TAIL OF THE PRION PROTEIN TRIGGERS UNFOLDED PROTEIN RESPONSE AND NEURODEGENERATION

This chapter contains unpublished data as well as parts that are adapted or reproduced from the following manuscript:

Membrane tethering of the flexible tail of PrP triggers prion-like neurodegeneration

Paolo Dametto[1], Claire Bridel[1,$], Asvin Lakkaraju[1], Lukas Villiger[1], Tracy O'Connor[1], Uli S. Herrmann[1], Pawel Pelczar[2], Thomas Rülicke[3], Donal McHugh[1,#], Arlind Adili[1], and Adriano Aguzzi[1†]

[1] Institute of Neuropathology, University Hospital Zurich, Switzerland

[2] Institute of Laboratory Animal Science, University of Zürich, Switzerland

[3] Institute of Laboratory Animal Science, University of Veterinary Medicine Vienna, Austria

[$] Current Address: Department of Neurosciences, University Hospital of Geneva, Switzerland

[#] Current Address: Institute of Experimental Immunology, University of Zurich, Switzerland

[†]Corresponding author:

Adriano Aguzzi

Institute of Neuropathology, University Hospital of Zurich

Schmelzbergstrasse 12, CH-8091 Zurich, Switzerland

Tel: +41-44-255-2108, Email: adriano.aguzzi@usz.ch

Author contributions

PD performed cloning to generate the Flp-In 293 cell lines, Western blots, immunohistochemical and immunofluorescent stainings, FACS, RT-PCR, survival analyses, and generated the sFT mouse. PD made Figures 2.1A, 2.2-2.9, 2.11-2.14, and 2.17-2.28. AL and LV performed the experiments shown in Figure 2.15 and Figure 2.16. CB made the FTgpi mouse and performed the experiments shown in Figure 2.1.B and 2.10. TR and PP performed pronuclear microinjections. TOC supervised parts of the work.

INTRODUCTION

THE CONTROVERSIAL ROLE OF THE FLEXIBLE TAIL (FT) OF PrP^C

PrP^C consists of an unstructured, flexible N-terminal tail (FT, residues 23-128) hinged to a structured globular domain (GD, residues 129-231) comprising three α-helices (α1, α2 and α3) and two-stranded antiparallel β-sheets [45]. Although unstructured, the amino acid sequence of the FT identifies a number of recognizable motifs: the signal peptide (SP), the small 'charge cluster 1' (CC1), a series of octapeptide repeats (OR), the 'charge cluster 2' (CC2), and the hydrophobic core (HC) – a stretch of 20 hydrophobic amino acids linking the FT with the GD (Figure 1.3). CC2 and HC together form the central domain (CD). All these motifs have been reported to interact with a broad range of proteins, conferring a number of potential, yet poorly understood, attributes to the FT, ranging from neurotrophic to neurotoxic properties [100], Clearly, the true function of these domains is still to be determined.

A ROLE FOR FT IN NEUROPROTECTION

Several mouse models carrying deletions in the HC domain ($PrP_{\Delta 32\text{-}121}$, $PrP_{\Delta 32\text{-}134}$ and $PrP_{\Delta 111\text{-}134}$, collectively denoted as 'ΔPrP'), demonstrate the intrinsic neuroprotective role of the PrP HC motif [100]. Expression of ΔPrP, or neuronal expression of Doppel, which resembles the GD of PrP^C but lacks the FT section, cause demyelination in the CNS and peripheral nerves, indicating that PrP^C, through its HC domain, is required for myelin maintenance [2,81,101]. Amino acids 23-90, encompassing the CC1 and OR domains, also showed neuroprotective properties – Doppel induced neurodegeneration when ectopically expressed in the CNS [96], but this phenotype was completely reversed when the first 133 aa of PrP^C were fused to Doppel (NH_2-$PrP_{(1\text{-}133)}$-Doppel) [102]. Importantly, when either CC1 or OR were removed from the chimera protein, Doppel-mediated toxicity could not be inhibited [103]. Moreover, it has been shown that the N-terminal fragment of PrP (N1), which contains the CC1, OR and CC2 domains, also displays *in vivo* and *in vitro* neuroprotective functions by modulating the p53 pathway [104].

The entire or partial loss of HC leads to very severe neurological disorders and early postnatal death in newborn mice [2,56,105], whereas mice carrying shorter deletions within the FT did not display neurological symptoms [2]. Importantly, introduction of one copy of wt PrP^C abrogated the deleterious effect in ΔPrP mice [56].

A ROLE FOR FT IN NEUROTOXICITY

The mechanism by which ΔPrP mutations leads to neurodegeneration *in vivo* is not known. Recently, *in vitro* studies showed how ΔPrP mutants induce spontaneous large cationic unspecific channel activity in HEK293 cells [106], suggesting that neurotoxicity could be elicited by the formation of a pore in the plasma membrane, which would destabilize the membrane potential. Deletion of the small CC1 domain from these variants reverses toxicity both *in vitro* [106] and *in vivo* [107], highlighting the importance of FT domains, in particular CC1, in modulating neurotoxicity in these models. Furthermore, mice expressing PrP^{C} devoid of CC1 display reduced susceptibility to prion infection and greatly reduced levels of PrP^{Sc} [108], suggesting that CC1 may not be essential for, but dramatically improves, prion propagation.

Further evidence supporting the pivotal role of the FT domain in PrP-induced toxicity has been demonstrated by Sonati et al [99]. Antibodies targeting the α1 and α3 helices of the GD are neurotoxic, and we recently found that their toxicity is strictly dependent on an intact FT [99]. These phenomena may be explained through an allosteric mechanism of action: conformational transitions in the GD may influence the topology of the FT relative to the plasma membrane or other cellular constituents, and eventually trigger a cascade of untoward events. In support of the idea that FT domains are crucial for PrP-induced toxicity, removal of the OR region from the FT, or pretreatment with anti-OR antibodies, abolishes the toxicity of anti-GD antibodies, indicating that an intact FT is required to transmit these toxic signals [99].

OUTLINE OF THIS WORK

Currently, controversial opinions surround the physiological and pathological role of FT. In light of our recent findings [99], I focused on the neurotoxic properties of FT. In order to clarify the mechanisms by which FT exerts detrimental actions *in vivo*, we generated transgenic mice expressing the FT fused to a GPI anchor but devoid of the entire GD ($PrP_{\Delta 141-225}$, henceforth termed 'FTgpi'). FTgpi mice experience progressive, inexorably lethal neurodegeneration. In contrast, mice expressing untethered, soluble FT (sFT) do not experience any pathology. Immunofluorescence and fluorescence-activated cell sorting (FACS) analysis showed that most FTgpi was retained in the ER with only a minor fraction reaching the plasma membrane. FTgpi triggered chronic ER stress *in vivo* at an early time point, which in turn induced apoptosis, potentially explaining the neuronal death observed in the cerebellum of FTgpi mice, where the protein is mostly expressed. These phenomena are strikingly similar to those observed in prion infections [67], suggesting that aberrant localization of FT or acquisition of illegitimate FT topologies may underlie the toxicity observed in these diseases. Therefore, FTgpi mice may be a useful tool for further investigation into the mechanisms of toxicity underlying human prion diseases.

RESULTS

GENERATION OF TRANSGENIC MICE AND ANALYSIS OF PROTEIN EXPRESSION

To investigate the ability of FT to elicit toxicity *in vivo*, a redacted version of the prion protein lacking the GD but retaining the GPI anchor signal ($PrP_{\Delta 141\text{-}225}$ or FTgpi; Figure 2.1A) was cloned into the 'half-genomic' pPrPHG backbone, which contains the *Prnp* gene devoid of intron #2 [54]. The resulting construct was injected into pronuclei of $Prnp^{+/+}$ mice. Potential founders were screened by tail PCR for the presence of the transgene, and six founders were identified as carriers. Three transgenic lines (FTgpi155, FTgpi157, and FTgpi177) were selected for further analysis on the basis of transgenic protein expression levels in the CNS (Figure 2.1B). FTgpi was visualized by western blot as a double band at 15 kDa and 17 kDa, potentially suggesting that FTgpi assumes different transmembrane topologies affecting cleavage of its signal peptide. The highest FTgpi-expressing founder, FTgpi157, and its offspring died before further analysis could be performed. This was the first indirect observation suggesting that FTgpi could be toxic.

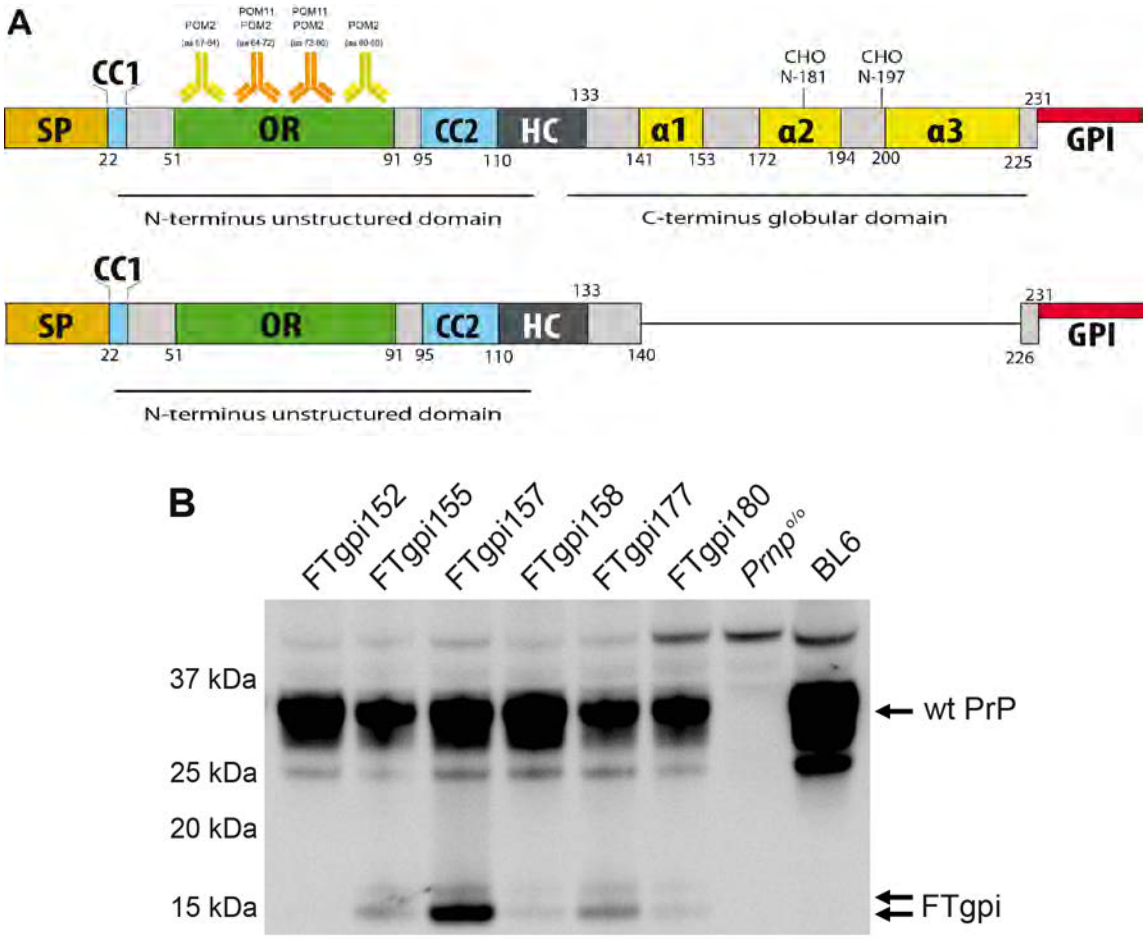

Figure 2.1. Layout of FTgpi protein and founder FTgpi expression level. *(**A**) Scheme of wild-type PrP and FTgpi utilized for the generation of the transgenic mouse. SP: signal peptide; OR: octapeptide repeats; CC2: charge cluster 2; HC: hydrophobic core; α1 α2 α3: α-helices; GPI: glycosylphosphatidylinositol anchor. POM2 binds the degenerate epitope QPHGGG/SW (aa 57-64, 64-72, 72-80, 80-88) whereas POM11 recognizes the epitope QPHGGSW (aa 64-72, 72-80) of the FT [1]. (**B**) Whole brains of FTgpi, Prnp$^{o/o}$ (here and henceforth used as a negative control) and B6/J-Hsd1 mice (BL6, here and henceforth used as positive control) were analyzed by Western blotting using POM11. Arrows: FTgpi protein (15 and 17 kDa). The FTgpi157 founder mouse showed the highest expression levels of FTgpi.*

The two remaining lines (FTgpi155 and FTgpi177) were crossed with *Prnp*$^{o/o}$ mice to obtain offspring on a *Prnp*$^{o/o}$ background. Transgenic mRNA levels in FTgpi155 brains were ~6-fold higher than *Prnp* mRNA in C57BL/6 mice (BL6; Figure 2.2A), yet FTgpi protein levels were just 15% (FTgpi155) and 5% (FTgpi177) of total PrP^{C} in BL6 brains (Figure 2.2B), suggesting that the FTgpi protein undergoes very rapid degradation.

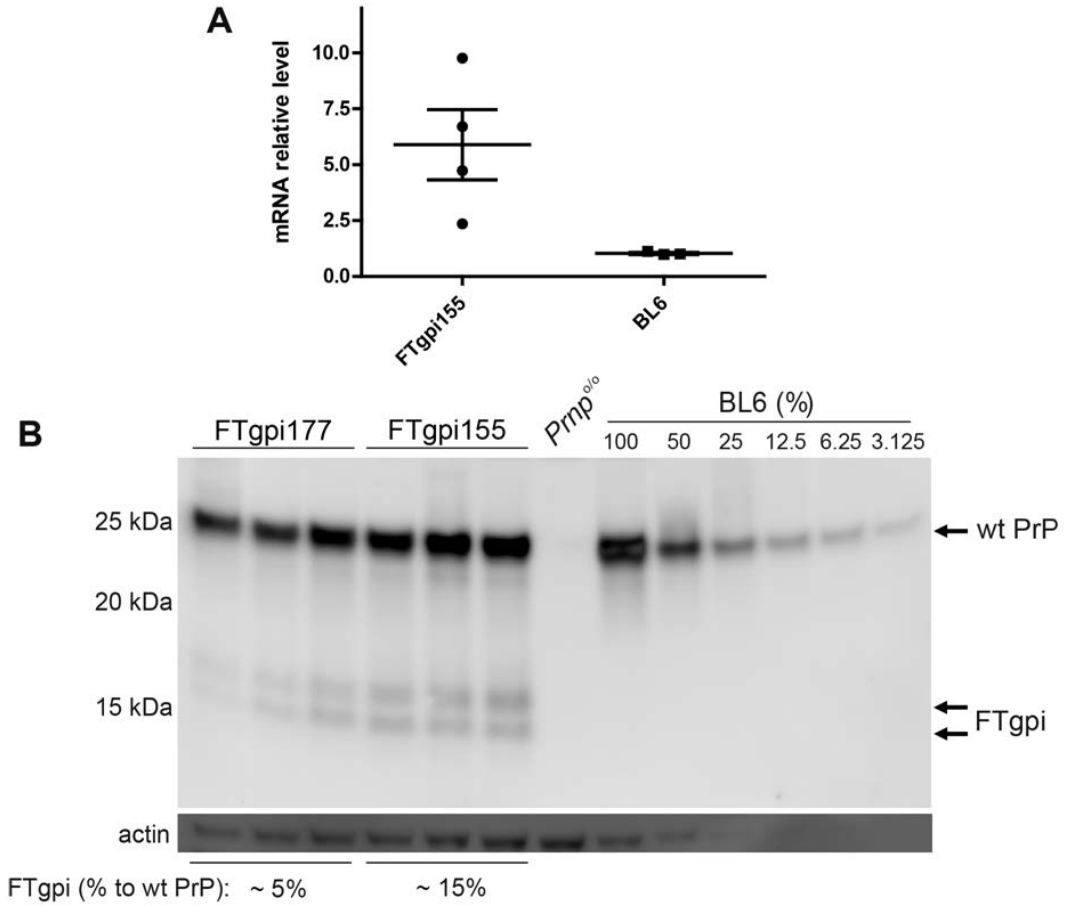

Figure 2.2. mRNA and protein level of FTgpi protein. *(**A**) Transgenic FTgpi and wt PrP transcription quantified by Real-Time PCR (RT-PCR). FTgpi mRNA was approximately 6-fold higher than Prnp mRNA. (**B**) Brain homogenates were subjected to PNGase F treatment. FTgpi155 and FTgpi177 mouse lines displayed protein levels of ~15% and ~5%, respectively, compared to a calibration curve with serially diluted BL6 brain (not shown). Western blots using POM2.*

PATHOLOGICAL PHENOTYPES OF MICE EXPRESSING FTGPI

All FTgpi transgenic lines were maintained in both *Prnp*$^{+/+}$ and *Prnp*$^{o/o}$ genetic backgrounds. We used the ZyFISH technique [109] to reliably discriminate between homo- and hemizygous transgene carriers. Mice were monitored according to a previously published four-degree clinical score [2]. Both the FTgpi155 and the FTgpi177 line developed a phenotypically similar form of ataxia. Since each line was derived from an independent pronuclear microinjection leading to unique chromosomal integration events, I concluded that the phenotype was induced by the expression of the transgene rather than by insertional mutagenesis.

The first sign of disease (~9 weeks) observed in FTgpi155 *Prnp*$^{+/+}$ was shivering, followed by mild limping and hind limb weakness. At later stages (~12 weeks), mice tended to fall on both sides while walking in the cage (Figure 2.3, left panel). In addition, mice were placed on a

metal grid and monitored for 5 min to assess their walking proficiency (cage grid test). At later stages of the disease (~14 weeks), these tests always resulted in positive scores, with both legs consistently falling through the grid (Figure 2.3, central and right panels). No paralysis was observed.

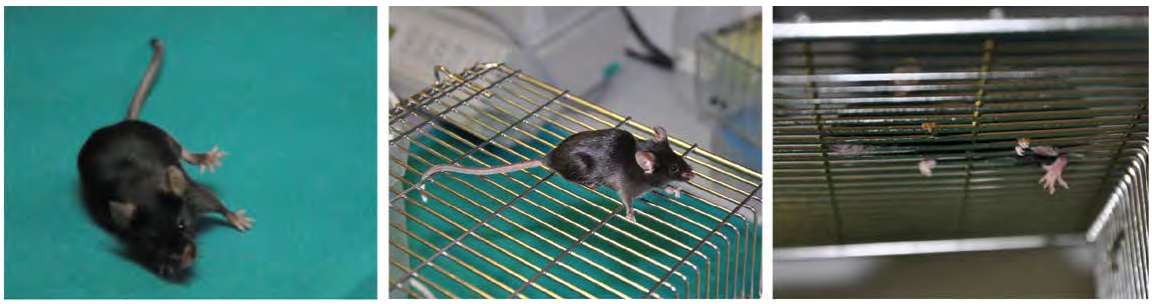

Figure 2.3. FTgpi mice phenotype. *Typical clinical phenotypes at terminal stage. Left panel: FTgpi155$^{+/+}$ mouse showing ataxia symptoms at 14 weeks of age. Central and right panel: representation of a grid test. At 14 weeks of age, FTgpi155$^{+/+}$ legs repeatedly falling through the grid.*

The higher-expressing lines, FTgpi155 *Prnp*$^{+/+}$ and FTgpi155 *Prnp*$^{o/o}$, developed signs of disease and died significantly earlier (median ± standard deviation: 109 ± 6.7 and 111 ± 24 days, respectively, p<0.0001) than the lower expressing lines FTgpi177 *Prnp*$^{+/+}$ and FTgpi177 *Prnp*$^{o/o}$ (242 ± 127 and 479 ± 178 days, respectively, p<0.0001), indicating that FTgpi toxicity was dose-dependent (Figure 2.4). Co-expression of PrP^{C} did not improve the survival of FTgpi mice (Figure 2.4). This suggests that the mechanism of toxicity is different from that of the deletion mutants, PrP$_{\Delta 94\text{-}134}$ and PrP$_{\Delta 32\text{-}134}$ [2,56], which are dose-dependently rescued by co-expression of PrP^{C} [2]. On the contrary, PrP^{C} seemed to worsen the phenotype in FTgpi177 mice, as FTgpi177 *Prnp*$^{+/+}$ died significantly earlier that FTgpi177 *Prnp*$^{o/o}$ mice (Figure 2.4, orange and green lines). This phenomenon did not occur in FTgpi155 mice, perhaps because FTgpi expression was saturating.

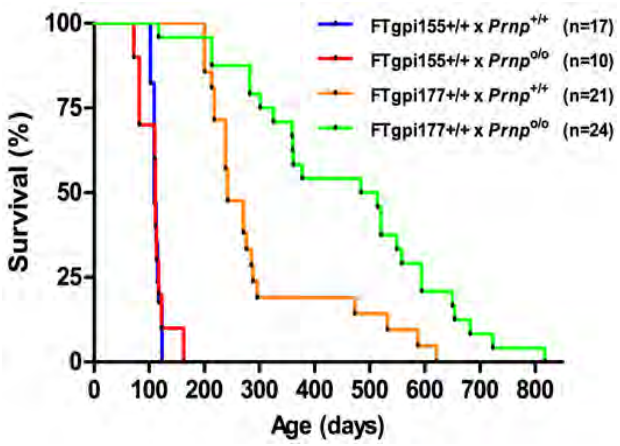

Figure 2.4. Survival curves of FTgpi mice. *Absence (x Prnp$^{o/o}$) or presence (x Prnp$^{+/+}$) of full-length PrP. The number of mice is indicated in the legend. Higher expressor FTgpi155 Prnp$^{+/+}$ and FTgpi155 Prnp$^{o/o}$ mice died significantly earlier than FTgpi177 Prnp$^{+/+}$ ($p<0.0001$) and FTgpi177 Prnp$^{o/o}$ ($p<0.0001$) mice respectively, suggesting that toxicity is dose-dependent. FTgpi177 Prnp$^{+/+}$ mice died significantly earlier than FTgpi177 Prnp$^{o/o}$ mice ($p<0.001$), indicating that PrP^{C} may exacerbate the phenotype. Statistics: Log-Rank (Mantel-Cox) test.*

FTGPI INDUCES CEREBELLAR DEGENERATION

Histological examination of brain sections of clinically affected FTgpi mice revealed conspicuous pathological changes in the cerebellum. All FTgpi lines displayed a similar phenotype consisting of progressive loss of cerebellar granule neurons (CGNs) in both hemispheres (Figure 2.5, arrows), substantial reduction in the width of the granule cell layer, widespread atrophy (Figure 2.5, H&E), and intense astrocytosis (Figure 2.5, GFAP).

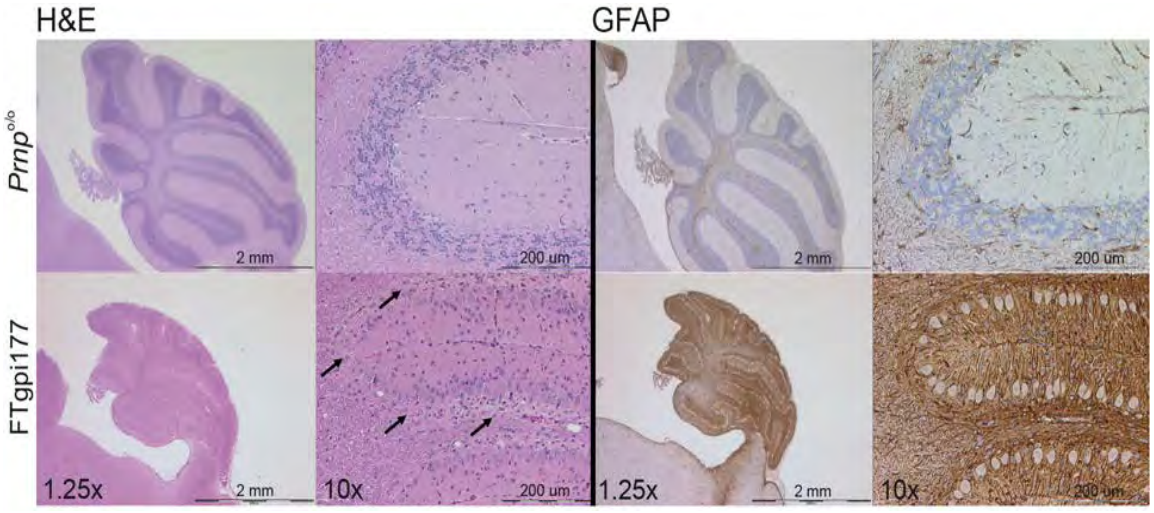

Figure 2.5.Brain histology of FTgpi mice. *(**H&E**) H&E staining showing severe atrophy of the cerebellum and conspicuous loss of CGNs in FTgpi177 mice compared to controls (left panels; arrows indicate loss of CGNs); (right panels) GFAP-stained cerebellum showing widespread astrogliosis in FTgpi177 mice.*

Interestingly, Purkinje cells were well-preserved. As the "half-genomic" pPrPHG vector is not expressed in Purkinje cells [110], this suggests that FTgpi toxicity is cell-autonomous and does not propagate to other cell types. No obvious pathology was present in other regions of the brain, likely due to the lower expression level of FTgpi (Figure 2.6).

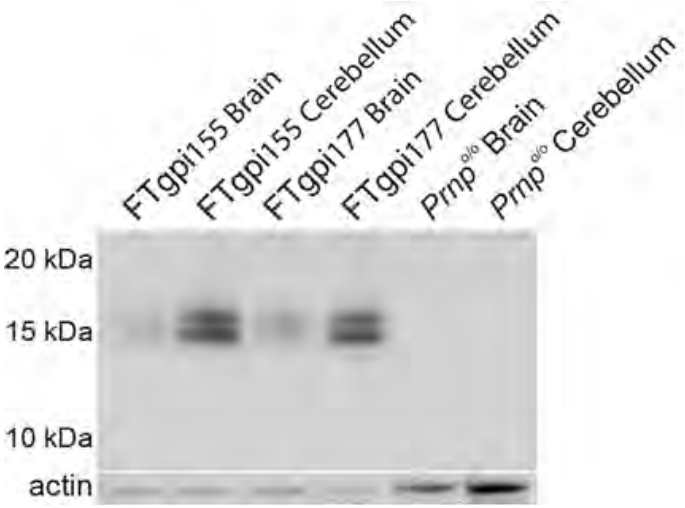

Figure 2.6. FTgpi expression level in brain and cerebellum. *Both FTgpi155 and FTgpi177lines showed increased FTgpi expression in the cerebellum. Western blot was probed with POM2 antibody.*

No other organs of the body had detectable levels of FTgpi (Figure 7A) and immunohistochenical analyses revealed that all were found to be pathologically unaffected by the FTgpi transgene (Figure 7B).

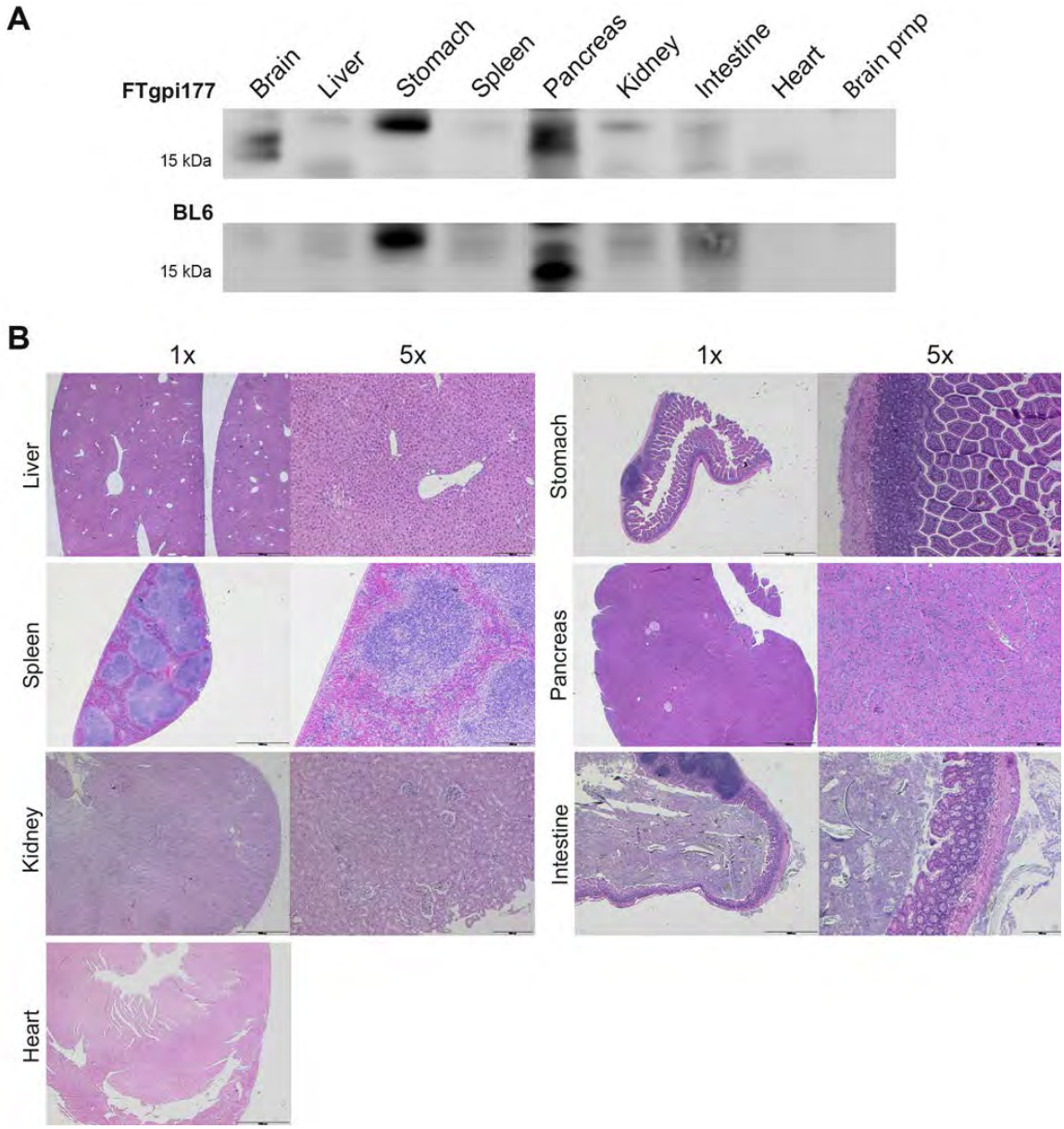

Figure 2.7. H&E staining of FTgpi177 organs *(**A**) Western blotting using POM11 show FTgpi expression exclusively in the brain. Unspecific bands are present in both FTgpi and BL6 blots. (**B**) No abnormalities were reported in liver, spleen, kidney, heart, stomach, pancreas and intestine.*

Terminal deoxynucleotidyl transferase dUTP nick end labeling (TUNEL) detects DNA fragmentation resulting from apoptosis or other forms of cell death. CGNs of FTgpi177 mice already showed nuclear TUNEL signals at 5 weeks of age, which became widespread by 10 weeks (Figure 2.8A). Strikingly, mice did not show any symptoms at this stage. At 28 weeks, the signal was reduced, probably due to the removal of dead neurons by microglia.

4',6-diamidino-2-phenylindole (DAPI) staining confirmed the progressive loss of CGNs in the cerebellum (Figure 2.8A), which was further reflected in progressive decrease of FTgpi expression over time (Figure 2.8B).

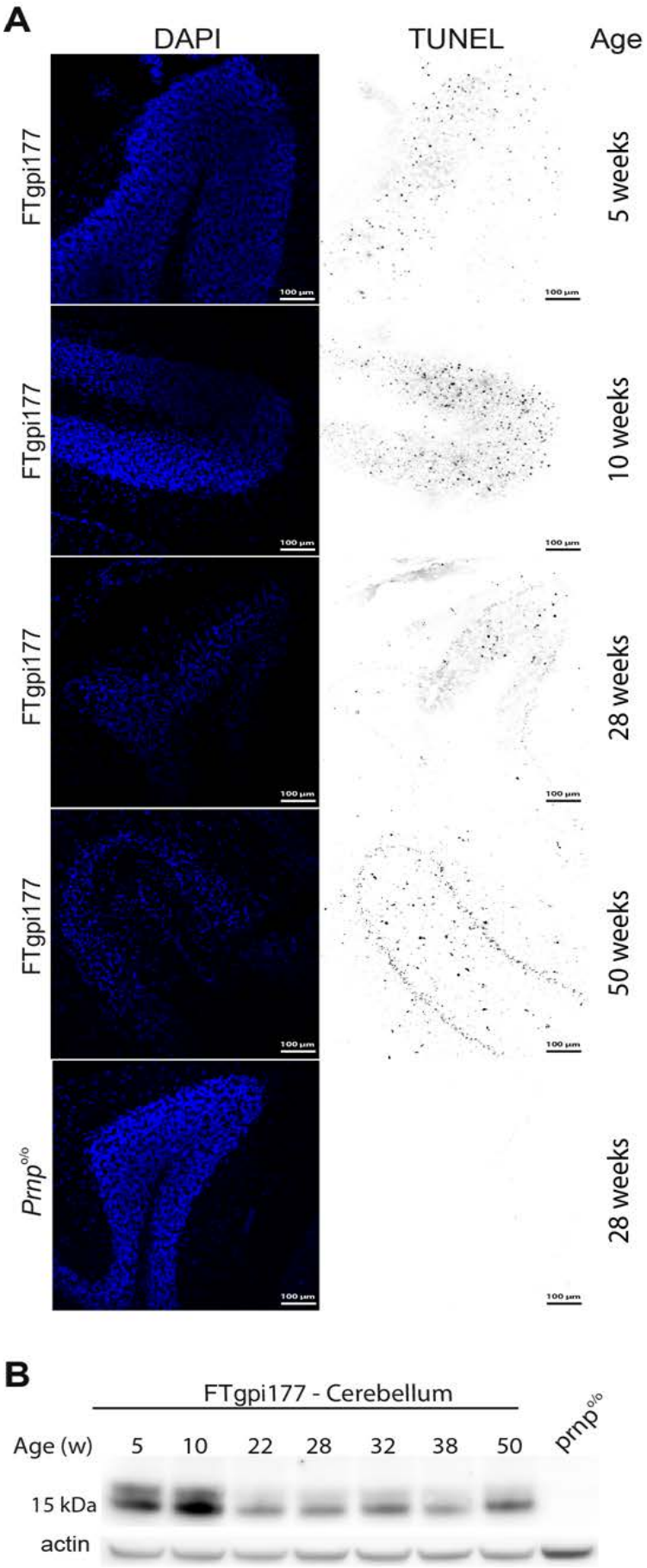

Figure 2.8. Cerebellar pathology in FTgpi mice. *(**A**) Cerebellar frozen sections were stained with DAPI (blue) and TUNEL (red) to reveal nuclei and fragmented DNA, respectively. A gradual loss of CGNs is evident in the granular layer. Numerous TUNEL^{+} cells were detected at 10 weeks in FTgpi mice. Frozen sections of age-matched Prnp$^{o/o}$ controls were stained at all respective time points (shown at 28 weeks) and did not reveal any TUNEL^{+} cells. (**B**) Western blot using POM11 showed FTgpi protein expression decreasing over time in the cerebellum, possibly as a consequence of the progressively reduced number of neurons.*

At 50 weeks, TUNEL^{+} cells shifted from the granular layer to the molecular layer and white matter (Figure 2.8A), and the TUNEL signal became localized to the cytoplasm of microglia (Iba1^{+} cells) (Figure 2.9A), suggesting neuronophagia by the latter. Accordingly, microglia showed a strong cytoplasmic FTgpi signal (Figure 2.9B).

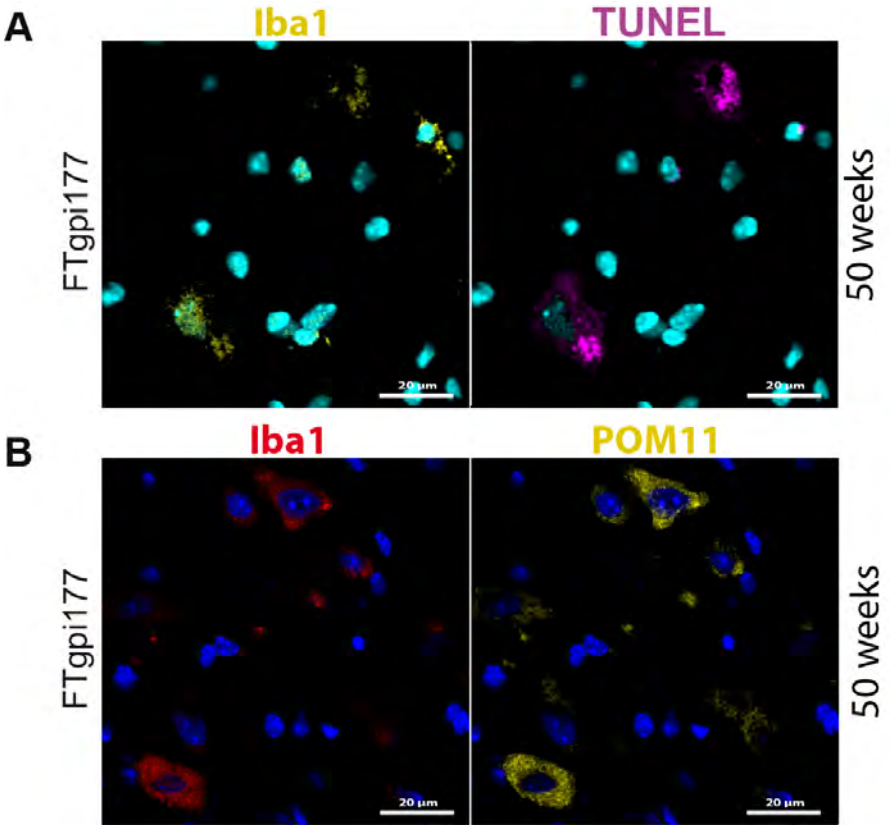

Figure 2.9.Microglia engulfing dead CGNs. *(**A**) Cerebellar frozen sections were stained with DAPI (blue), Iba1 (yellow) and TUNEL (purple) to reveal nuclei, fragmented DNA, and microglia respectively. TUNEL signal localized to the cytoplasm of microglia. (**B**) Cerebellar frozen sections were stained with DAPI (blue), Iba1 (red) and POM11 (yellow) to reveal nuclei, microglia, and FTgpi. A strong FTgpi signal was detected in the cytoplasm of microglia.*

FTGPI IS RETAINED IN THE ER

In order to study the biogenesis of FTgpi, the wild-type PrP^{C} and FTgpi reading frames were cloned into the expression plasmid pBMN, which was used to generate retroviral particles using the Phoenix Retrovirus Expression System (Orbigen). These particles were employed to infect HPL cells, a hippocampal cell line which lacks PrP^{C} expression [111], in order to create stably-transfected cell lines expressing either FTgpi or PrP^{C}. FTgpi lacks the two N-

glycosylation sites that are located in the GD, and was expressed as an unglycosylated 15 kDa protein in HPL cells (Figure 2.10).

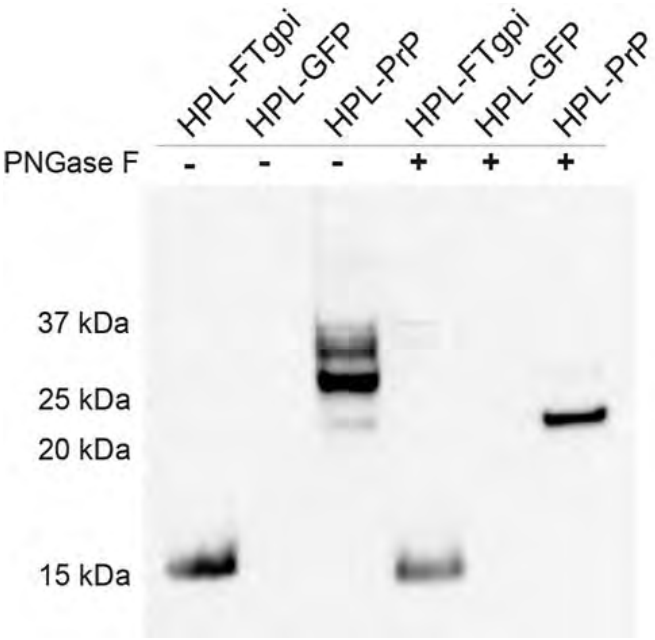

Figure 2.10. FTgpi expression in HPL cells. *Stably transfected HPL cell lysates were subjected to PNGase F treatment as indicated and analyzed by Western blotting using POM11. FTgpi does not have glycosylation sites and appears as a single band at 15 kDa.*

In order to obtain insight into the mechanism of FTgpi toxicity, I compared the subcellular localization of FTgpi and PrP. The surface of live HPL cells stably transfected with either full-length PrP^C or FTgpi was co-stained with the plasmalemmal marker CmDil and POM11, an antibody against the FT of PrP^C which recognizes both PrP^C and FTgpi [1]. As expected, PrP^C was highly expressed and colocalized with CmDil, whereas no immunofluorescent signal was detected for FTgpi (Figure 2.11A), although the total FTgpi expression level was similar to that of PrP^C (Figure 2.10).

FACS analysis on live cells confirmed that much less FTgpi was present on the plasma membrane than PrP^C, as the FTgpi signal (Figure 2.11B, red line) was slightly stronger than the background (grey line, HPL-GFP) but much weaker than PrP^C (blue line). This suggests that FTgpi undergoes abnormal processing, and that its transport to the plasma membrane may be impaired.

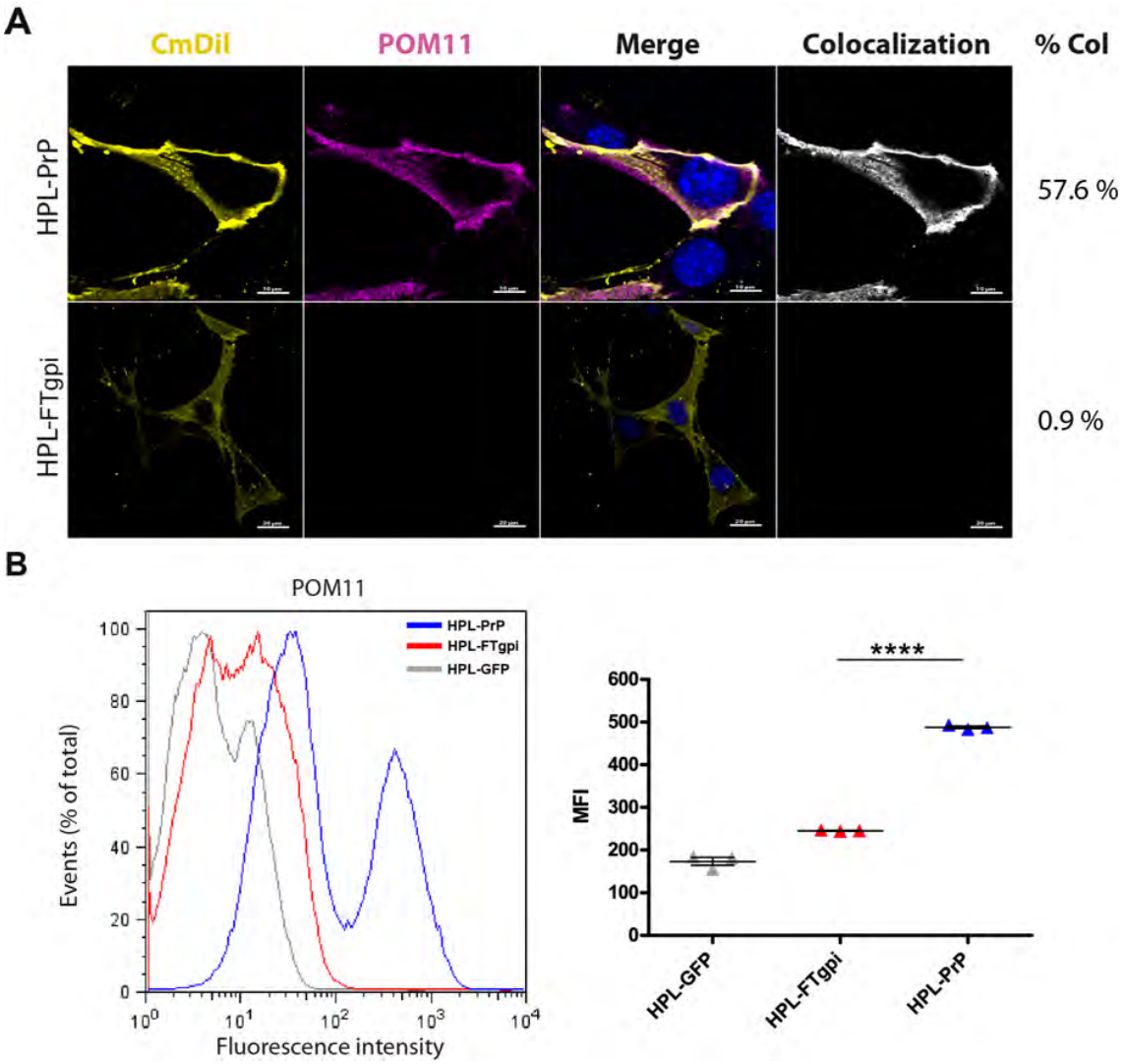

Figure 2.11. Immunofluorescence on stably transfected HPL-PrP and HPL-FTgpi cells. FTgpi does not reach the plasma membrane. *POM11 stains both PrP and FTgpi. (**A**) Cells were stained with the surface marker CmDil (yellow), fixed, and stained with POM11 followed by Alexa 647 anti-mouse IgG secondary antibody (purple), and counter-stained with DAPI (blue) to visualize the nuclei. As expected, PrP showed colocalization with the surface marker CmDil (yellow), whereas FTgpi failed to be expressed on the plasma membrane. Confocal images were processed with Imaris;* Colocalization was calculated using the function ImarisColoc. *(**B**) FACS analysis: cells were stained with POM11, followed by Alexa 647 anti-mouse IgG secondary antibody. Each plot is representative of three biological replicates (left panel; HPL-GFP [grey line, background fluorescence], HPL-FTgpi [red line] and HPL-PrP [blue line, positive control]). Median fluorescence intensity (MFI) was dramatically lower for HPL-FTgpi compared with HPL-PrP (right panel), indicating its scarce expression on the plasma membrane. ****P<0.0001 by unpaired two tails t-test.*

Next, fixed and permeabilized cells were co-stained with calnexin, an ER marker, and POM11. Both PrP^C and FTgpi were found to colocalize with calnexin, confirming their presence in the ER (Figure 2.12).

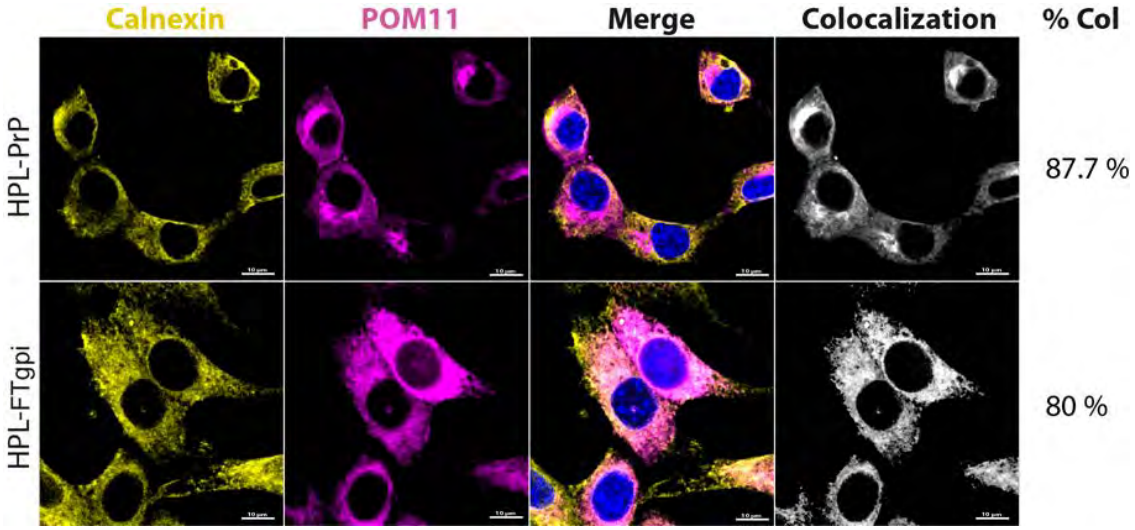

Figure 2.12. Immunofluorescence on stably transfected HPL-PrP and HPL-FTgpi cells. FTgpi localizes in the ER lumen. Cells were fixed, permeabilized and stained with calnexin antibody, to label the ER, and with POM11, followed by Alexa 555 anti-rabbit (yellow) and Alexa 647 anti-mouse (purple) IgG secondary antibodies, respectively. Blue: DAPI nuclear stain. Both PrP and FTgpi showed colocalization within the ER. *Confocal imagines were processed with Imaris;* Colocalization was calculated using the function ImarisColoc.

Conversely, PrP^C was found to co-localize within the Golgi, as expected, but FTgpi was not (Figure 2.13A). In addition, cells were stained solely with POM11 to compare the intracellular distribution of PrP versus FTgpi (Figure 2.13B). The vast majority of HPL-PrP showed a characteristic Golgi-like staining (Figure 2.13B, white arrows), which was absent within HPL-FTgpi cells. This suggests that FTgpi was unable to leave the ER.

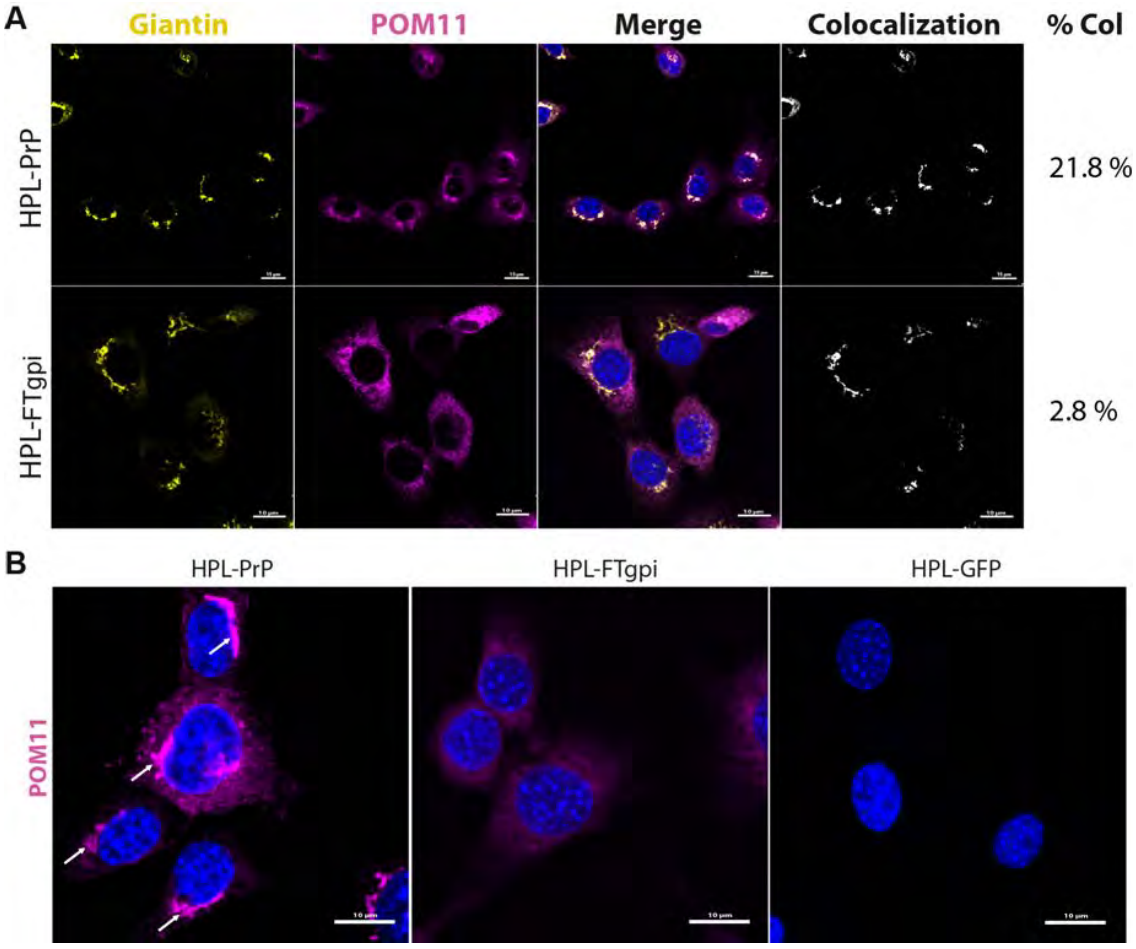

Figure 2.13. Immunofluorescence on stably transfected HPL-PrP and HPL-FTgpi cells. FTgpi does not reach the Golgi apparatus. *(**A**) Cells were fixed, permeabilized, and stained with giantin antibody labeling the Golgi apparatus (yellow), as well as POM11 (purple), followed by Alexa 647 anti-mouse and Alexa 555 anti-rabbit IgG secondary antibodies., Blue: DAPI. PrP partially but specifically colocalized with giantin, indicating that most PrP was in the ER. However, only a faint colocalization signal was detected in HPL-FTgpi. (**B**) Cells were fixed and stained with POM11 (purple), followed by Alexa 647 anti-mouse IgG secondary antibody, and reacted with DAPI (blue) to stain the nuclei. White arrows point at the characteristic Golgi-staining, which is widely present in HPL-PrP cells, whereas HPL-FTgpi cell do not show such signal. HPL-GFP were transfected with the pBMN empty-vector and used as control for unspecific signals. Confocal imagines were processed with Imaris; colocalization was calculated using the function ImarisColoc.*

Co-staining with LAMP2, a lysosome marker, did not show colocalization with either PrP^C or FTgpi (Figure 2.14).

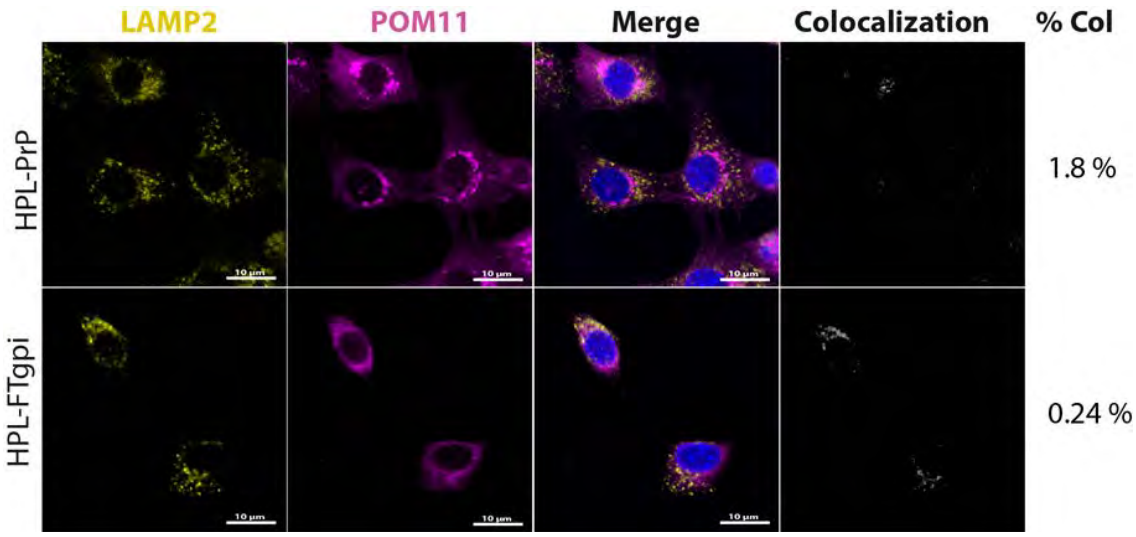

Figure 2.14. Immunofluorescence on stably transfected HPL-PrP and HPL-FTgpi cells. FTgpi does not localize in lysosomes. Cells were fixed and stained with LAMP2 antibody to mark the lysosomes (yellow) and POM11 (purple), followed by Alexa 647 anti-mouse and Alexa 555 anti-rabbit IgG secondary antibodies, and reacted with DAPI (blue) to stain the nuclei. Neither PrP nor FTgpi showed colocalization with LAMP2. Confocal imagines were processed with Imaris; colocalization was calculated using the function ImarisColoc.

FTGPI IS DEGRADED BY PROTEASOMES

The expression level of FTgpi protein in mouse brains was only ~15% of that of PrP^C in wild-type mice, despite much higher mRNA levels, suggesting that FTgpi may be actively degraded *in vivo*. Using HPL cells expressing either PrP or FTgpi, we quantified the expression level of these proteins by Western blot upon treatment with a battery of compounds that selectively inhibited either lysosomes (NH_4Cl, Bafilomycin, Leupeptin) or proteasomes (MG132, Lactacystin) after 4 and 8 h. PrP^C resides physiologically on the plasma membrane, where it is endocytosed and recycled to the membrane [112] or alternatively degraded through lysosomes [113]. As anticipated, PrP^C level increased upon lysosomal inhibition (Figure 2.15A), for which NH_4Cl, which inhibits lysosome acidification, was particularly effective. Bafilomycin and Leupeptin, which specifically inhibit the vacuolar-type H+-ATPase and the cysteine, serine and threonine peptidases, respectively, also increased PrP^C expression levels in cells, albeit not as dramatically as NH_4Cl.

In contrast, FTgpi expression was not altered with lysosomal inhibition; however, it was significantly increased upon proteasome inhibition (Figure 2.15B). This suggests that FTgpi

could be retro-translocated from the ER into the cytosol to be degraded by the proteasome machinery.

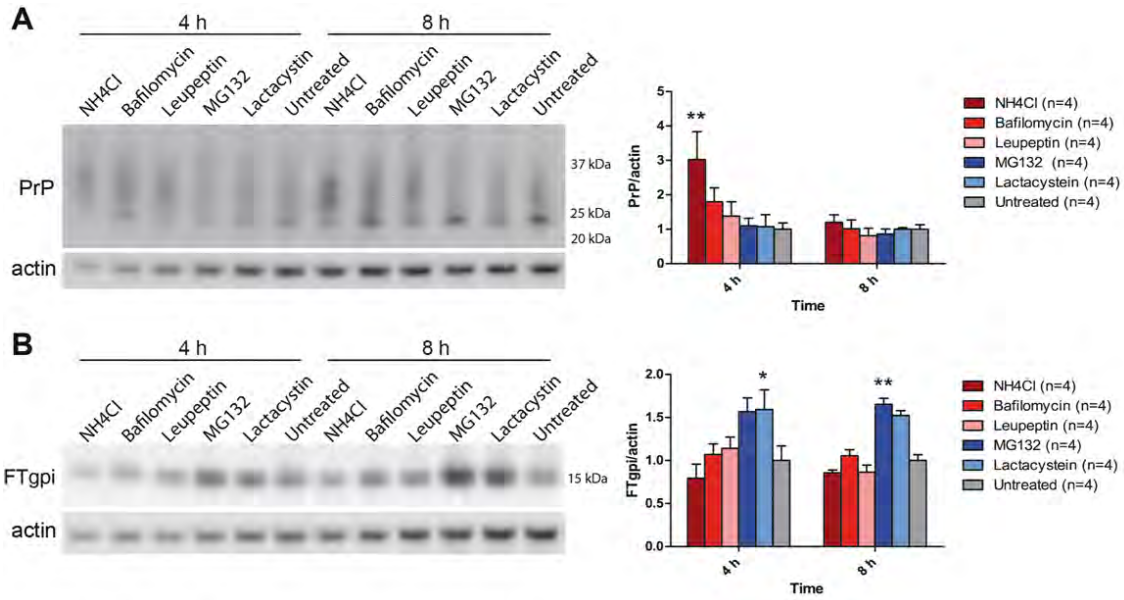

Figure 2.15. NGPI is degraded through proteasomes. *HPL-PrP and HPL-NGPI cells were treated for 4 and 8 h with either lysosomes inhibitors (NH_4Cl, Bafilomycin, Leupeptin) or proteasomes inhibitors (MG132, Lactacystin). (**A**) Lysates of HPL-PrP cells were analyzed by Western blotting using POM11. The level of PrP increased significantly upon treatment with lysosomes inhibitors. Graph: quantification of the respective Western blots. (**B**) Lysates of HPL-FTgpi cells were analyzed by Western blotting using POM11. The level of FTgpi specifically increased upon treatment with proteasome inhibitors. Each bar indicates the mean ±SEM of 4 biological replicates. **P<0.01 and *P<0.05 by two-way ANOVA with Bonferroni multiple comparisons post-test (each bar is compared to the Untreated).*

Some of these drugs may have pleiotropic effects. For instance, proteasome inhibitors (e.g. MG132) could induce transcriptional up-regulation of the cytomegalovirus promoter, which in turn could substantially enhance synthesis of ectopic proteins [114]. We therefore investigated the mechanism of FTgpi clearance using an alternative method in order to confirm the data. We used pulse-chase experiments in combination with Bafilomycin and MG132. We transiently transfected HPL cells with either FTgpi or PrP^C, then I metabolically labeled the cells with [^{35}S]methionine/cysteine for 1 h and either harvested directly or chased for different intervals of time in ^{35}S-free culture medium before lysis. FTgpi and PrP were immunopurified with POM2, and analyzed by SDS-PAGE. As anticipated, PrP^C turnover was significantly reduced upon lysosomal inhibition and its half-life ($T_{1/2}$) could not be measured, whereas a $T_{1/2}$ of approximately 4 h was obtained with proteasome inhibition, which was comparable to unhibited cells (Figure 2.16A). In contrast, FTgpi degradation was drastically impaired upon proteasome inhibition, yet it was unaffected by lysosomal inhibition ($T_{1/2}$ ~ 2.2

h) compared to the untreated condition ($T_{1/2}$ ~ 2.6 h) (Figure 2.16B). This confirmed that cells degrade FTgpi through the proteasome machinery.

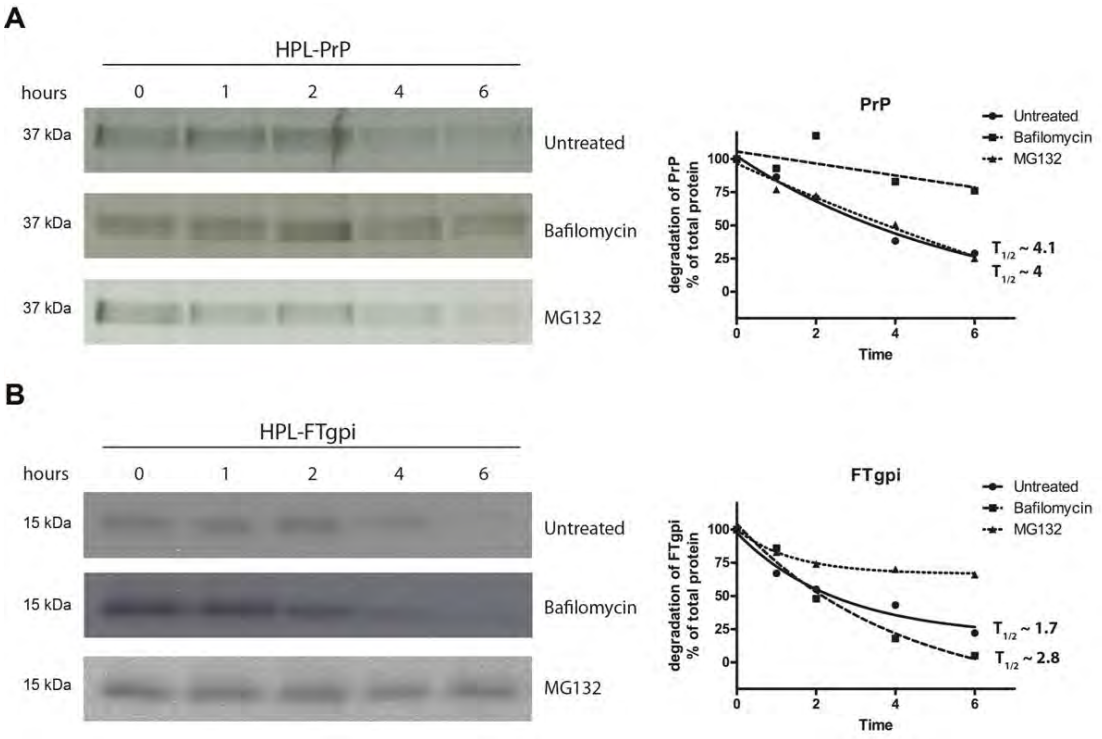

Figure 2.16. FTgpi is degraded through proteasomes. *HPL cells were transiently transfected with PrP or FTgpi, and metabolically labeled with [^{35}S]Met/Cys for 20 min at 37 °C. Then, cells were either lysed after the pulse or incubated in culture medium without ^{35}S at 37 °C for 1, 2, 4, 6, and 8 h, respectively, in presence of either DMSO (untreated), Bafilomycin (a lysosomes inhibitor) or MG132 (a proteasomes inhibitor). Proteins were immunoprecipitated with POM2 and subjected to SDS-PAGE and autoradiography. (**A**) Left panel: PrP turnover was impaired upon treatment with Bafilomycin but not MG132. Right panel: evaluation of autoradiograms: the amounts of protein are expressed as percentage of total protein rescued directly after the labeling period and plotted as a function of the chase time points. (**B**) Left panel: FTgpi turnover was impaired upon treatment with MG132 but not Bafilomycin. The data points were fitted to an exponential curve using nonlinear regression analysis.*

FTGPI INDUCES CHRONIC ER STRESS *IN VITRO*

Our observations on the cellular turnover of FTgpi, together with the fact that FTgpi contains an exposed core of 20 hydrophobic amino acids that is likely to be targeted by the ER quality control system, raised the possibility that FTgpi may elicit ER stress and the unfolded protein response (UPR). The UPR is mediated by three families of signal transducers: Activating Transcription Factor 6 (ATF6), Protein kinase-like Endoplasmic Reticulum Kinase (PERK) and

Serine/threonine-protein-kinase/endoribonuclease (IRE1), which sense the conditions of protein folding in the ER lumen and relay the information to the cell through many different mechanisms, including regulated proteolysis (ATF6), translational control (PERK) and nonconventional mRNA splicing (IRE1) [115].

I used stably transfected HPL cells to measure ER stress markers by immunoblot. HPL-FTgpi cells exhibited significantly increased phosphorylation levels of both PERK (Figure 17A) and eIF2α (Figure 17B) when compared with HPL-GFP. Hence, FTgpi robustly activates the PERK pathway. Moreover, C/EBP-homologous protein (CHOP) expression was also found to be slightly increased (Figure 17C), and its mRNA was significantly augmented (Figure 17D).

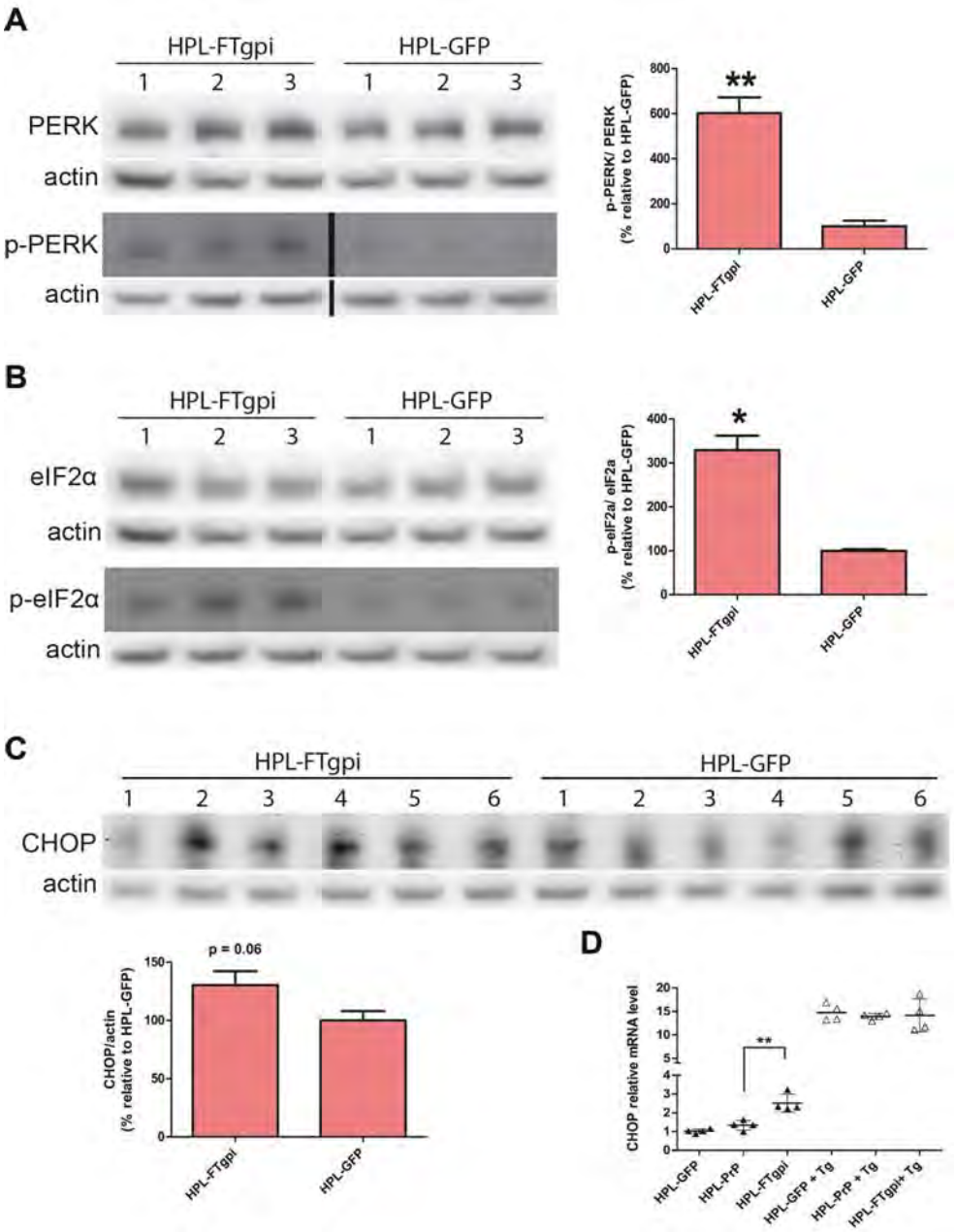

Figure 2.17. FTgpi induces ER stress in vitro. *Cell lysates were analyzed by Western blot. Numbers denote independent experiments. p-PERK (**A**) and p-eIF2α (**B**) were significantly higher in HPL-FTgpi than in HPL-GFP cells. p-PERK blot: non-consecutive lanes of the same blot. p-PERK/PERK and p-eIF2α/eIF2α ratios were calculated after values were normalized with actin. (**C**) CHOP was also found to be increased in HPL-FTgpi cells. (**D**) CHOP mRNA was quantified by RT-PCR. Thapsigargin (Tg)-treated cells were used as positive control. CHOP was significantly upregulated in HPL cells expressing FTgpi. (**A-B-C**) Each bar indicates the average ± SEM of 3 or 6 biological replicates. ** P<0.01 and *P<0.05 by unpaired two-tails t-test (each bar is compared to HPL-GFP). (**D**) Each sample is representative of 4 biological replicates. Error bars indicate averages ± SEM. **P<0.01 by one-way ANOVA with Bonferroni multiple comparisons post-test (each sample is compared to HPL-GFP).*

Similar results were obtained when HPL-FTgpi were compared to HPL-PrP cells (Figure 2.18).

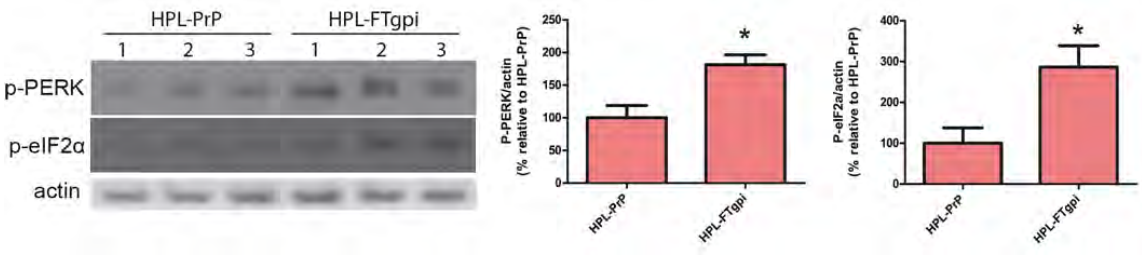

Figure 2.18. FTgpi, but not PrP, triggers ER stress in HPL cells*. Cell lysates were analyzed by Western blot using the indicated antibodies. Numbers: biological replicates. (**A**) p-PERK and p-eIF2α were significantly increased in HPL-FTgpi cells. Values were normalized with actin. Each bar indicates the mean ±SEM of 3 biological replicates. *P<0.05 by unpaired two-tails t-test (each bar is compared to HPL-PrP).*

Next, I investigated the status of the IRE1 pathway by examining specifically the spliced version of XBP1. Thapsigargin (Tg)-treated cells were used as positive controls, as Tg robustly induces ER stress. Surprisingly, the level of spliced XBP1 in HPL-FTgpi cells was not altered compared to HPL-PrP (Figure 2.19). Secondly, I assessed the mRNA expression level of the most common markers of ER stress, whose expression is increased by the activation of ATF6 (GRP78, HERP1, EDEM1, ERP72, HSP40) [116,117]. Only HERP1 was found to be slightly upregulated (Figure 2.19). Together these data suggest that IRE1and ATF6 may not be key players in the process leading to toxicity *in vitro*.

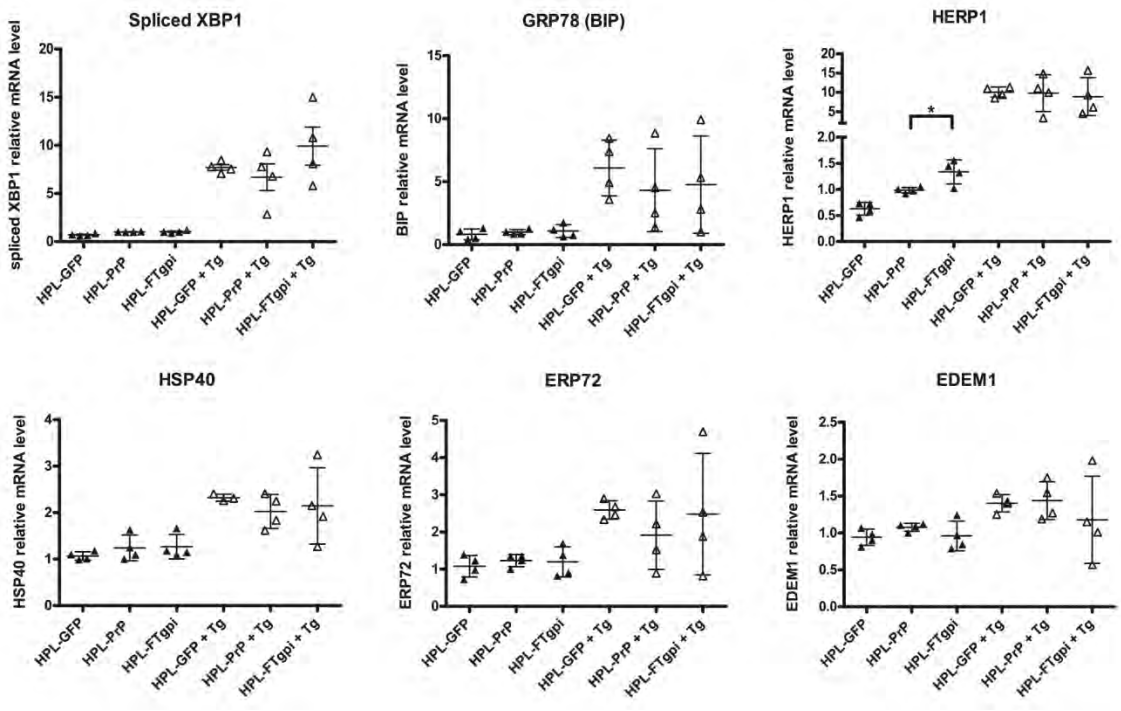

Figure 2.19. Transcriptional analysis of additional ER stress markers. *Tg: Thapsigargin. Cells were treated with 0.5 µM Tg for 3 h at 37°C in order to induce ER stress as positive controls for our primers. mRNA levels were quantified by RT-PCR. Major players involved in the IRE1 and ATF6 pathways, such as spliced XBP1 and BIP respectively, were unaltered in vitro. Black triangles: non-treated cells; white triangles: Tg-treated cells. *P<0.05 by one-way ANOVA with Bonferroni multiple comparisons post-test.*

FTGPI INDUCES CHRONIC ER STRESS *IN VIVO*

In order to verify the involvement of ER stress *in vivo*, I performed the same analysis using mRNA derived from cerebellum of asymptomatic FTgpi155 *Prnp*$^{o/o}$ mice. mRNA levels of spliced XBP1, BIP, CHOP, and HSP40 were all significantly upregulated compared to age-matched *Prnp*$^{o/o}$ control mice (Figure 2.20A), indicating that FTgpi causes a comprehensive ER stress response *in vivo*, where IRE1, PERK and ATF6 seem to be all involved. Importantly, ER stress was detected in FTgpi mice at a stage where no cerebellar degeneration was yet to be observed, suggesting that ER stress is an upstream event that may lead to the subsequent neurodegenerative process.

Increased phosphorylation levels of PERK were also observed in cerebellar homogenates of FTgpi mice (Figure 2.20B), supporting the evidence of ongoing ER stress *in vivo*.

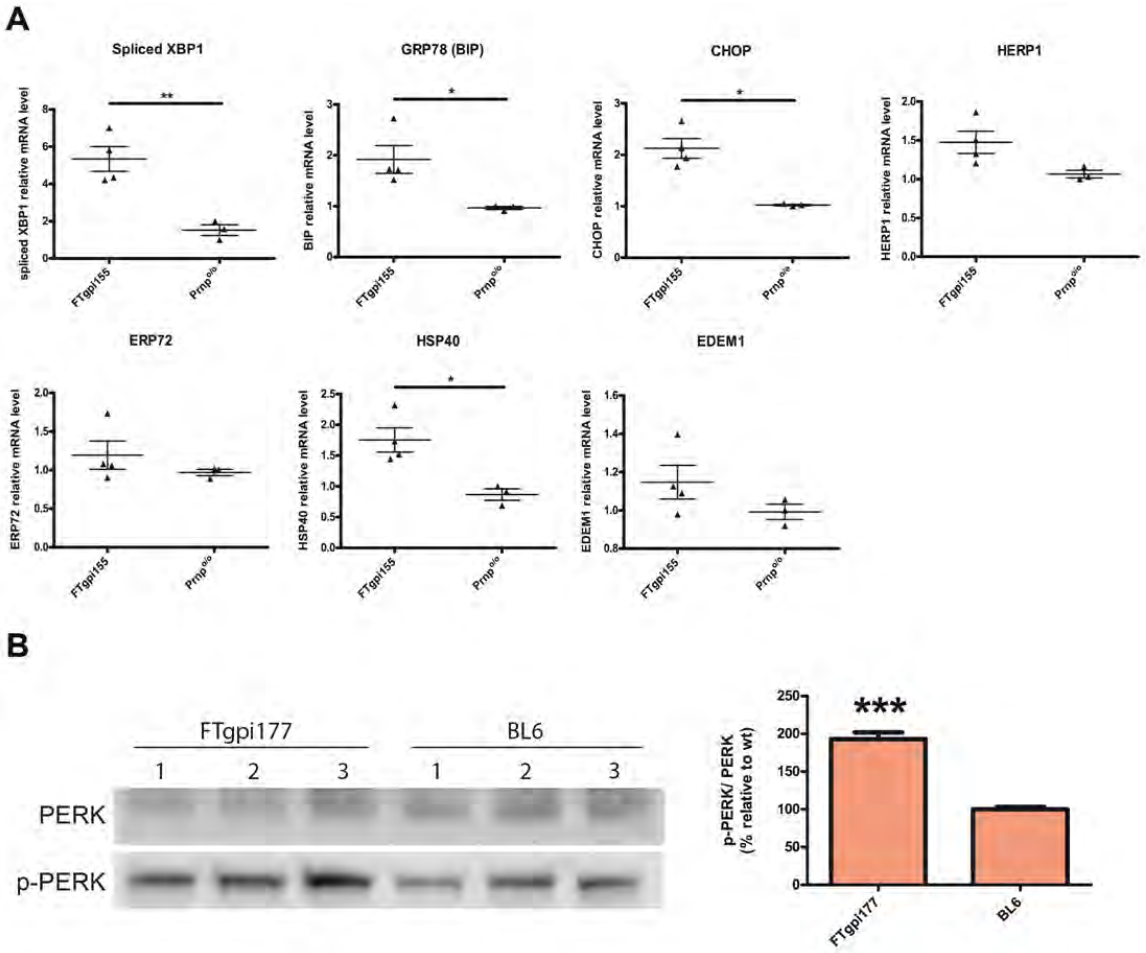

Figure 2.19. Figure 2.20. FTgpi induces ER stress in vivo *(**A**) mRNA was extracted from cerebellum of FTgpi155 and Prnp$^{o/o}$ mice. mRNA levels of ER stress markers were quantified by RT-PCR. XBP1, BIP and CHOP were found to be significantly upregulated. *P<0.05 and **P<0.01 by unpaired two-tails t-test. (**B**) Cerebellum homogenates of FTgpi177 and Prnp$^{o/o}$ mice were analyzed by Western blot. p-PERK was increased in cerebellum of FTgpi177 mice. The blot was first probed with a p-PERK antibody, stripped for 20 min, and then re-probed with PERK antibody. Each bar indicates the mean ±SEM of 3 biological replicates. *** P<0.001 by unpaired two-tails t-test (each bar is compared to BL6).*

FTGPI BINDS 'BINDING IMMUNOGLOBULIN PROTEIN' (BIP) *IN VIVO*

BIP binds to IRE1, PERK and ATF6 in unstressed cells and dissociates from these UPR sensors during acute ER stress. In ER stress conditions, a chronic presence of unfolded proteins would saturate the free pool of chaperones, titrating BIP away from IRE1, hence activating the UPR signaling [118,119]. Further, it has been shown that misfolded proteins in the ER that do not interact with BIP failed to induce the UPR [119]. I examined whether FTgpi interacts with BIP by immunoprecipitation experiments. I pulled down FTgpi on brain homogenates of FTgpi155 mice using POM2. I found that POM2 specifically co-precipitated BIP in samples where FTgpi

was expressed, whereas no band was detected in *Prnp*$^{o/o}$ control mice (Figure 2.21). I concluded that FTgpi binds BIP *in vivo.*

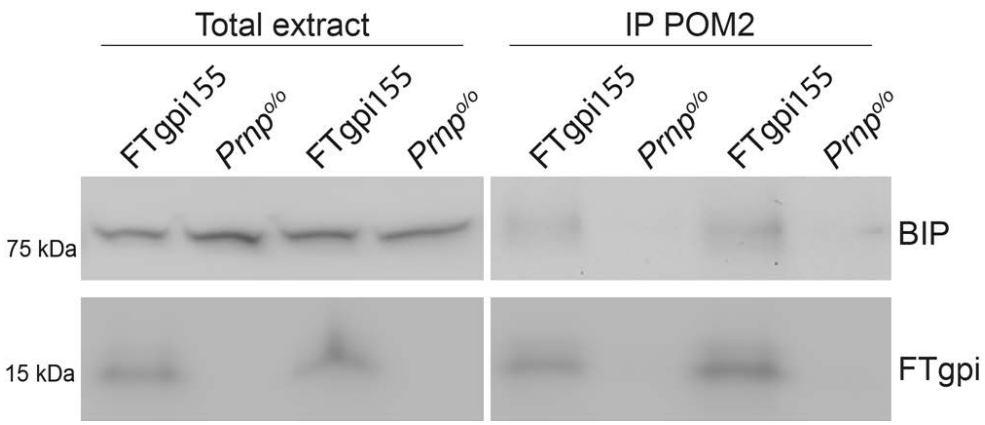

Figure 2.21. FTgpi binds BIP in vivo. *Brain homogenates of FTgpi155 and Prnp*$^{o/o}$ *mice were incubated overnight with POM2 to precipitate FTgpi. Precipitates were analyzed by Western blot. Left panel: total extract. Right panel: immunoprecipitates, showing that BIP specifically co-precipitated with FTgpi, as no signal was detected in Prnp*$^{o/o}$ *mice.*

THE HC DOMAIN IS REQUIRED FOR FTGPI CYTOTOXICITY

Our previous investigations indicated that FTgpi elicits ER stress by triggering the UPR, primarily through the activation of PERK *in vitro*. I then sought to define the domains of FTgpi required for activating this pathway. I employed the Flp-In™ 293 T-Rex cell line (Invitrogen) to generate stably transfected cell lines ensuring a homogenous expression of our proteins of interest. The following constructs were cloned into the pcDNA5/FRT vector: PrP, FTgpi, an anchorless version of FTgpi (sFT or $PrP_{\Delta 141-254}$), and an anchorless version of FTgpi devoid of the HC domain ($sFT_{\Delta HC}$ or $PrP_{\Delta 112-254}$). Cells transfected with the empty vector were defined as HEK-pcDNA5. Upon co-transfection with our vectors and pOG44, which encodes the Flp recombinase, hygromycin-resistant clones were pooled together. HEK-PrP expressed sizeable levels of PrP^{C} protein, whereas all other mutants failed to express high levels (Figure 2.22A). All mutants with low protein expression also displayed low mRNA level (Figure 2.22B), suggesting that negative selection occurred against those mutants, possibly because of their toxicity.

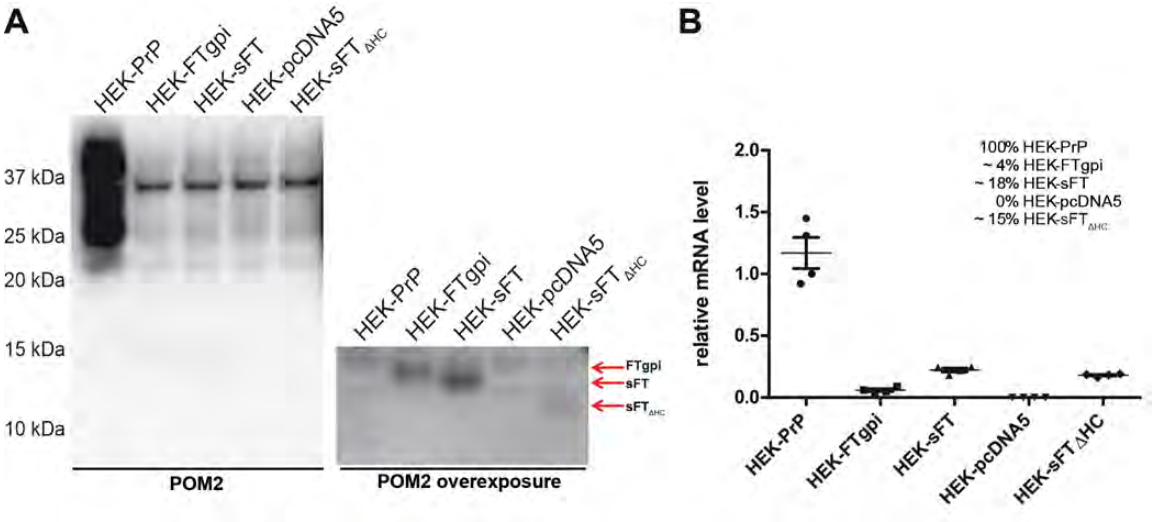

Figure 2.22. Poor expression level of FTgpi, sFT and $sFT_{\Delta HC}$ in stably transfected Flp-In™ 293 T-Rex cells. *Flp-In™ 293 T-Rex cells were stably transfected by using pcDNA5/FRT vector containing the coding sequence for PrP, FTgpi, sFT or $sFT_{\Delta HC}$, and the respective cell lines were generated. (**A**) Cell lysates were analyzed by Western blot using POM2. HEK-PrP cells show a strong signal, whereas the other lines failed in expressing comparable levels of protein. Overexposure of the blot allowed the detection of FTgpi, sFT and $sFT_{\Delta HC}$. (**B**) mRNA level was quantified by RT-PCR. mRNA of HEK-PrP was set as 100%.*

Notably, despite the low expression levels, HEK-FTgpi induced higher phosphorylation of eIF2α than HEK-pcDNA5 (Figure 2.23). HEK-PrP also displayed increased phosphorylation of eIF2α (Figure 2.23), albeit to a lesser degree than HEK-FTgpi, which was expected considering the exceptionally high expression of the protein. Interestingly, HEK-sFT cells showed a comparable level of p-eIF2α as seen with HEK-FTgpi (Figure 2.23), suggesting that anchoring to the membrane may not be crucial to trigger ER stress. Conversely, HEK-$sFT_{\Delta HC}$ cells do not show increased phosphorylation of eIF2α, indicating that deletion of the HC suffices to alleviate FTgpi-induced ER stress.

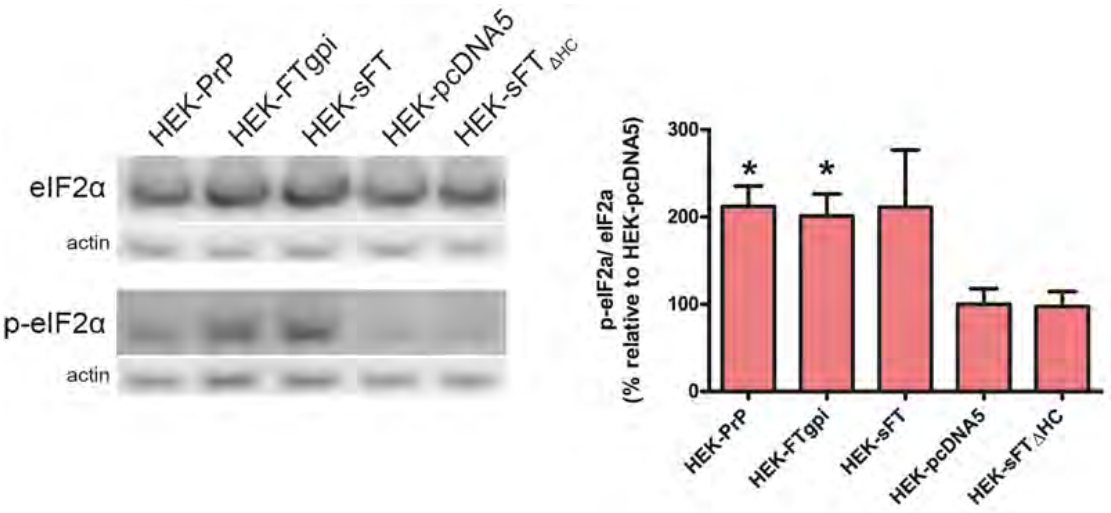

Figure 2.23. FTgpi induces phosphorylation of eIF2α in HEK cells. *Cell lysates were analyzed by Western blot using eIF2α and p-eIF2α antibodies. p-eIF2α/p-eIF2α ratio was calculated after values were normalized to actin. Each bar indicates the mean ±SEM of 3 biological replicates. *P<0.05 by unpaired two-tails t-test (each bar is compared to HEK-pcDNA5).*

FTGPI INFLUENCES PROTEIN KINASE B (AKT) PHOSPHORYLATION LEVEL

The AKT cascade is a critical pathway regulating cell survival, and its deactivation deprives cells of signals allowing them to withstand apoptotic stimuli [120]. Sustained phosphorylation of eIF2α inactivates AKT by moderating its phosphorylation state [121]. I found decreased phosphorylation of AKT in HEK-PrP, HEK-FTgpi, and HEK-sFT cells (Figure 2.24A). As for eIF2α, deletion of the HC abrogates the effect on AKT (Figure 2.24A). A similar signal was also detected in HPL cells (Figure 2.24B).

Hence, chronic deactivation of AKT may be involved in the loss of CGNs observed *in vivo*.

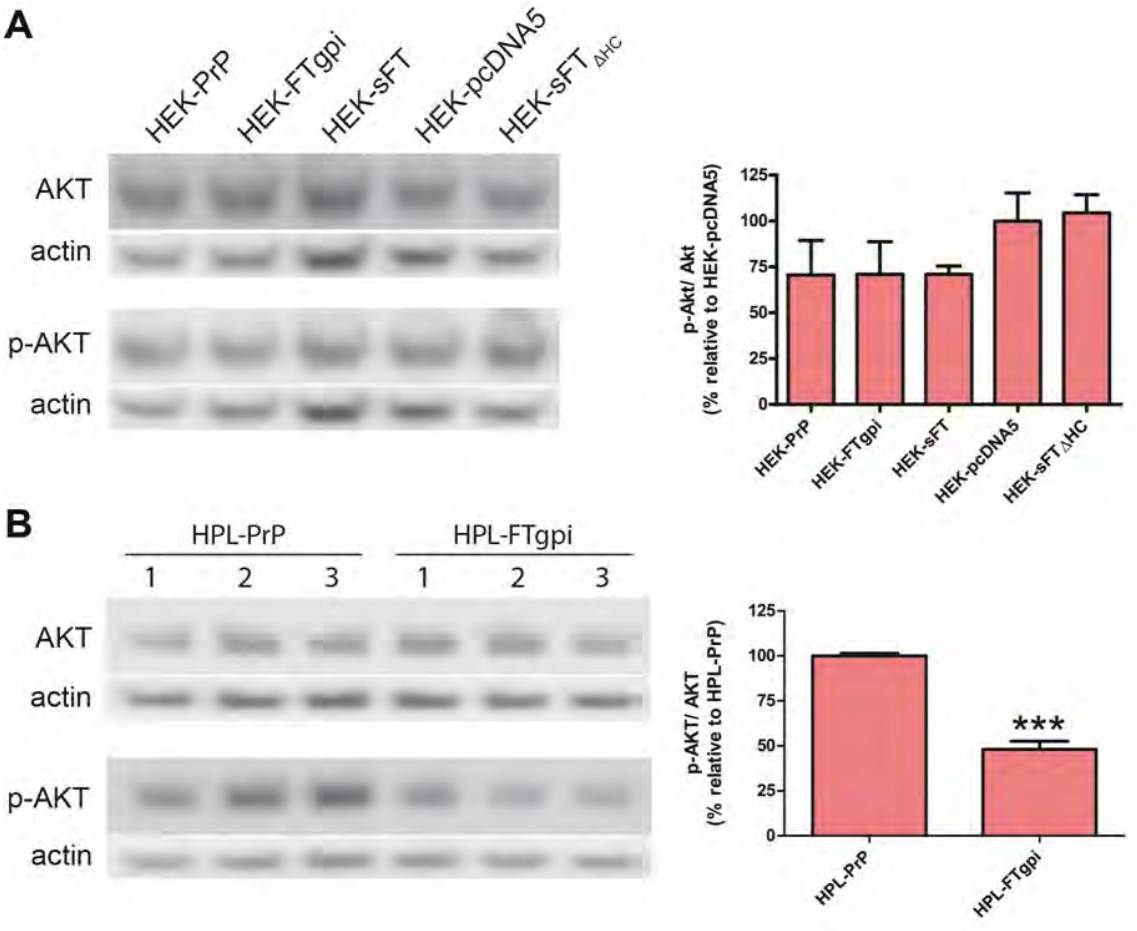

Figure 2.24. FTgpi reduces AKT phosphorylation in vitro. *Cell lysates were analyzed by Western blot using AKT and p-AKT antibodies. p-AKT/AKT ratio was calculated after values were normalized to actin. (**A**) HEK cells (**B**) HPL cells. Numbers: biological replicates. p-AKT was significantly decreased in both HEK- and HPL-FTgpi cells. Each bar indicates the mean ±SEM of 3 biological replicates. *** P<0.001 by unpaired two-tails t-test (each bar is compared to (**A**) HPL-pcDNA5 or (**B**) HPL-PrP).*

Therefore, I tested the level of phosphorylated AKT *in vivo*. Unlike *in vitro*, I found increased levels of phosphorylated AKT in cerebellar homogenates of FTgpi177 mice (Figure 2.25), suggesting that differences could be present between the *in vitro* and *in vivo* models. The discrepancy has been discussed in the Discussion session.

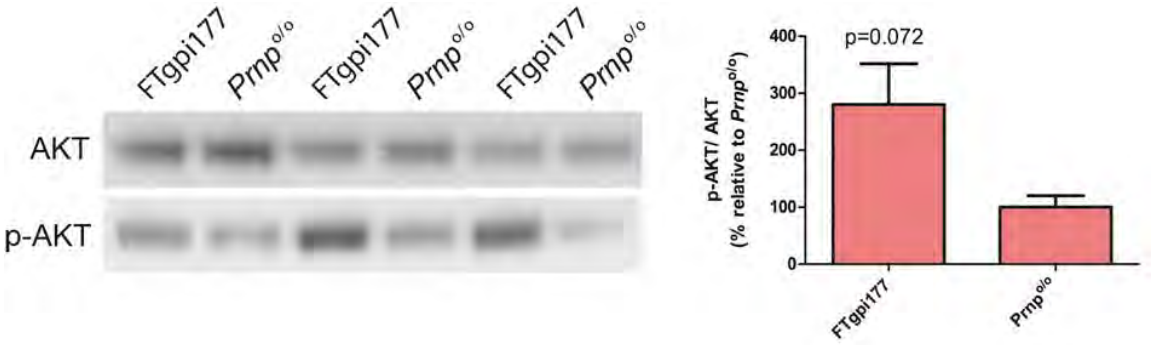

Figure 2.25. FTgpi increases AKT phosphorylation in vivo. *Cerebellum homogenates of FTgpi177 and Prnp$^{o/o}$ mice were analyzed by Western blot. p-AKT was increased in cerebellum of FTgpi177 mice. Blot was first decorated with p-AKT antibody, stripped for 20 min, and stained with AKT.*

FTGPI DECREASES ERK1/2 PHOSPHORYLATION *IN VITRO*

Since increased phosphorylated levels of the extracellular-signal-regulated kinases (ERK1/2) promotes cell survival in CGNs [122], I measured levels of phosphorylated ERK1/2 in our HEK cells. Decreased phosphorylation of ERK1/2 in HEK-FTgpi and HEK-sFT cells was detected (Figure 2.26), suggesting that activation of the ERK1/2 signaling pathway could be impaired. The reduced activation of this pathway may contribute to toxicity. Again, in HEK-sFT$_{\Delta HC}$ cells, where the FTgpi lacks the HC domain, ERK1/2 was not down-regulated (Figures 2.26). Taken together, these data suggest that HC is required for triggering the cascade of events leading to neurotoxicity.

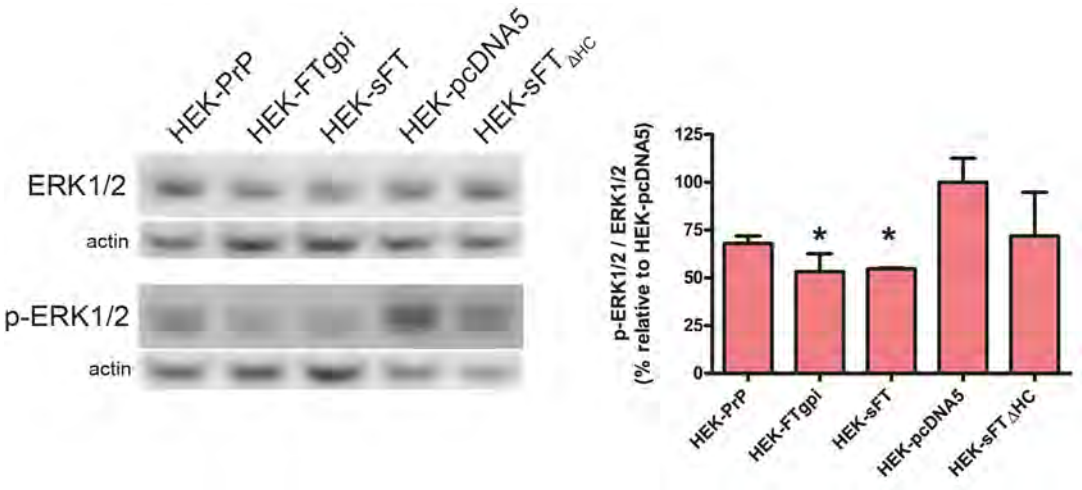

Figure 2.26. FTgpi decreases ERK1/2 phosphorylation in vitro. *Cell lysates were analyzed by Western blot using ERK1/2 and p-ERK1/2 antibodies. p-ERK1/2 /ERK1/2 ratio was calculated after values were normalized to actin. Each bar indicates the mean ±SEM of 3 biological replicates. *P<0.05 by unpaired two-tails t-test (each bar is compared to HEK-pcDNA5).*

MICE EXPRESSING $sFT_{\Delta HC}$ DO NOT DEVELOP NEURODEGENERATION

In order to confirm the previous results *in vivo*, I used the "half-genomic" pPrPHG vector to generate mice expressing the soluble secreted FT domain of PrP^C ($PrP_{\Delta 112-254}$ or $sFT_{\Delta HC}$). The transgenic line $sFT_{\Delta HC}138$ was selected and crossed with $Prnp^{o/o}$ mice to obtain offspring on a $Prnp^{o/o}$ background. $sFT_{\Delta HC}$ protein level was assessed by enzyme-linked immunosorbent assay ELISA to be 4.5% of total PrP^C in BL6 brains (Figure 2.27A). $sFT_{\Delta HC}$ was detected on Western blot upon immunoprecipitation with POM2 and it appeared as a band at 12 kDa (Figure 2.27B).

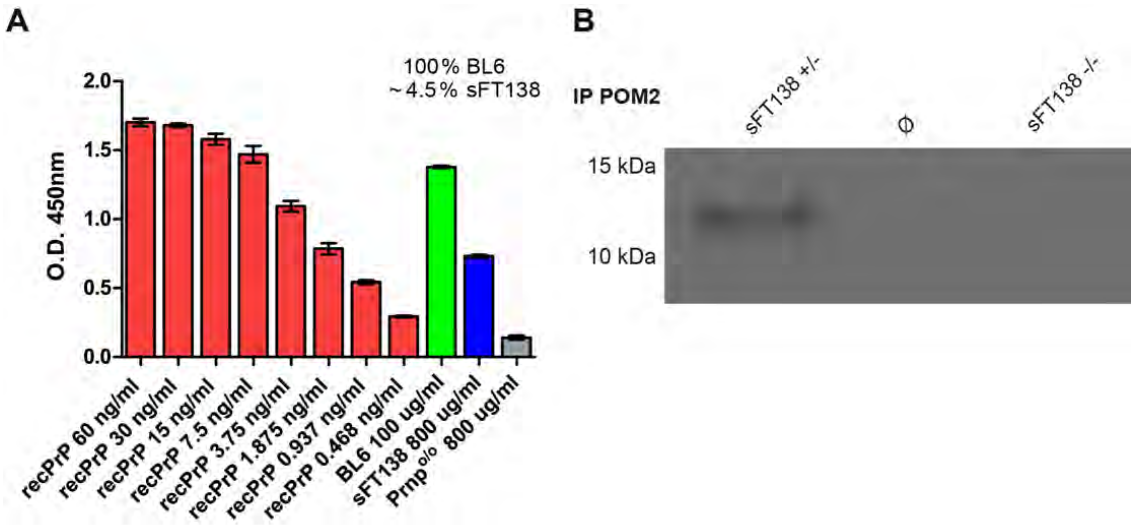

Figure 2.27. $sFT_{\Delta HC}138$ mice do not develop neurodegeneration. *(**A**) BL6, $sFT_{\Delta HC}138$ and $Prnp^{o/o}$ brain homogenates were analyzed by ELISA. Serially-diluted recombinant PrP23-231 (recPrP, red bars) was used to establish the standard curve. Upon data normalization, $sFT_{\Delta HC}138$ mice (blue bar) were found to express a protein level of 4.5% compared to a BL6 mouse (green bar). (**B**) IP with POM2 was performed overnight on 10 mg of total protein (brain homogenate). The blot (stained with biotinylated-POM2) showed a band of ~ 12 kDa, corresponding to the $sFT_{\Delta HC}$ protein expressed by a transgene positive mouse ($sFT_{\Delta HC}138+/-$). A transgene negative littermate ($sFT_{\Delta HC}138-/-$) was used as negative control.*

$sFT_{\Delta HC}138$ mice were observed for at least 700 days and were found to have a normal lifespan. In addition, they did not show motor alterations and did not develop neurodegeneration. H&E and GFAP staining of cerebellar sections from mice up to 90 weeks of age did not display any abnormalities (Figure 2.28).

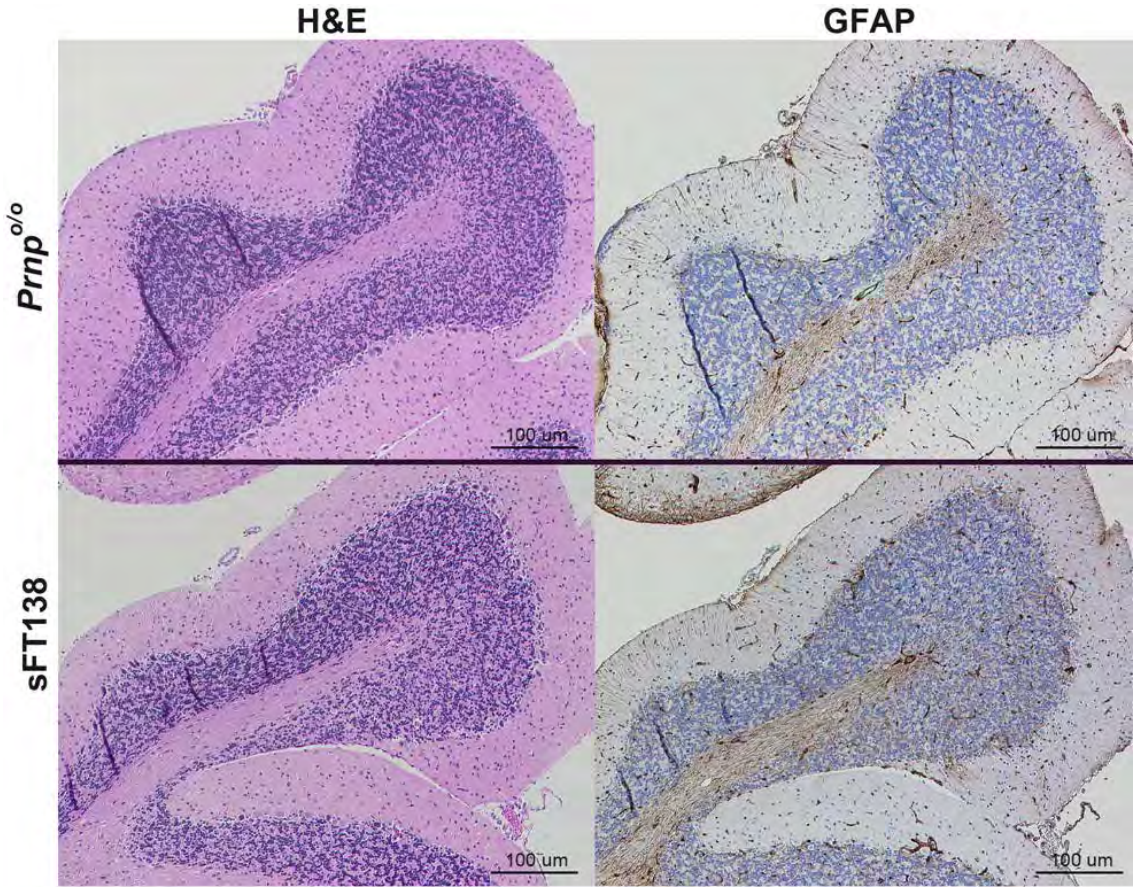

Figure 2.28. sFT$_{\Delta HC}$138 mice do not develop neurodegeneration. H&E and GFAP staining of paraffin-embedded cerebellar sections from 90 weeks old Prnp$^{o/o}$ and sFT$_{\Delta HC}$138 mice. sFTΔHC138+/- and sFTΔHC138-/- sections showed indistinguishable patterns.

DISCUSSION AND OUTLOOK

We recently uncovered a critical role for the FT of PrP^C as the effector domain of PrP^C-mediated neuronal death [99]. Ligands targeting the α1 and α3 helices of the PrP^C globular domain induced rapid neurotoxicity in cerebellar organotypic cultured slices. Toxicity was prevented by deletions of the OR domain, suggesting that the FT has neurotoxic properties and is required to transmit the toxic signals originating from the globular domain [99]. In light of this data, we generated a mouse line expressing a membrane-anchored version of the FT (FTgpi) of PrP^C and found the protein to be a potent neurotoxin. Mice expressing FTgpi developed severe ataxia and die within few weeks. Similar to other mice with interstitial PrP deletions (collectively referred to as "ΔPrP") [56], FTgpi mice experienced massive loss of CGNs. However, the phenotype was not ameliorated (and was possibly exacerbated) by co-expressing wild-type PrP^C, indicating that the mechanism of toxicity differs from that of other ΔPrP mice.

FTgpi induces chronic ER stress leading to neurodegeneration

Unexpectedly, FTgpi retained the typical ER retention phenotype; however, only a small fraction of the protein was found to reach the plasma membrane. Degradation was predominantly mediatedby the proteasome, unlike the full-length protein which was mainly degraded by lysosomes. These observations, along with the unstructured nature of the protein and its exposed hydrophobic domain, led us to speculate that FTgpi may trigger ER stress. Interestingly, of the three branches of the UPR, FTgpi selectively activated the PERK pathway, which protects cells by transiently dampening cellular protein synthesis, thus reducing misfolded protein load and thereby restoring ER homeostasis [123]. However, when chronically activated, PERK signaling promotes cell death by inducing CHOP, which in turn promotes the transcription of Bcl-2-like protein 11 (BIM) [124,125], a proapoptotic protein, and by downregulating the antiapoptotic BCL-2 protein [125]. This cascade protects the organism from rogue cells in which the fidelity of their signaling components cannot be guaranteed [115].

In many instances, the UPR tries to modulate the protein folding capacity of the ER by increasing the activity of the IRE1 and ATF6 pathways [71,115,116]. The activation of these pathways was not observed in FTgpi-expressing cultured cells, but mouse cerebelli exhibited a comprehensive ER stress response with significantly increased levels of spliced XPB1, BIP, CHOP and HSP40. This discrepancy may reflect the increased capacity of immortalized cells to deal with stress, activation of adaptive response pathways to deal with the stress, or the

secondary recruitment of multiple cell types *in vivo*. Apart from accumulating in the ER, the FTgpi also interacts with BiP, a key chaperone responsible for protein folding in the ER. The binding between BiP and FTgpi could sequester the availability of BiP to other essential proteins, which are its obligate substrates.

The proposed signaling network elicited by FTgpi is represented in Figure 2.29.

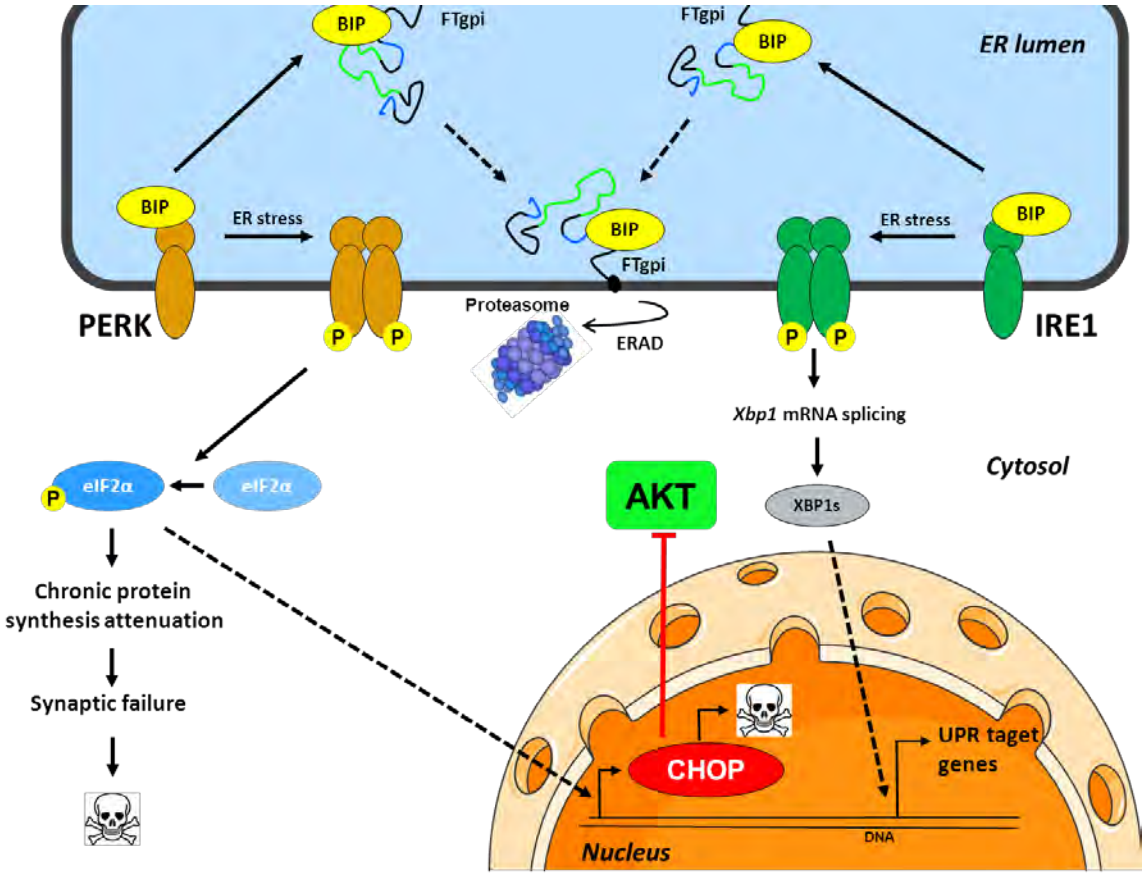

Figure 2.29. Scheme depicting the UPR pathways raised by FTgpi.

Hydrophobic patterns are often targeted by the ER quality control machinery [126], and indeed removal of the hydrophobic core (HC) from FTgpi prevented hyperphosphorylation of eIF2α. In the context of FTgpi, the HC cannot be shielded by the folded globular domain of PrP^{C}, which is missing. Thus, it could chronically engage a specific sub-module of the quality control, leading to ER stress and activation of PERK.

Sustained PERK activation modulates AKT phosphorylation [121]. In particular, AKT activation is increased by short-term exposure, but is down-regulated by long-term exposure, to ER stress [127]. Accordingly, decreased phosphorylation of AKT was observed in both HPL and HEK cells. AKT has a highly conserved role in blocking apoptosis and promoting cell survival by regulating the activation of multiple downstream targets [128], thus chronic deactivation of

AKT may increase the susceptibility of CGNs to cellular stresses. The increased phosphorylation of AKT found *in vivo* but not *in vitro*. may result from the release of ATP by numerous apoptotic CGNs which in turn stimulates astrocytic AKT phosphorylation via P2Y receptors [129,130], contributing to the astrogliosis observed in older FTgpi mice. This suggests that, although AKT could be deactivated at the level of single CGN, it remains activated within the rest of the brain.

Prolonged UPR activity is concomitant with chronic ER stress-associated cell death [131]. FTgpi-induced ER stress may cause the neuronal death observed in FTgpi mice. Importantly, ER stress was detectable in very young FTgpi mice, before any apparent histological or clinical signs of neurodegeneration. One interesting avenue to explore in future studies would be to see if pharmacological inhibition of PERK prevents neurodegeneration in FTgpi mice.

Possible involvement of ER stress in human prion diseases

Several mutations in the human prion protein gene (*PRNP*) have been associated with human prion diseases, such as Creutzfeldt-Jakob disease (CJD), Gerstmann-Sträussler-Scheinker syndrome (GSS) and fatal familial insomnia (FFI) [3]. The molecular mechanism by which these *PRNP* mutants lead to neurodegeneration is not well understood. Missense mutations can affect the structure of a protein, altering its subcellular localization, function, and structure, as demonstrated in a range of studies on the prion protein [132-137] as well as other proteins, such as the CFTR receptor [138] and the TPMT protein [139]. Evidence of ER stress has been found in humans affected with sporadic and vCJD [140] and in SH-SY5Y cells expressing a familial CJD-associated PrP mutant [141]. Therefore, we speculate that disease-associated mutations in the *PRNP* gene introduce thermodynamic instability to the prion protein, which leads to a partial or total misfolding of PrP, exposing the HC, which could trigger the same pathway observed in FTgpi. In light of our new findings, the mechanism of toxicity of these mutant versions of PrP^{C} clearly deserves further investigations.

FTgpi as a model to investigate mechanisms of toxicity in prion infections

ER dysfunctions have been observed in cases of prion infections. Nanomolar concentrations of purified PrP^{Sc} from mouse scrapie brain induce apoptosis in N2A neuroblastoma cells, and toxicity was associated with increased release of intracellular calcium from the ER, a strong upregulation of UPR-inducible chaperones, and a higher sensitivity to ER stress-induced cell death [142,143]. In another study, brain tissue samples from animals naturally infected with BSE showed upregulation of genes involved in ER stress responses, including ER chaperones,

heat shock proteins Grp94 and the chaperone Grp170 [144]. Further, abnormal upregulation of protein disulfide isomerase (PDI), Grp79 and Grp58 was detected in 263K infected hamster brain tissues [145].

Recently, prion-infected mice showed sustained UPR induction, protracted eIF2α phosphorylation and PERK activation [67]. Repression of translation resulted in the loss of critical proteins that leads to synaptic dysfunctions and neuronal death [67]. Strikingly, this mechanism is similar to the signaling pathway evoked by FTgpi in transgenic mice. Although at this stage it is still unclear how the prion infection activates ER stress, one can hypothesize that the abrogation of the ubiquitin proteasome system within a prion-infected body could lead to accumulation of misfolded proteins in the ER, thereby inducing ER stress. Prion infections have been shown to impair post-Golgi trafficking of membrane proteins [146,147], therefore it is also reasonable to assume this could lead to the accumulation of such proteins in the ER resulting in ER stress. Alternatively, small amounts of PrP^{Sc} may enter the ER and activate ER stress, either by inducing the misfolding of the endogenous PrP^{C} and exposure of its HC, and/or through direct binding to the UPR sensor IRE1 and PERK. In support of the latter, there is increasing evidence of direct binding of misfolded proteins to IRE1 and PERK and subsequent UPR activation [148,149]. A recent study showed that a specific compound targeting the PERK pathway of the UPR prevented neurodegeneration in prion-infected mice, both in animals treated at the preclinical stage and also later in disease [150].

ER stress and FTgpi: beyond prion diseases

ER deregulation might have an important part to play in a range of other neurological disorders. Altered level of p-PERK, p-eIF2α and CHOP levels are seen in patients with Parkinson's disease (PD) [68,151], Alzheimer's diseases (AD) [69,152,153], Huntington's disease (HD) [154,155], as well as in amyotrophic lateral sclerosis (ALS) [70,71]. Although the subcellular localization of protein misfolding can differ between these disorders, the interdependence of protein folding throughout the cells suggests that ER dysfunctions could be the final common pathway for many neurological diseases [156]. It is not well understood if ER stress is the cause or an effect of these diseases. UPR activation has been mostly detected in post mortem human brains and cell based models [157]. Animal models for AD, PD and HD often do not produce neuronal cell death [158], a major hallmark of these diseases, hence detection of signaling pathways evoked by these disorders could be problematic.

FTgpi pathogenesis suggests that ER stress is an upstream phenomenon in the chain of events leading to neurodegeneration, it is exacerbated by higher level of FTgpi, and it is a relatively slow and cumulative process, which leads in the long term to the death of CGNs. Being upstream, it could be a suitable target for therapeutic approaches. It is becoming increasingly clear that manipulation of common pathways such as protein translation and protein degradation, rather than disease-specific approaches, could lead to new, broader therapeutic strategies. Furthermore the resemblance between the mechanisms leading to neurodegeneration elicited by prions and FTgpi, suggest that FTgpi mice may represent a useful tool for further investigations of the mechanisms of toxicity underlying human prion diseases. Moreover, FTgpi mice are particularly suitable for assessment of potential new treatments, as ER stress occurs as an upstream event and is the main cause of toxicity. Therefore, we believe that FTgpi mice may represent a useful tool in the hunt for an effective treatment option.

MATERIALS AND METHODS

Construction of transgenes

To create the FTgpi construct, total mouse brain cDNA was amplified using the primer set SY6 and SY7 which introduce BamHI and SalI cloning sites at the 3' and 5' ends of the ORF of PrP. PrP was cloned into the cloning vector pBSK (pBSK-PrP). This plasmid served as a template for the following cloning steps. An XbaI cloning site was introduced by PCR in the PrP ORF just before amino acid 225. The primer sets used were SY6/SY6a and SY7a/SY7. An amino-terminal insert was amplified from pBSK-PrP using the primer set SY6/SY8 which introduces BamHI and XbaI cloning sites before the start codon and after amino acid 140, respectively. pBSK-PrP and the amino-terminal insert were digested with BamHI and XbaI, and the open vector and the insert were ligated, to generate a construct consisting of the first 140 amino acids of PrP directly linked amino acid 226 ($PrP_{\Delta 141-225}$). Primers: SY6 fw (5'-CGC GGA TCC AAT TTA GGA GAG CCA AGC AGA-3'), SY6a rev (5'-CGC TCT AGA ACG TCG CCC GTC GTA ATA GGC-3'), SY7a fw (5'-CGC TCT AGA GAC GGG AGA AGA TCC AGC AGC-3'), SY7 rev (5'-ACG CGT CGA CCA CGA GAA TGC GAA GGA ACA-3'), SY8 rev (5'-ACG CTC TAG ACC AGT CGT TGC CAA AAT G-3').

To create the $sFT_{\Delta HC}$ construct, the "half-genomic" pPrPHG plasmid containing the wild-type PrP was used as template. Primer set BspE5' and sFT3' were used to generate a 2842bp amplicon containing the $sFT_{\Delta HC}$ sequence, and to introduce a BspEI and a StuI cloning sits at the 5' and 3' ends respectively. The "half-genomic" pPrPHG plasmid was then digested either with SalI and BspEI or SalI and StuI; an 8435bp and a 2379bp fragment were respectively isolated from gel, purified, and mixed with the previous amplicon in a three-way ligation reaction, in order to obtain the "half-genomic" pPrPHG plasmid expressing the $sFT_{\Delta HC}$ transgene. Primers: BstE5' fw (5'-CAA GCA TTT AAG CCA GTC CGG AGC GGT GA -3'), sFT3' rev (5'-CCT ATC TCA CAC ATG CTT GAG GTT GGT TTT TGG -3').

Generation of transgenic mice

The phg plasmids containing the $PrP_{\Delta 141-225}$ (FTgpi) ORF and $PrP_{\Delta 112-254}$ (sFT) were propagated in Escherichia coli XL1 blue, the minigene were excised with NotI and SalI, processed as described [54], and injected into fertilized *Prnp*$^{+/+}$ oocytes (B6D2F1/Crl) by standard procedures [159]. The transgene positive founders were crossed with *Prnp*$^{o/o}$ ZHI mice in order to obtain transgene-positive mice on a *Prnp*$^{o/o}$ background. FTgpi transgene was identified by PCR using the exon 2 forward primer pE2 and the non-coding region at 3' of exon 3 reverse primer 3'NC . The fragment size of the transgene was 647bp. The $sFT_{\Delta HC}$

transgene was identified by PCR using the forward primer pE2 and the reverse primer sFT3'. The fragment size of the transgene was 417 bp. In order to outbreed the *Prnp*$^{+}$ allele, PCR analysis was carried out using primers P10 (forward primer, *Prnp* exon 3), 3'NC (reverse primer), and P3 (reverse primer, neoR gene); P10 and 3'NC gave a 542 bp signal for the *Prnp*$^{+}$ allele and P3 and 3'NC gave a 362 bp product for the *Prnp*^{0} allele. In the PCR, the transgene was also detected as a 269 bp product. Primers: pE2 (5'-CAA CCG AGC TGA AGC ATT CTG CCT-3'), 3'NC (5'-CCC TCC CCC AGC CTA GAC CAC GA-3'), P10 (5'-GTA CCC ATA ATC AGT GGA ACA AGC CCA GC-3'), P3 (5'-ATT CGC AGC GCA TCG CCT TCT ATC GCC-3'), sFT3' rev (5'-CCT ATC TCA CAC ATG CTT GAG GTT GGT TTT TGG -3').

Morphological analysis

Brains were removed and fixed in 4% formaldehyde in PBS, pH 7.5, paraffin embedded, and cut into 2-4 µM sections. Sections were stained with hematoxylin and eosin (H&E) and commercial antibodies to GFAP (glial fibrillary acidic protein; activated astrocytes). The same protocol was applied to livers, spleens, kidneys, hearts, stomachs, pancreas and intestines.

TUNEL staining

5 µM frozen sections were fixed with 1% paraformaldehyde in PBS, pH 7.4, for 10 min at room temperature (RT), rinsed twice in PBS, permeabilized with a solution of Ethanol:Acetic acid (2:1) for 5 min at -20°C, rinsed twice with PBS, and then stained using ApopTag® Plus In Situ Apopotosis Fluorescein Detection kit, according to the manufacturer's directions (Millipore). Cell nuclei were counterstained with DAPI. Sections were mounted with Fluorescent Mounting Medium (Dako) and imaged on a CLSM Leica SP5 ZMB. Co-staining TUNEL and Iba1 on frozen sections: 5 µM slices were cut and put on glass slides, fixed 10 min in 1% paraformaldehyde in PBS, washed 2X with PBS, 2 min in 50% acetone, 2 min in 100% acetone, 2 min in 50% acetone, washed 2X with PBS and 1X with PBS-T. Slides were treated 10 min with Protein block serum free (Dako), incubated 2 h at RT with Iba1 diluted in 0.3% Triton in PBS, washed 2X with PBS, 1X with PBS-T, incubated with anti-rabbit Alexa467 secondary antibodies diluted in 0.3% Triton in PBS 1 h at RT with 1 ug/ml DAPI. Slides were washed 2X with PBS, 1X with PBS-T, and stained using ApopTag® Plus In Situ Apopotosis Fluorescein Detection kit, according to the manufacturer's directions (Millipore). Sections were mounted with Fluorescent Mounting Medium (Dako) and imaged on a Olympus Fluoview FV10i.

Immunofluorescence staining

Cells were grown on Cultureslides, 8-well (BD Biosciences), washed 1X PBS and fixed with 4% formalin in PBS, pH 7.4, for 15 min at RT. After washing 2X with ice-cold PBS, cells were permeabilized with 0.3% Triton X-100 in PBS for 5 min at RT, rinsed 1x with PBS, and incubated for 40 min in blocking solution (1% FBS in PBS) for 40 min at RT. Cells were rinsed 1x with PBS and incubated with primary antibody (POM11, giantin, LAMP2) diluted in washing buffer (1%BSA, 0.25% Triton X-100 in PBS) overnight at 4°C. After washing 2X with PBS, cells were incubated with Alexa Fluor®-conjugated 555- anti-mouse or 647-secondary anti-rabbit or anti-rat antibodies (Invitrogen, Molecular Probes) diluted 1:5000 in washing buffer for 2 h at RT, and incubated with 1 ug/ml DAPI (4',6-diamidino-2-phenylindole, Invitrogen). Permeabilization with 100% methanol at -20°C for 10 min was performed when calnexin was used as a primary antibody. Surface staining with CmDil: CM-Dil was diluted in cell culture media (OPTI-MEM, 10% FBS, Glutamax) at a concentration of 0.5 ug/ml, immediately before labelling. Cells were incubated at 37°C for 5 min, then at 4°C for 15 min, washed 1X with PBS and fixed in 4% formalin. Primary and secondary antibodies stainings were performed as previously described. Cells were mounted with Fluorescent Mounting Medium (Dako) and imaged on a CLSM Leica SP5 ZMB. Confocal imagines were processed with Imaris; colocalization was quantified using the function ImarisColoc after setting the thresholds.

Generation of stably transfected Flp-In™-293 cells

Flp-In™-293 cells were maintained in Dulbecco's Modified Eagle Medium (Life Technologies, 31966-021) supplemented with 10% fetal bovine serum and penicillin/streptomycin.

PrP, FTgpi, sFT and $sFT_{\Delta HC}$ constructs were cloned into the pcDNA™5/FRT vector. Flp-In™-293 cells were transfected with the respective pcDNA™5/FRT and pOG44 vectors using Lipofectamine 2000 (Invitrogen) according to the manufacturer's directions. Clones were selected for 15 days in 250µg/ml Hygromycin and subsequently maintained in 100µg/ml Hygromycin.

Western blot analysis

Cerebellums were homogenized using TissueLyser LT for 5 min in 10 vol of lysis buffer (0.5% Nonidet P-40, 0.5% 3-[(3-cholamidopropyl)dimethylammonio]-1-propanesulfonate (CHAPS), protease inhibitors (complete Mini, Roche), phosphates inhibitors (PhosphoSTOP, Roche) in PBS, and centrifuged at 1000g for 5 min at 4°C to remove debris prior to analysis by SDS-PAGE

(Novex® NuPAGE® 10% Bis-Tris Gels). After electrophoresis, samples were transferred to nitrocellulose membranes (PROTRAN®, Whatman®). Membranes were blocked with 5% milk 1 h at RT and incubated overnight in Tris-buffered saline-Tween (TBS-T) at 4°C with primary antibodies, followed by incubation with a secondary Peroxidase-Goat Anti-Mouse IgG (H+L) (#62-6520) or Peroxidase-Goat Anti-Rabbit IgG (H+L) (#111.035.045), used at 1:10000 1 h at RT. Membranes were developed with Luminata Crescendo (Millipore) and images were acquired using Stella imaging system (Raytest). Cells were homogenized on ice using a 30G syringe in lysis buffer, centrifuged at 1000g for 5 min at 4°C to remove debris prior to analysis by SDS-PAGE (E-PAGE™ 48 wells 8%). After electrophoresis, samples were transferred using the iBlot system (Invitrogen). For deglycosylation, denatured total protein was incubated at 37°C for 4 h with 500 U PNGase F (New England Biolabs) according to the manufacturer's instructions.

Immunoprecipitation

Protein extraction from the mouse cerebellum was performed using mechanical lysis in IP buffer (HBS buffer (pH 6.8) with 2% CHAPS and cocktail of protease inhibitors (Roche)). This was followed by centrifugation at 8000 rpm for 10 min. The amount of protein in the lysate was estimated using BCA assay and 500 µg of the protein was used for the immunoprecipitation assays. For the cell lines, lysis was performed for 20 min at 4°C in IP buffer followed by centrifugation for 10 min at 10000 g. In both cases supernatants were precleared and incubated for 16 h at 4°C with antibodies and dynabeads. For immunoprecipitation of BiP 2 U/ml of Apyrase was added to the lysate to deplete ATP. After immunoprecipitation, the beads were washed for three times with the IP buffer and resuspended in the sample buffer (2x) after the final wash. The samples were heated at 95°C for 5 min and migrated on 12% Tris-Bis gels with the MOPS buffer.

Pulse chase Assays

To monitor the half-life of FTgpi and PrP^C, HPL cells were transfected with mammalian expression plasmids of the two proteins. 24 h post transfection, the cells were either treated with DMSO, MG132 (10µM) or bafilomycin (250 nM) for 2 h followed by incubation in starvation medium (DMEM without methionine and cysteine) for 40 min along with the drugs to deplete the endogenous stores of methionine and cysteine. The cells were then labeled with 50µCi/ml ^{35}S-methionine/cysteine for 20 min followed by a chase in normal medium at different time points. After the chase, the cells were harvested in isotonic HEPES buffer (pH-

6.8) containing 2%CHAPS and protease inhibitor cocktail. Post nuclear supernatants were obtained by centrifuging the sample at 10000g for 10 min. FTgpi and PrP^{C} were immunoisolated from the post nuclear supernatant by overnight incubation with POM2 antibody followed by incubation with Dynabeads for 2h at 4°C. The immunoprecipitates were migrated on a 12% Tris-BIS gels followed by fixation and drying of the gels. The dried gels were exposed to phosphoscreen and the radiolabelled products were revealed using a film.

Sandwich ELISA

96-well plates were coated with 400 ng/ml of purified antibody POM2 overnight at 4°C. Plates were washed 4X with PBS containing 0.1% (vol/vol) Tween 20 (PBST), and blocked with 5% TopBlock (Invitrogen) for 2hrs at RT. Plates were incubated with serially-diluted recPrP23-231 for the standard curve, sFT138 (800 ug/ml), BL6 (100 ug/ml) and *Prnp*$^{o/o}$ (800 ug/ml) brain homogenates in PBST containing 1% TopBlock. After 2 h at RT, plates were washed extensively and then probed with biotinylated POM11 at a concentration of 100 ng/ml in PBST containing 1% TopBlock, for 1hr at RT. Subsequently, after washing, plates were incubated with horseradish peroxidase conjugated avidin (1:1000 dilution, Pharmigen) for 1h at RT. Plates were developed with TMB Stabilized Chromagen (SB01, Invitrogen), and optical density was measured at 450nm.

FACS analysis

Cells were harvested with EDTA 10 mM, washed 2X in PBS, resuspended in ice-cold FACS buffer (2%FBS, 2mM EDTA in PBS) and incubated with 1:500 POM11 antibody for 30 min on ice. Cells were then washed 2X with ice-cold FACS buffer and incubated for 30 min on ice with Alexa Fluor®-conjugated 647 anti-mouse, protected from light. Cells were washed 3X with ice-cold FACS buffer and transferred into micro-FACS tubes. Data was acquired using FACSCalibur™ (BD Biosciences).

Antibodies

Mouse monoclonal anti-PrP antibodies POM1, POM2, POM11 [1] were diluted 1:5,000 for Western blot; anti-PERK (#3192), anti-p-PERK (#3179), anti-eIF2α (#9722), anti-p-eIF2α (#9721), anti-CHOP (#5554), anti-AKT (#4685), anti-p-AKT (#4060), anti-Erk1/2 (#9107), anti-p-Erk1/2 (#4370) (Cell Signaling) were diluted 1:1000 for Western Blot; actin antibody (Millipore AG, MAB1501R) was used at 1:10000 for Western blot. Immunofluorescence: anti-calnexin (Abcam, ab22595) was used at 4 ug/ml, anti-giantin (Abcam, ab24586) was used at

1/1000, anti-lamp2 (Abcam, ab25339) was used at 1/100, anti-Iba1 (Abcam, ab5076) was used at 1/100, and POM11 was used at 1/1000. Co-staining TUNEL and Iba1: anti-Iba1 (Wako, 019-19741) was used at 1:500.

mRNA analysis

Cerebellar RNA was isolated using RNeasy Plus Universal Mini Kit (QIagen), according to the manufacturer's manual. After reverse transcription (QuantiTect Rev. Transcription Kit, QIagen), cDNA was used for RT-PCR to quantify FTgpi and PrP mRNA levels using the following primers: pE2 fw (5'-CAA CCG AGC TGA AGC ATT CTG CCT-3'), sFT ORF rev (5'-AGG TGC CAC CCT GAG GTG GGT AA-3'). GAPDH was used to standardize expression levels using primers GAPDH fw (5'-CCA CCC CAG CAA GGA GAC T-3') and GAPDH rev (5'-GAA ATT GTG AGG GAG ATG CT-3'). RT-PCR was performed using SYBR-green (Roche) and determination of ΔΔCT-values was done on a ViiA™ 7 real-time system (Applied Biosystems). Cell mRNA was isolated using RNeasy Mini Kit (QIagen), according to the manufacturer's manual. After reverse transcription (QuantiTect Rev. Transcription Kit, QIagen), cDNA was used for RT-PCR to quantify the ER stress related genes; CHOP: fw (5'-CTT CAC TAC TCT TGA CCC TGC-3'), rev (5'-CTA GTT CTT CCT TGC TCT TCC TC-3'). Spliced-Xbp1 primers: fw (5'-TGC TGA GTC CGC AGC AGG TG-3'), rev (5'-CAT GAC AGG GTC CAA CTT GTC-3'). BIP primers: fw (5'-CGA GGA GGA GGA CAA GAA GG-3'), rev (5'-CAC CTT GAA TGG CAA GAA CT-3'). HERP 1 primers: fw (5'-CAT CTC TAG GCC TGA GGC TG-3'), rev (5'-GTT CCT GAT GCA GCA GTG GCA-3'). ERP72 primers: fw (5'-TGG ACA CCT CCA CCT GAA GTC-3'), rev (5'-CTC ATA CTC AGG GGC AAG TTT C-3'). HSP40 primers: fw (5'-GAT CTG CCA CTG CTT CTC TAA G-3'), rev (5'-CCT GAG CAG CTT CAT AAT CC-3'). EDEM1 primers: fw (5'-GTT CTG ATA GGG GAT GTG GAA G-3'), rev (5'-GAG GAG ATA TGT GGA CTC CAC-3'). GAPDH was used to standardize expression levels. RT-PCR was performed using SYBR-green (Roche) and determination of ΔΔCT-values was done on a ViiA™ 7 real-time system (Applied Biosystems).

CHAPTER 3

OVEREXPRESSION OF SHADOO IN PERIPHERAL NERVES DOES NOT RESCUE THE POLYNEUROPATHY IN *PRNP*$^{o/o}$ MICE

INTRODUCTION

SHADOO, A PROTEIN WITH SIMILARITY TO THE PRION PROTEIN FT

Shadoo (Sho) is the third member of the prion gene family, and was discovered in 2003 by *in silico* analysis. The protein was coined Shadoo, the Japanese word for 'shadow', and the gene was termed *Sprn* ('shadow of the prion protein'), and appeared to be widely conserved in nature [98]. Sho was predicted to be extracellular and GPI-anchored, which was then confirmed experimentally [97]. Sequence comparison with PrP^C shows: a highly conserved N-terminal signal sequence and a hydrophobic region of 20 residues with strong homology. Furthermore, although Sho does not have an octarepeat domain, it has an Arginine-rich basic region containing up to six tetrarepeats. Conversely, the C-terminal of Sho contains a glycosylation site but no structure, hence it has little homology with PrP^C GD [98] (Figure 3.1). The circular dichroism spectrum of recombinant murine Sho is consistent with a random coil configuration [97]. Overall, Sho strongly resembles PrP^C FT.

Unlike Doppel, Sho expression is restricted to the CNS, which may have implications for prion-associated CNS phenomena. Initial findings led to the hypothesis of a possible functional link between mammalian PrP and Sho proteins.

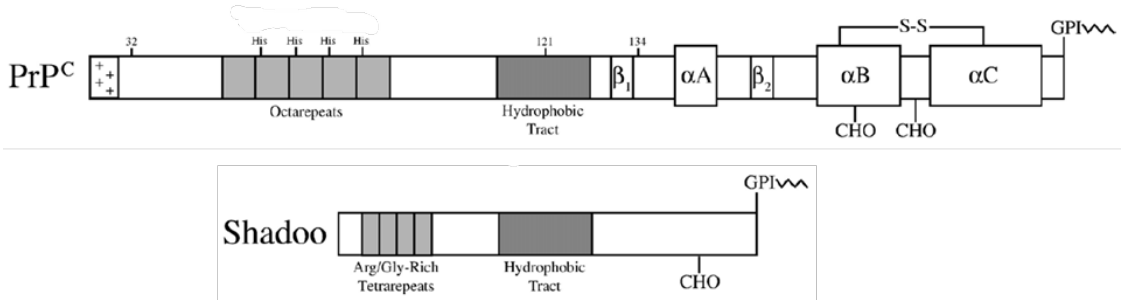

Figure 3.1 Structural comparison between PrP and Sho. *Sho resembles PrP FT. In particular, the hydrophobic tract (in dark grey) shares high homology.*

Prnp$^{o/o}$ mice show only a mild phenotype despite PrP^C being implicated in multiple cellular processes. Therefore, it has been hypothesized that an alternative protein (π) exists, which is able to compensate for the absence of PrP^C [91] *in vivo*. Following its discovery, investigators

appointed Sho as the π protein, primarily because of the high homology of the HC domain (Figure 3.1). The HC domain, as previously mentioned, is crucial for PrP^C neurotrophic properties and myelin maintenance.

SHADOO HAS PRP^C-LIKE PROTECTIVE PROPERTIES

ΔPrP mutants and Doppel are able to induce cell death when transfected into wild type cerebellar granule neurons (CGNs) [97,103]. As anticipated, cotransfection of wt PrP^C reduced the toxic activity of both ΔPrP and Doppel in this model. Interestingly, cotransfection of wt Sho also significantly ameliorated the toxic phenotype of ΔPrP and Doppel [97]. Given the similarities between the HC domains of Sho and PrP, and HC intrinsic properties, this domain was a strong candidate for the 'active site' of Sho. Therefore, a mutant version of Sho lacking the HC domain was generated ($Sho_{\Delta 62\text{-}77}$). When cotransfected in CGNs along with Doppel and ΔPrP, $Sho_{\Delta 62\text{-}77}$ could not exert its neurotrophic effect [97]. Moreover, knockdown of Sho in *Prnp*$^{o/o}$ embryos induced lethality [160]. Taken together, these results pointed at Sho as the potential π protein.

SHADOO IN PRION INFECTIONS

Sho protein level is strikingly reduced in prion-infected animals, whereas no differences were observed in mice models of Alzheimer's disease, suggesting Sho depletion may be specific for prion diseases [97].

Follow-up experiments showed that Sho protein levels were decreased in the brains of mice, hamsters, voles, and sheep infected with different natural and experimental prion strains. Furthermore, Sho levels were inversely proportional to levels of PrP^{Sc} [161].

Its apparent involvement in prion diseases led to investigators to believe that Sho may offer new insights into the homeostatic mechanisms involved in detection and clearance of misfolded proteins that drive prion disease pathogenesis.

Therefore, mice overexpressing Sho, driven by the *Prnp* promoter, were generated (Tg*Sprnp*24551 mice) [162]. In these mice, levels of Sho are 2.5-fold higher than the endogenous protein, whereas PrP^C level is not altered. When Tg*Sprnp*24551 mice were challenged with prions, the incubation period and onset of clinical symptoms were not different between the various cohorts, suggesting that Sho does not modulate the chemical events that shape the neurological disease phase of prion infection [162]. Nevertheless, scientists concluded that the potent drop in Sho protein occurring during the preclinical phase of the disease could be used as a marker for early detection of prion infections.

SHADOO IS NOT THE Π PROTEIN

Westaway and coworkers generated Sho knockout mice (S*prn*$^{o/o}$ mice) [163]. S*prn*$^{o/o}$ mice are viable and have a normal life span. Prion-infected S*prn*$^{o/o}$ mice have incubation times and clinical symptoms that are not notably different from prion-infected wild type mice [163]. Importantly, double-knockout mice deficient in both Sho and PrP^{C} (S*prn*$^{o/o}$ *Prnp*$^{o/o}$) are also fertile and viable up to a mean of 690 days of age [163]. These data reduce the impetus for equating Sho with the notional π protein, and contradict the previous results that showed lethality in double-knockout embryos.

OUTLINE OF THIS WORK

Mice lacking the HC of PrP^{C} or *Prnp*$^{o/o}$ mice develop CDP in the peripheral nerve but not in the CNS [2] [81], suggesting that HC is essential for peripheral myelin maintenance. Sho carries a domain with high homology to the HC of PrP^{C} and it has been shown to have PrP^{C}-like neuroprotective features.

I posit that, because Sho is expressed in the CNS and is functionally homologous to the neuroprotective function of the HC of PrP^{C}, it therefore rescues the CDP phenotype (in the CNS) induced by HC-deficient mice. The abrogation of the CDP does not occur in peripheral nerves, possibly due to the lack of Sho expression. Therefore, I wished to test the hypothesis that expression of Sho in the peripheral nerve would prevent CDP in *Prnp*$^{o/o}$ mice.

Mice expressing ~2.5-fold transgenic Sho, driven by the *Prnp* promoter, were kindly provided by Dr. David Westaway *(University of Alberta, Centre for Research in Neurodegenerative Diseases)* and crossed with *Prnp*$^{o/o}$ mice. In these mice, I found that Sho does not revert the CDP phenotype present in the peripheral nerves, thus refuting our initial hypothesis, and contributing to the evidence indicating that Sho is not the potential partner/surrogate of PrP^{C}.

RESULTS

SHADOO IS NOT EXPRESSED IN PERIPHERAL NERVES

Sho is predominantly expressed in the CNS, although limited expression of Sho has been detected by RT-PCR in non-brain tissues such as lung and stomach [98]. Sho has not been detected in testis, liver, gut spleen, heart, kidney and skeletal muscle [98]. The expression of Sho in peripheral nerves has not previously been investigated.

In order to assess the expression of Sho in peripheral nerves, I collected whole brains (as positive controls) and dorsal root ganglions (DRGs) from wild type mice; extracted the mRNA, translated into cDNA, and multiplied by a 40 cycles PCR reaction. I used two different pairs of primers, one pair annealing to the 3' untranslated region (Sho_3' primer) and one pair annealing to the ORF (Sho_ORF primer) of the *Sprn* gene. Actin was used an additional positive control for the PCR reaction and quality of cDNA. As anticipated, I detected Sho in brain cDNA, whereas I could not detected a signal in DRG cDNA, indicating that Sho is not expressed in peripheral nerves (Figure 3.2).

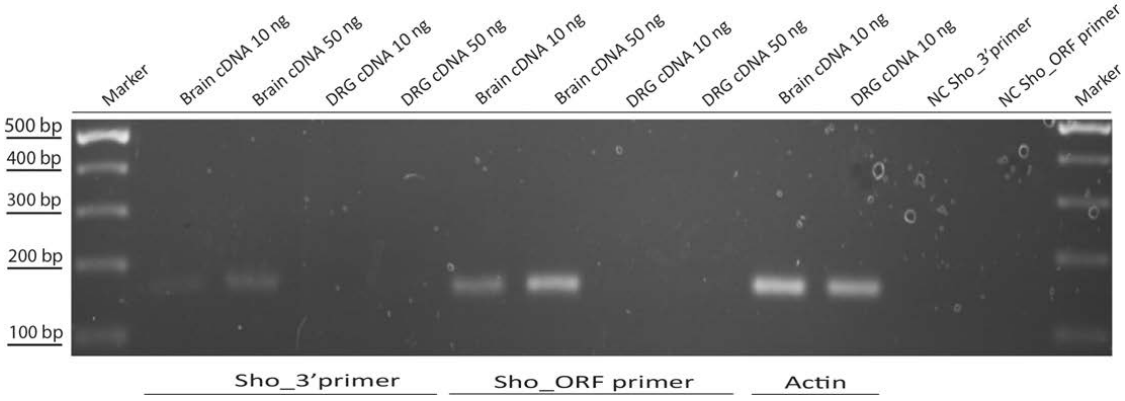

Figure 3.2. Sho is not expressed in peripheral nerves. *mRNA was obtained from mouse tissue whole brains and dorsal root ganglions (DRGs) of wild type mice. Sho signal was selectively detected in the brain tissue but not in DRGs, indicating that Sho is absent in peripheral nerves.*

GENERATION OF TRANSGENIC MICE OVEREXPRESSING SHADOO ON A *PRNP*$^{0/0}$ BACKGROUND

PrP^{C} is physiologically expressed in the peripheral nervous system, thus the *Prnp* promoter allows the expression of the gene in peripheral nerves [76]. Mice overexpressing transgenic Sho ≈ 2.5 fold under the *Prnp* promoter (Tg*Sprn*24551 or *Sprn*) *[162]*, originally on a FVB genetic background ($Prnp^{+/+}$), were crossed with $Prnp^{o/o}$ mice in order to obtain a mouse line over-expressing Sho, driven by the *Prnp* promoter, on a $Prnp^{o/o}$ background (Figure 3.3).

The CDP observed in *Prnp*$^{o/o}$ mice has 100% penetrance at 50 weeks [81]. Therefore, once the new line was established, mice were aged up to 50 weeks and, only then, were subsequently examined.

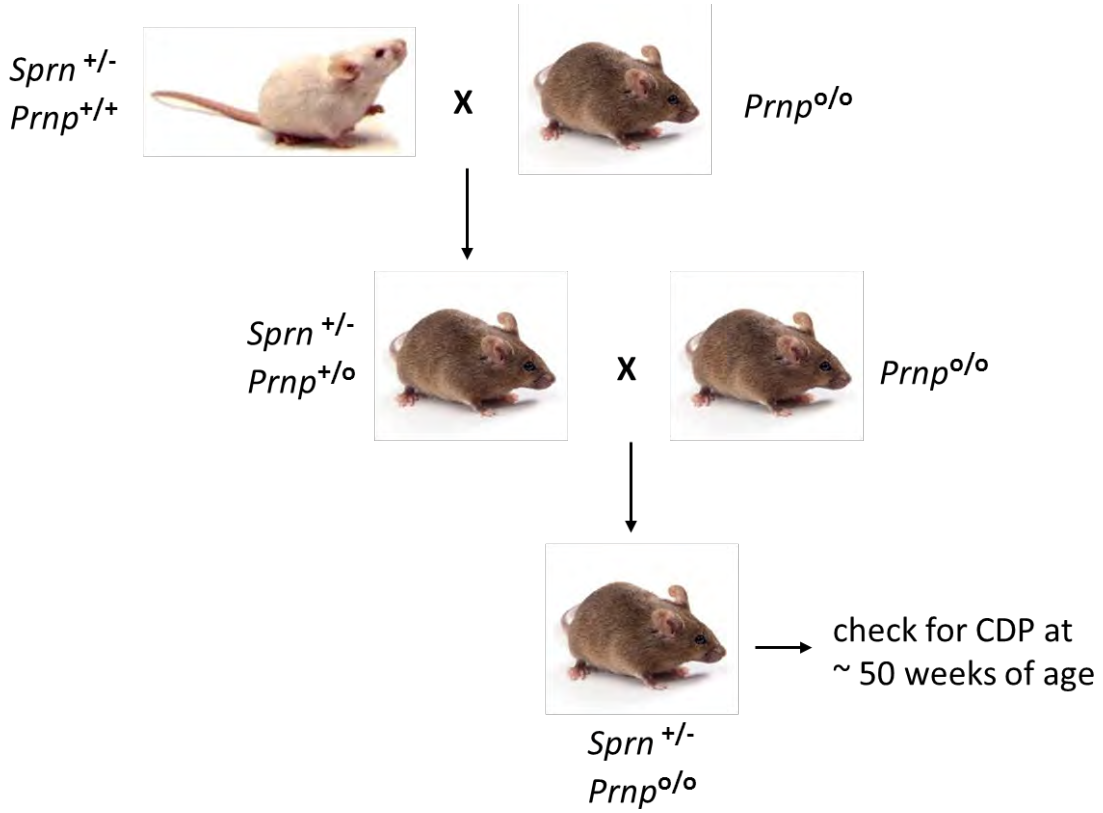

Figure 3.3. Breeding strategy. *Sprn* mice were crossed twice with *Prnp*$^{o/o}$ mice in order to obtain the mouse line *Sprn*$^{+/-}$ *Prnp*$^{o/o}$

SHADOO DOES NOT RESCUE THE POLYNEUROPATHY OBSERVED IN *PRNP*$^{0/0}$ MICE

Sciatic nerves were collected from 50 week-old *Sprn*$^{+/-}$ *Prnp*$^{o/o}$, *Sprn*$^{-/-}$ *Prnp*$^{o/o}$ and *Sprn*$^{-/-}$ *Prnp*$^{+/o}$ littermates. *Sprn*$^{-/-}$ *Prnp*$^{+/o}$ mice were used as a 'healthy nerve' positive control, as these mice still retain a *Prnp* allele; *Sprn*$^{-/-}$ *Prnp*$^{o/o}$ mice were used as a 'degenerated nerve' positive control [81].

Representative toluidine blue-stained 'semi-thin' cross sections of sciatic nerves are shown in Figure 3.4

As anticipated, no signs of neuropathy were detected in *Sprn*$^{-/-}$ *Prnp*$^{+/o}$ mice. Conversely, all *Sprn*$^{+/-}$ *Prnp*$^{o/o}$ and *Sprn*$^{-/-}$ *Prnp*$^{o/o}$ mice that were included in these assessments showed CDP, which was 100% penetrant and conspicuous in all peripheral nerves (Figure 3.4). Structural

abnormalities, such as aberrant or redundant myelin loops and supernumerary myelin sheaths were detected in both *Sprn*$^{+/-}$ *Prnp*$^{o/o}$ and *Sprn*$^{-/-}$ *Prnp*$^{o/o}$ mice. Morphological alterations in *Sprn*$^{+/-}$ *Prnp*$^{o/o}$ mice were less pronounced, yet qualitatively similar to those of *Sprn*$^{-/-}$ *Prnp*$^{o/o}$ mice (Figure 3.4).

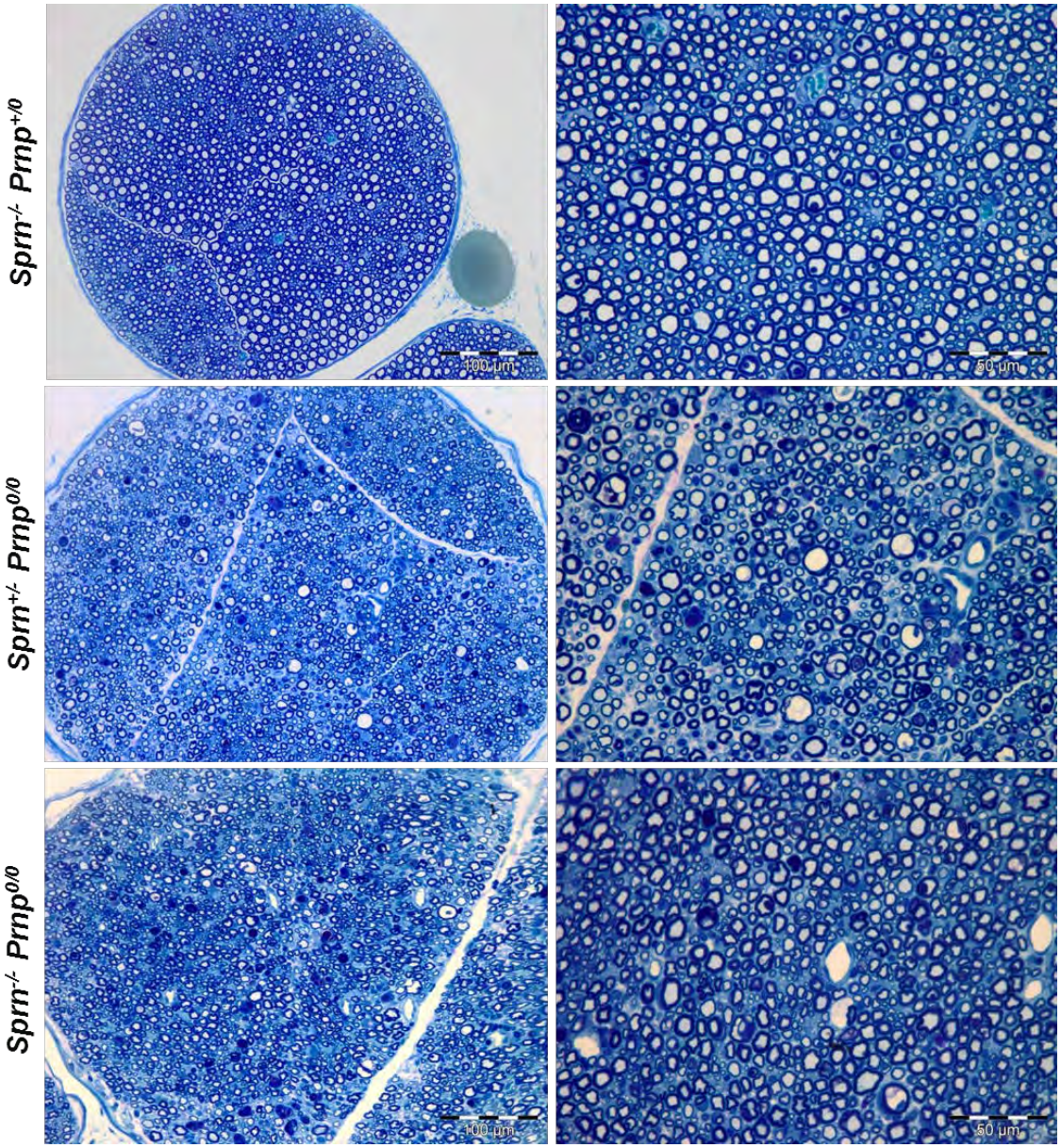

Figure 3.4. Sprn*$^{+/-}$ *Prnp*$^{o/o}$ *mice are affected by CDP. *Toluidine blue-stained 'semi-thin' cross sections of sciatic nerves of Sprn*$^{-/-}$ *Prnp*$^{+/o}$*, Sprn*$^{+/-}$ *Prnp*$^{o/o}$ *and Sprn*$^{-/-}$ *Prnp*$^{o/o}$ *mice, all approximately 50 weeks of age. Sho does not rescue the CDP observed in Sprn*$^{-/-}$ *Prnp*$^{o/o}$*mice.*

I used software developed in house [81] to analyze the axon size-density distribution in these nerves. Large fibers were predominantly found to be affected by the lack of PrP^{C}, as

previously reported [81], and Sho was found not to be able to revert the phenotype, although a very mild effect was observed for axons of 45-50 µm^2 (Figure 3.5).

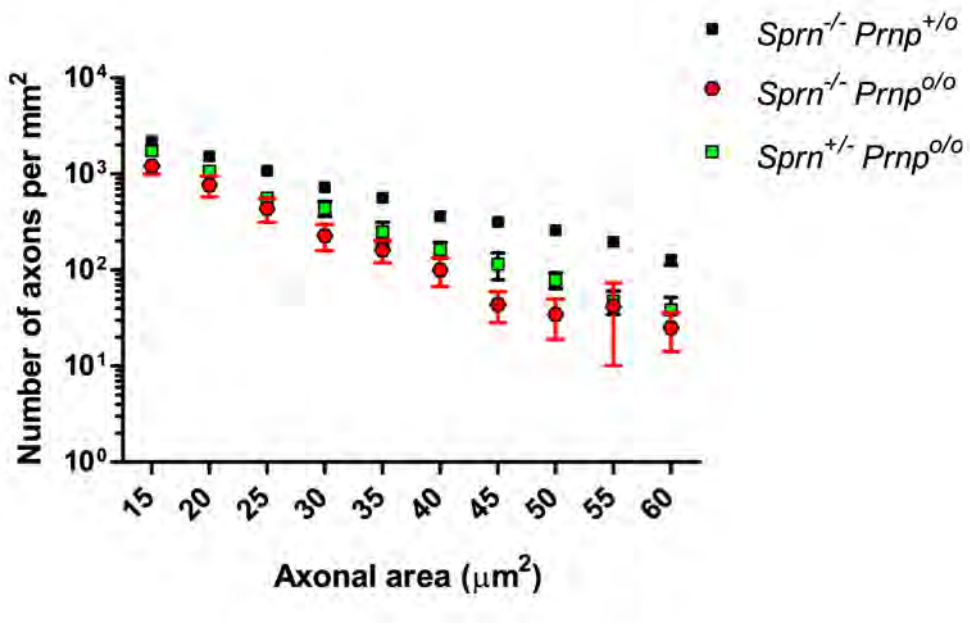

Figure 3.5. Sho does not revert the phenotype induced by the lack of PrP^C. *Morphometrical analysis of sciatic nerves. Axonal density within nerves (number of axons per mm^2) was quantified morphometrically and plotted against the cross-sectional areas (µm^2) of axons (axonal density-size distribution). Error bars, s.e.m.*

In conclusion, our studies indicate that Sho does not significantly influence the onset and development of CDP associated with the lack of PrP^C in adult mice.

BEHAVIORAL EXPERIMENTS

I performed a series of behavioral experiments (hot plate test, grip test, rotarod) to identify any subtle differences between Sprn$^{+/-}$ *Prnp$^{o/o}$* and *Sprn$^{-/-}$ Prnp$^{o/o}$* mice.

In the hot plate assay, the mouse is placed on the surface of a hot plate, which is maintained at 52.5 °C [164]. The latency of the mouse to raise and lick hind paws, to flutter or to jump up is recorded. The latency of these reflexes is dependent, among other variables, upon the time for afferent conduction of the impulse coming from the peripheral system to the spinal cord dorsal horn neurons [165].

Our group previously reported that the time lag to licking was significantly longer in *Prnp$^{o/o}$* mice compared to wild type mice [81]. Therefore, I wished to test whether Sho was able to

decrease the response of *Prnp*$^{o/o}$ mice to heat. Responses were found to be not significantly different between Sprn$^{+/-}$ *Prnp*$^{o/o}$ and *Sprn*$^{-/-}$ *Prnp*$^{o/o}$ mice, both at 13-18 weeks and 50 weeks of age (Figure 3.6), reinforcing the histological observation that Sho does not ameliorate the CDP.

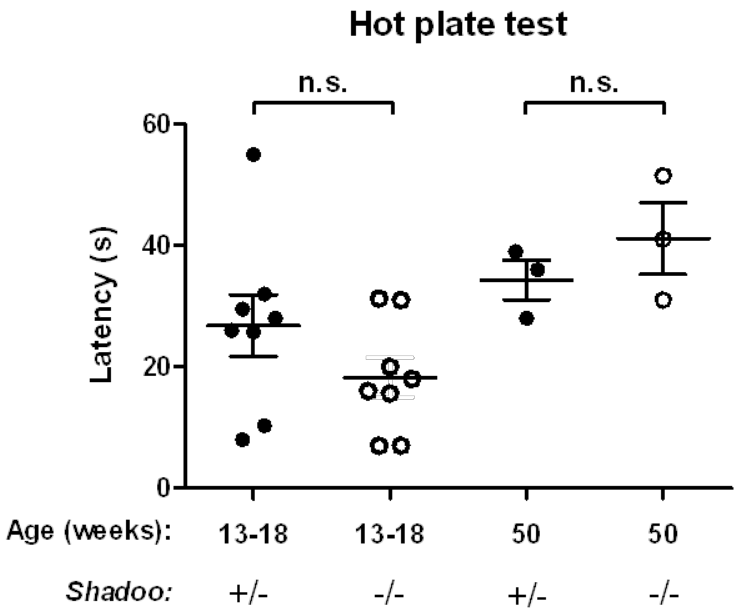

Figure 3.6. Hot plate test. *Mice were individually placed onto a metal plate that was maintained at a constant temperature of 55°C (± 0.4°C). The time to a response to the heat, such as shaking of the hind paws, licking of the hind paws and jumping, was recorded. Responses to heat were not significantly different between Sho +/- and Sho -/- mice. All mice are on a Prnp*$^{o/o}$ *background*

The grip strength test is used to measure the neuromuscular function, as maximal muscle strength of forelimbs and combined forelimbs and hind limbs. These are assessed by the grasping applied by the mouse on a grid that is connected to a sensor [165]. I previously observed that grip strength was significantly weakened in 50-week-old *Prnp*$^{o/o}$ mice compared to the controls [81]. Here, I assessed if there was any difference in strength between Sprn$^{+/-}$ *Prnp*$^{o/o}$ and *Sprn*$^{-/-}$ *Prnp*$^{o/o}$ mice, and found that there was no significant difference in performance between the two groups (Figure 3.7).

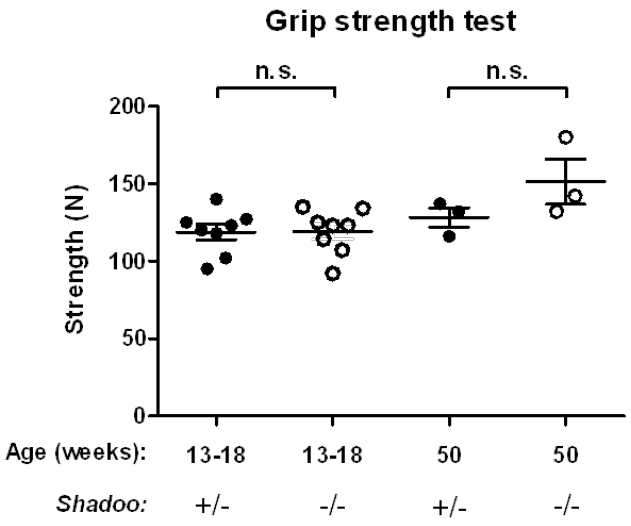

Figure 3.7. Grip strength test. *Each mouse was pulled by the tail and thus exerted a force on the wire, which was attached to a mechanical spring force gauge calibrated in Newton. No statistically significant differences in grip strength were observed between Sho +/- and Sho -/- mice. All mice are on a* $Prnp^{o/o}$ *background.*

Motor coordination, balance and ataxia can be tested with the rotarod test. The rotarod measures the ability of the mouse to maintain balance on a rotating rod [166]. This task requires an intact cerebellar function and motor coordination [167].

On accelerating rotarods, the time to fall was similar for 13-18 weeks and 50-week-old $Sprn^{+/-}$ $Prnp^{o/o}$ mice compared with their negative ($Sprn^{-/-}$ $Prnp^{o/o}$) littermates (Figure 3.8).

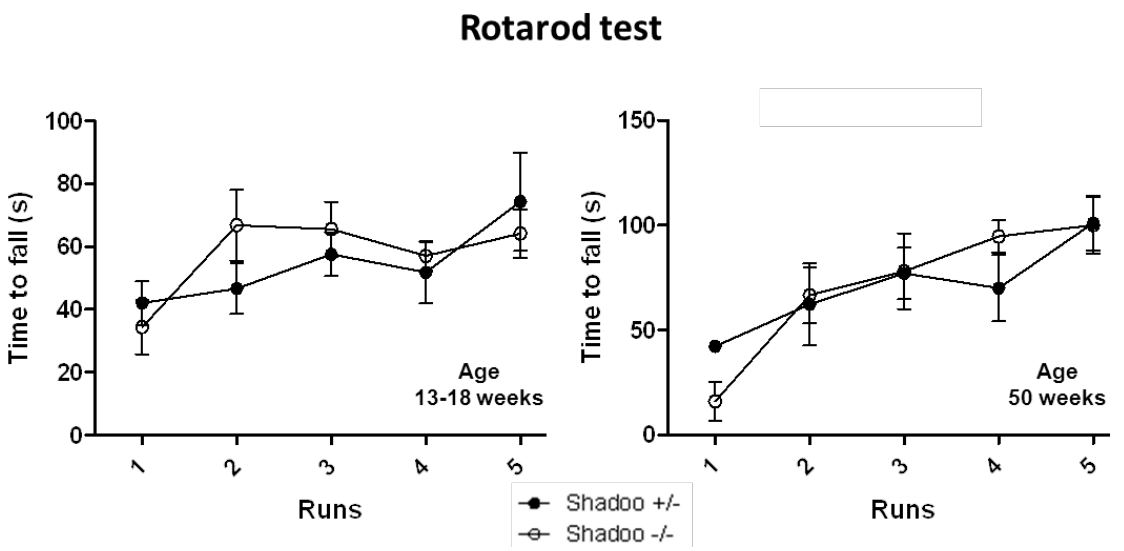

***Figure 3.8. Rotarod test**. Mice were placed on accelerating rotating drums. The time to fall was evaluated when the animals dropped from the drums. Sho +/- mice showed no difference in performance on the rotarod test when compared to Sho-/- mice at 13-18 weeks (left panel) and 50 weeks of age (right panel). All mice are on a Prnp$^{o/o}$ background.*

In agreement with the histological results, all behavioral experiments suggest that Sho does not ameliorate the CDP at the level of peripheral nerves, as no differences were observed between Sprn$^{+/-}$ *Prnp*$^{o/o}$ and *Sprn*$^{-/-}$ *Prnp*$^{o/o}$ mice.

DISCUSSION AND OUTLOOK

In this study, I demonstrated that specific overexpression of Sho in peripheral nerves of *Prnp*$^{o/o}$ mice could not alleviate the CDP which invariably affect these animals. Histological examinations and behavioral experiments showed that Sho does not influence the development of the polyneuropathy. Sections of sciatic nerves from Sprn$^{+/-}$ *Prnp*$^{o/o}$ still displayed the classic hallmarks of the CDP, such as aberrant or redundant myelin loops, supernumerary myelin sheaths and axon morphology irregularities, which has been previously described [81]. Moreover, no differences were observed from a battery of behavioral experiments. Taken together, these results clearly reject our initial hypothesis that Sho could act as the substitute protein for PrP^{C} in the CNS, where Sho is expressed and where no CDP in observed in *Prnp*$^{o/o}$ mice.

At the initiation of this project, there was a paucity of knowledge concerning Sho. I knew the similarities between Sho and FT of PrP^{C}, and evidence that indicated the PrP^{C}-like neuroprotective activity of Sho in a range of assays *in vitro [97]*. Furthermore, double knockout of *Prnp* and *Sprn* in mouse embryos induced embryonic lethality [160]. These early-stage results and the firm desire of the scientific community to identify the physiological function of PrP^{C}, led to the speculation that Sho, defined as the shadow of PrP^{C}, is the π protein and potentially the substitute/partner to PrP^{C} in signaling and in the involvement in prion diseases.

Follow-up studies have, however, reduced the hype surrounding Sho. The most important report came from Westaway et al, who generated a double knockout mouse (*Sprn*$^{-/-}$ *Prnp*$^{o/o}$) which was viable and fertile up to 690 days, contrary to expectations [163]. Furthermore, absence of Sho did not significantly impact the temporal and clinical manifestation of prion infections. Overall, these results reduced the impetus for associating Sho with the π protein.

Although Sho has some PrP^{C}-like protective properties [97], and could be useful as a marker of prion infections [162] and to dissect the behavior of PrP^{Sc} in the cell [161], Sho is not involved in myelin maintenance, as initially hypothesized, therefore, the identity of the substitute protein still remains elusive and subject to investigation. Nonetheless, this work provides further knowledge on the role and function of Sho.

MATERIALS AND METHODS

Mice

We housed mice and performed animal experiments in accordance with the Swiss Animal Protection Law and in compliance with the regulations of the veterinary office (canton Zürich). We included the following mice in our study: *Prnp*$^{o/o}$ on a mixed C57BL/6;129Sv background [60]. We bred FVB/NCr-Tg(HaPrPcos-Sprn)24551/Mri mice (Tg*Sprn*24551 or *Sprn*) [162] with *Prnp*$^{o/o}$ mice to obtain *Sprn*$^{+/-}$ *Prnp*$^{o/o}$ and *Sprn*$^{-/-}$ *Prnp*$^{o/o}$.

PCR analysis

Whole brains and DRGs were extracted from wild type mice. mRNA was isolated using RNeasy Plus Universal Mini Kit (QIagen), according to the manufacturer's instructions. Following reverse transcription (QuantiTect Rev. Transcription Kit, QIagen), cDNA was amplified by PCR to detect Sho using the following primers: Sho_3' fw (5'-TGT TTA GCA TCT GGC ACA GC-3'), Sho_3' rev (5'-GAT GGC TGA TAG CAG GGG TA-3'), Sho_ORF fw (5'-CTG GAG GAC GAT GAG AAT GG-3'), Sho_ORF rev (5'-GAA GCA GTT CTA GGG CAC CA-3'), actin fw (5'-GAC AGG ATG CAG AAG GAG AT-3'), and actin rev (5'-TTG CTG ATC CAC ATC TGC TG-3').

PCR parameters: denaturation (94°C, 2 min), 40 cycles amplification (three steps: 94°C, 30 sec_55°C, 30 sec_72°C, 50 sec), final elongation (72°C, 5 min).

Ultrastructural investigations

We embedded sciatic nerves in Epon using standard procedures and stained 'semi-thin' sections (500 nm) with toluidine blue. For morphometric analysis of axon size-density distribution, we captured images of 'semi-thin' sections from three mice per genotype and analyzed these using a semi-automatized software developed in house. We plotted axonal density against axonal size.

Behavioral experiments

In order to assess the functionality of the peripheral proprioceptive system, muscle strength, locomotion and motor coordination in mice, hot plate test, grip strength test and RotaRod were used respectively. Tests were performed on consecutive days to allow the mice to recover between each testing session.

Hot Plate Test: during the hot plate test, the animals were individually placed onto a metal plate (ITC Life Science, Series 8, PE 34, Woodland Hills, USA) that was maintained at a

constant temperature of 55°C (± 0.4°C). The time to a response to the heat, such as shaking of the hind paws, licking of the hind paws and jumping (all 4 paws in the air), was recorded. Each test was stopped after 60s.

Grip Test: the test consists of a mechanical spring force gauge, calibrated in Newton with a maximal capacity of 3N (Medio-Line Spring scale, metric, 300g, Pesola AG, Baar, Switzerland), which is attached to a trapezoidal steel wire for mice to grasp. Each mouse was pulled by the tail and thus exerted a force on the wire. When the pulling force applied on the wire exceeded the grip strength, the mouse would let go of the wire and the force indicated on the gauge was determined. The grip strength was measured five times per mouse, and then the median value for each animal was captured for statistical analysis.

Rotarod: the Rotarod consists of five rotating drums which accelerate continuously from 4 to 40 rpm (Ugo Basile, model 47600, Comerio, Italy). The maximum speed was attained after 245s. Five animals were tested simultaneously and the time and number of rotations was evaluated when the animals dropped from the drums (cut off time was 300s). The test was repeated five times per animal and the mean values per mouse were captured for statistical analysis.

REFERENCES

1. Polymenidou M, Moos R, Scott M, Sigurdson C, Shi YZ, et al. (2008) The POM monoclonals: a comprehensive set of antibodies to non-overlapping prion protein epitopes. PLoS ONE 3: e3872.

2. Baumann F, Tolnay M, Brabeck C, Pahnke J, Kloz U, et al. (2007) Lethal recessive myelin toxicity of prion protein lacking its central domain. EMBO J 26: 538-547.

3. Aguzzi A, Baumann F, Bremer J (2008) The prion's elusive reason for being. Annu Rev Neurosci 31: 439-477.

4. Bolton DC, McKinley MP, Prusiner SB (1982) Identification of a protein that purifies with the scrapie prion. Science 218: 1309-1311.

5. Prusiner SB (1982) Novel proteinaceous infectious particles cause scrapie. Science 216: 136-144.

6. Griffith JS (1967) Self-replication and scrapie. Nature 215: 1043-1044.

7. Alper T, Haig DA, Clarke MC (1966) The exceptionally small size of the scrapie agent. Biochem Biophys Res Commun 22: 278-284.

8. Alper T, Cramp WA, Haig DA, Clarke MC (1967) Does the agent of scrapie replicate without nucleic acid? Nature 214: 764-766.

9. Basler K, Oesch B, Scott M, Westaway D, Walchli M, et al. (1986) Scrapie and cellular PrP isoforms are encoded by the same chromosomal gene. Cell 46: 417-428.

10. Oesch B, Westaway D, Walchli M, McKinley MP, Kent SB, et al. (1985) A cellular gene encodes scrapie PrP 27-30 protein. Cell 40: 735-746.

11. Weissmann C (1991) A 'unified theory' of prion propagation. Nature 352: 679-683.

12. Prusiner SB, Scott MR, DeArmond SJ, Cohen FE (1998) Prion protein biology. Cell 93: 337-348.

13. Aguzzi A, Haass C (2003) Games played by rogue proteins in prion disorders and Alzheimer's disease. Science 302: 814-818.

14. DeArmond SJ (1993) Alzheimer's disease and Creutzfeldt-Jakob disease: overlap of pathogenic mechanisms. Curr Opin Neurol 6: 872-881.

15. Sponarova J, Nystrom SN, Westermark GT (2008) AA-amyloidosis can be transferred by peripheral blood monocytes. PLoS ONE 3: e3308.

16. Westermark GT, Westermark P (2010) Prion-like aggregates: infectious agents in human disease. Trends Mol Med 16: 501-507.

17. Eisele YS, Obermuller U, Heilbronner G, Baumann F, Kaeser SA, et al. (2010) Peripherally applied Abeta-containing inoculates induce cerebral beta-amyloidosis. Science 330: 980-982.

18. Ashe KH, Aguzzi A (2013) Prions, prionoids and pathogenic proteins in Alzheimer disease. Prion 7: 55-59.

19. Aguzzi A, Calella AM (2009) Prions: protein aggregation and infectious diseases. Physiol Rev 89: 1105-1152.

20. Williams ES, Young S (1980) Chronic wasting disease of captive mule deer: a spongiform encephalopathy. J Wildl Dis 16: 89-98.

21. Aguzzi A, Sigurdson C, Heikenwalder M (2007) Molecular Mechanisms of Prion Pathogenesis. Annu Rev Pathol.

22. Sigurdson CJ (2008) A prion disease of cervids: chronic wasting disease. Vet Res 39: 41.

23. Aguzzi A, Polymenidou M (2004) Mammalian prion biology: one century of evolving concepts. Cell 116: 313-327.

24. Wilesmith JW (1988) Bovine spongiform encephalopathy. Vet Rec 122: 614.

25. Aguzzi A, Glatzel M (2006) Prion infections, blood and transfusions. Nat Clin Pract Neurol 2: 321-329.

26. Owen F, Poulter M, Collinge J, Crow TJ (1990) Codon 129 changes in the prion protein gene in Caucasians. Am J Hum Genet 46: 1215-1216.

27. Aguzzi A, Weissmann C (1996) Spongiform encephalopathies: a suspicious signature. Nature 383: 666-667.

28. Bruce ME, Will RG, Ironside JW, McConnell I, Drummond D, et al. (1997) Transmissions to mice indicate that 'new variant' CJD is caused by the BSE agent. Nature 389: 498-501.

29. Hill AF, Desbruslais M, Joiner S, Sidle KC, Gowland I, et al. (1997) The same prion strain causes vCJD and BSE. Nature 389: 448-450, 526.

30. Collinge J, Whitfield J, McKintosh E, Beck J, Mead S, et al. (2006) Kuru in the 21st century--an acquired human prion disease with very long incubation periods. Lancet 367: 2068-2074.

31. Gajdusek DC, Zigas V (1957) Degenerative disease of the central nervous system in New Guinea; the endemic occurrence of kuru in the native population. N Engl J Med 257: 974-978.

32. Duffy P, Wolf J, Collins G, DeVoe AG, Streeten B, et al. (1974) Letter: Possible person-to-person transmission of Creutzfeldt-Jakob disease. N Engl J Med 290: 692-693.

33. Will RG (2003) Acquired prion disease: iatrogenic CJD, variant CJD, kuru. Br Med Bull 66: 255-265.

34. Bernoulli C, Siegfried J, Baumgartner G, Regli F, Rabinowicz T, et al. (1977) Danger of accidental person-to-person transmission of Creutzfeldt-Jakob disease by surgery. Lancet 1: 478-479.

35. Hsiao K, Baker HF, Crow TJ, Poulter M, Owen F, et al. (1989) Linkage of a prion protein missense variant to Gerstmann-Straussler syndrome. Nature 338: 342-345.

36. Tateishi J, Kitamoto T, Hashiguchi H, Shii H (1988) Gerstmann-Straussler-Scheinker disease: immunohistological and experimental studies. Ann Neurol 24: 35-40.

37. Gerstmann J (1957) Some notes on the Gerstmann syndrome. Neurology 7: 866-869.

38. Lugaresi E, Medori R, Montagna P, Baruzzi A, Cortelli P, et al. (1986) Fatal familial insomnia and dysautonomia with selective degeneration of thalamic nuclei. N Engl J Med 315: 997-1003.

39. Tateishi J, Brown P, Kitamoto T, Hoque ZM, Roos R, et al. (1995) First experimental transmission of fatal familial insomnia. Nature 376: 434-435.

40. Collins S, McLean CA, Masters CL (2001) Gerstmann-Straussler-Scheinker syndrome,fatal familial insomnia, and kuru: a review of these less common human transmissible spongiform encephalopathies. J Clin Neurosci 8: 387-397.

41. Prusiner SB (1991) Molecular biology of prion diseases. Science 252: 1515-1522.

42. Stahl N, Baldwin MA, Teplow DB, Hood L, Gibson BW, et al. (1993) Structural studies of the scrapie prion protein using mass spectrometry and amino acid sequencing. Biochemistry 32: 1991-2002.

43. Hosszu LL, Baxter NJ, Jackson GS, Power A, Clarke AR, et al. (1999) Structural mobility of the human prion protein probed by backbone hydrogen exchange. Nat Struct Biol 6: 740-743.

44. James TL, Liu H, Ulyanov NB, Farr-Jones S, Zhang H, et al. (1997) Solution structure of a 142-residue recombinant prion protein corresponding to the infectious fragment of the scrapie isoform. Proc Natl Acad Sci U S A 94: 10086-10091.

45. Riek R, Hornemann S, Wider G, Billeter M, Glockshuber R, et al. (1996) NMR structure of the mouse prion protein domain PrP(121-231). Nature 382: 180-182.

46. Weissmann C (2004) The state of the prion. Nat Rev Microbiol 2: 861-871.

47. Cohen FE, Pan KM, Huang Z, Baldwin M, Fletterick RJ, et al. (1994) Structural clues to prion replication. Science 264: 530-531.

48. Gajdusek DC (1988) Transmissible and non-transmissible amyloidoses: autocatalytic post-translational conversion of host precursor proteins to beta-pleated sheet configurations. J Neuroimmunol 20: 95-110.

49. Jarrett JT, Lansbury PT, Jr. (1993) Seeding "one-dimensional crystallization" of amyloid: a pathogenic mechanism in Alzheimer's disease and scrapie? Cell 73: 1055-1058.

50. Aguzzi A, O'Connor T (2010) Protein aggregation diseases: pathogenicity and therapeutic perspectives. Nat Rev Drug Discov 9: 237-248.

51. Aguzzi A, Sigurdson CJ (2004) Antiprion immunotherapy: to suppress or to stimulate? Nat Rev Immunol 4: 725-736.

52. Bueler H, Aguzzi A, Sailer A, Greiner RA, Autenried P, et al. (1993) Mice devoid of PrP are resistant to scrapie. Cell 73: 1339-1347.

53. Sailer A, Bueler H, Fischer M, Aguzzi A, Weissmann C (1994) No propagation of prions in mice devoid of PrP. Cell 77: 967-968.

54. Fischer M, Rulicke T, Raeber A, Sailer A, Moser M, et al. (1996) Prion protein (PrP) with amino-proximal deletions restoring susceptibility of PrP knockout mice to scrapie. EMBO J 15: 1255-1264.

55. Flechsig E, Shmerling D, Hegyi I, Raeber AJ, Fischer M, et al. (2000) Prion protein devoid of the octapeptide repeat region restores susceptibility to scrapie in PrP knockout mice. Neuron 27: 399-408.

56. Shmerling D, Hegyi I, Fischer M, Blattler T, Brandner S, et al. (1998) Expression of amino-terminally truncated PrP in the mouse leading to ataxia and specific cerebellar lesions. Cell 93: 203-214.

57. Budka H (2003) Neuropathology of prion diseases. Br Med Bull 66: 121-130.

58. Soto C, Satani N (2010) The intricate mechanisms of neurodegeneration in prion diseases. Trends Mol Med.

59. Almer G, Hainfellner JA, Brucke T, Jellinger K, Kleinert R, et al. (1999) Fatal familial insomnia: a new Austrian family. Brain 122 (Pt 1): 5-16.

60. Bueler H, Fischer M, Lang Y, Bluethmann H, Lipp HP, et al. (1992) Normal development and behaviour of mice lacking the neuronal cell-surface PrP protein. Nature 356: 577-582.

61. Brandner S, Raeber A, Sailer A, Blattler T, Fischer M, et al. (1996) Normal host prion protein (PrPC) is required for scrapie spread within the central nervous system. Proc Natl Acad Sci U S A 93: 13148-13151.

62. Brandner S, Isenmann S, Raeber A, Fischer M, Sailer A, et al. (1996) Normal host prion protein necessary for scrapie-induced neurotoxicity. Nature 379: 339-343.

63. Chesebro B, Trifilo M, Race R, Meade-White K, Teng C, et al. (2005) Anchorless prion protein results in infectious amyloid disease without clinical scrapie. Science 308: 1435-1439.

64. Mallucci G, Dickinson A, Linehan J, Klohn PC, Brandner S, et al. (2003) Depleting neuronal PrP in prion infection prevents disease and reverses spongiosis. Science 302: 871-874.

65. Ross CA, Poirier MA (2005) Opinion: What is the role of protein aggregation in neurodegeneration? Nat Rev Mol Cell Biol 6: 891-898.

66. Johnston JA, Ward CL, Kopito RR (1998) Aggresomes: a cellular response to misfolded proteins. J Cell Biol 143: 1883-1898.

67. Moreno JA, Radford H, Peretti D, Steinert JR, Verity N, et al. (2012) Sustained translational repression by eIF2alpha-P mediates prion neurodegeneration. Nature 485: 507-511.

68. Smith WW, Jiang H, Pei Z, Tanaka Y, Morita H, et al. (2005) Endoplasmic reticulum stress and mitochondrial cell death pathways mediate A53T mutant alpha-synuclein-induced toxicity. Hum Mol Genet 14: 3801-3811.

69. Hoozemans JJ, van Haastert ES, Nijholt DA, Rozemuller AJ, Eikelenboom P, et al. (2009) The unfolded protein response is activated in pretangle neurons in Alzheimer's disease hippocampus. Am J Pathol 174: 1241-1251.

70. Atkin JD, Farg MA, Walker AK, McLean C, Tomas D, et al. (2008) Endoplasmic reticulum stress and induction of the unfolded protein response in human sporadic amyotrophic lateral sclerosis. Neurobiol Dis 30: 400-407.

71. Doyle KM, Kennedy D, Gorman AM, Gupta S, Healy SJ, et al. (2011) Unfolded proteins and endoplasmic reticulum stress in neurodegenerative disorders. J Cell Mol Med 15: 2025-2039.

72. Stewart RS, Harris DA (2003) Mutational analysis of topological determinants in prion protein (PrP) and measurement of transmembrane and cytosolic PrP during prion infection. J Biol Chem 278: 45960-45968.

73. Harris DA, Lele P, Snider WD (1993) Localization of the mRNA for a chicken prion protein by in situ hybridization. Proc Natl Acad Sci U S A 90: 4309-4313.

74. Strumbo B, Ronchi S, Bolis LC, Simonic T (2001) Molecular cloning of the cDNA coding for Xenopus laevis prion protein. FEBS Lett 508: 170-174.

75. Rivera-Milla E, Stuermer CA, Malaga-Trillo E (2003) An evolutionary basis for scrapie disease: identification of a fish prion mRNA. Trends Genet 19: 72-75.

76. Moser M, Colello RJ, Pott U, Oesch B (1995) Developmental expression of the prion protein gene in glial cells. Neuron 14: 509-517.

77. Baker CA, Martin D, Manuelidis L (2002) Microglia from Creutzfeldt-Jakob disease-infected brains are infectious and show specific mRNA activation profiles. J Virol 76: 10905-10913.

78. Dodelet VC, Cashman NR (1998) Prion protein expression in human leukocyte differentiation. Blood 91: 1556-1561.

79. Ford MJ, Burton LJ, Morris RJ, Hall SM (2002) Selective expression of prion protein in peripheral tissues of the adult mouse. Neuroscience 113: 177-192.

80. Heikenwalder M, Zeller N, Seeger H, Prinz M, Klohn PC, et al. (2005) Chronic lymphocytic inflammation specifies the organ tropism of prions. Science 307: 1107-1110.

81. Bremer J, Baumann F, Tiberi C, Wessig C, Fischer H, et al. (2010) Axonal prion protein is required for peripheral myelin maintenance. Nat Neurosci 13: 310-318.

82. Steele AD, Emsley JG, Ozdinler PH, Lindquist S, Macklis JD (2006) Prion protein (PrPc) positively regulates neural precursor proliferation during developmental and adult mammalian neurogenesis. Proc Natl Acad Sci U S A 103: 3416-3421.

83. Watts JC, Huo H, Bai Y, Ehsani S, Won AH, et al. (2009) Interactome analyses identify ties of PrP and its mammalian paralogs to oligomannosidic N-glycans and endoplasmic reticulum-derived chaperones. PLoS Pathog 5: e1000608.

84. Martins VR, Beraldo FH, Hajj GN, Lopes MH, Lee KS, et al. (2010) Prion protein: orchestrating neurotrophic activities. Curr Issues Mol Biol 12: 63-86.

85. Riek R, Hornemann S, Wider G, Glockshuber R, Wuthrich K (1997) NMR characterization of the full-length recombinant murine prion protein, mPrP(23-231). FEBS Lett 413: 282-288.

86. Zahn R, Liu A, Luhrs T, Riek R, von Schroetter C, et al. (2000) NMR solution structure of the human prion protein. Proc Natl Acad Sci U S A 97: 145-150.

87. Alfa Cisse M, Louis K, Braun U, Mari B, Leitges M, et al. (2008) Isoform-specific contribution of protein kinase C to prion processing. Mol Cell Neurosci 39: 400-410.

88. Oliveira-Martins JB, Yusa S, Calella AM, Bridel C, Baumann F, et al. Unexpected tolerance of alpha-cleavage of the prion protein to sequence variations. PLoS ONE 5: e9107.

89. Sunyach C, Cisse MA, da Costa CA, Vincent B, Checler F (2007) The C-terminal products of cellular prion protein processing, C1 and C2, exert distinct influence on p53-dependent staurosporine-induced caspase-3 activation. J Biol Chem 282: 1956-1963.

90. Mange A, Beranger F, Peoc'h K, Onodera T, Frobert Y, et al. (2004) Alpha- and beta-cleavages of the amino-terminus of the cellular prion protein. Biol Cell 96: 125-132.

91. Watts JC, Westaway D (2007) The prion protein family: diversity, rivalry, and dysfunction. Biochim Biophys Acta 1772: 654-672.

92. Behrens A, Genoud N, Naumann H, Rulicke T, Janett F, et al. (2002) Absence of the prion protein homologue Doppel causes male sterility. EMBO J 21: 3652-3658.

93. Moore RC, Lee IY, Silverman GL, Harrison PM, Strome R, et al. (1999) Ataxia in prion protein (PrP)-deficient mice is associated with upregulation of the novel PrP-like protein doppel. J Mol Biol 292: 797-817.

94. Silverman GL, Qin K, Moore RC, Yang Y, Mastrangelo P, et al. (2000) Doppel is an N-glycosylated, glycosylphosphatidylinositol-anchored protein. Expression in testis and ectopic production in the brains of Prnp(0/0) mice predisposed to Purkinje cell loss. J Biol Chem 275: 26834-26841.

95. Luhrs T, Riek R, Guntert P, Wuthrich K (2003) NMR structure of the human doppel protein. J Mol Biol 326: 1549-1557.

96. Moore RC, Mastrangelo P, Bouzamondo E, Heinrich C, Legname G, et al. (2001) Doppel-induced cerebellar degeneration in transgenic mice. Proc Natl Acad Sci U S A 98: 15288-15293.

97. Watts JC, Drisaldi B, Ng V, Yang J, Strome B, et al. (2007) The CNS glycoprotein Shadoo has PrP(C)-like protective properties and displays reduced levels in prion infections. EMBO J 26: 4038-4050.

98. Premzl M, Sangiorgio L, Strumbo B, Marshall Graves JA, Simonic T, et al. (2003) Shadoo, a new protein highly conserved from fish to mammals and with similarity to prion protein. Gene 314: 89-102.

99. Sonati T, Reimann RR, Falsig J, Baral PK, O'Connor T, et al. (2013) The toxicity of antiprion antibodies is mediated by the flexible tail of the prion protein. Nature.

100. Beland M, Roucou X (2012) The prion protein unstructured N-terminal region is a broad-spectrum molecular sensor with diverse and contrasting potential functions. J Neurochem 120: 853-868.

101. Radovanovic I, Braun N, Giger OT, Mertz K, Miele G, et al. (2005) Truncated prion protein and Doppel are myelinotoxic in the absence of oligodendrocytic PrPC. J Neurosci 25: 4879-4888.

102. Baumann F, Pahnke J, Radovanovic I, Rulicke T, Bremer J, et al. (2009) Functionally relevant domains of the prion protein identified in vivo. PLoS ONE 4: e6707.

103. Drisaldi B, Coomaraswamy J, Mastrangelo P, Strome B, Yang J, et al. (2004) Genetic mapping of activity determinants within cellular prion proteins: N-terminal modules in PrPC offset pro-apoptotic activity of the Doppel helix B/B' region. J Biol Chem 279: 55443-55454.

104. Guillot-Sestier MV, Sunyach C, Druon C, Scarzello S, Checler F (2009) The alpha-secretase-derived N-terminal product of cellular prion, N1 displays neuroprotective function, in vitro and in vivo. J Biol Chem.

105. Li A, Christensen HM, Stewart LR, Roth KA, Chiesa R, et al. (2007) Neonatal lethality in transgenic mice expressing prion protein with a deletion of residues 105-125. EMBO J 26: 548-558.

106. Solomon IH, Khatri N, Biasini E, Massignan T, Huettner JE, et al. (2011) An N-terminal polybasic domain and cell surface localization are required for mutant prion protein toxicity. J Biol Chem 286: 14724-14736.

107. Westergard L, Turnbaugh JA, Harris DA (2011) A nine amino acid domain is essential for mutant prion protein toxicity. J Neurosci 31: 14005-14017.

108. Turnbaugh JA, Unterberger U, Saa P, Massignan T, Fluharty BR, et al. (2012) The N-terminal, polybasic region of PrP(C) dictates the efficiency of prion propagation by binding to PrP(Sc). J Neurosci 32: 8817-8830.

109. McHugh D, O'Connor T, Bremer J, Aguzzi A (2012) ZyFISH: a simple, rapid and reliable zygosity assay for transgenic mice. PLoS ONE 7: e37881.

110. Karapetyan YE, Saa P, Mahal SP, Sferrazza GF, Sherman A, et al. (2009) Prion strain discrimination based on rapid in vivo amplification and analysis by the cell panel assay. PLoS ONE 4: e5730.

111. Sakudo A, Onodera T, Ikuta K (2007) Prion protein gene-deficient cell lines: powerful tools for prion biology. Microbiol Immunol 51: 1-13.

112. Shyng SL, Huber MT, Harris DA (1993) A prion protein cycles between the cell surface and an endocytic compartment in cultured neuroblastoma cells. J Biol Chem 268: 15922-15928.

113. Bainton DF (1981) The discovery of lysosomes. J Cell Biol 91: 66s-76s.

114. Alvarez-Castelao B, Martin-Guerrero I, Garcia-Orad A, Castano JG (2009) Cytomegalovirus promoter up-regulation is the major cause of increased protein levels of unstable reporter proteins after treatment of living cells with proteasome inhibitors. J Biol Chem 284: 28253-28262.

115. Walter P, Ron D (2011) The unfolded protein response: from stress pathway to homeostatic regulation. Science 334: 1081-1086.

116. Cao SS, Kaufman RJ (2012) Unfolded protein response. Curr Biol 22: R622-626.

117. Samali A, Fitzgerald U, Deegan S, Gupta S (2010) Methods for monitoring endoplasmic reticulum stress and the unfolded protein response. Int J Cell Biol 2010: 830307.

118. Bertolotti A, Zhang Y, Hendershot LM, Harding HP, Ron D (2000) Dynamic interaction of BiP and ER stress transducers in the unfolded-protein response. Nat Cell Biol 2: 326-332.

119. Gardner BM, Pincus D, Gotthardt K, Gallagher CM, Walter P (2013) Endoplasmic reticulum stress sensing in the unfolded protein response. Cold Spring Harb Perspect Biol 5: a013169.

120. Song G, Ouyang G, Bao S (2005) The activation of Akt/PKB signaling pathway and cell survival. J Cell Mol Med 9: 59-71.

121. Appenzeller-Herzog C, Hall MN (2012) Bidirectional crosstalk between endoplasmic reticulum stress and mTOR signaling. Trends Cell Biol 22: 274-282.

122. Bonni A, Brunet A, West AE, Datta SR, Takasu MA, et al. (1999) Cell survival promoted by the Ras-MAPK signaling pathway by transcription-dependent and -independent mechanisms. Science 286: 1358-1362.

123. Lin JH, Li H, Zhang Y, Ron D, Walter P (2009) Divergent effects of PERK and IRE1 signaling on cell viability. PLoS ONE 4: e4170.

124. Puthalakath H, O'Reilly LA, Gunn P, Lee L, Kelly PN, et al. (2007) ER stress triggers apoptosis by activating BH3-only protein Bim. Cell 129: 1337-1349.

125. Hetz C (2012) The unfolded protein response: controlling cell fate decisions under ER stress and beyond. Nat Rev Mol Cell Biol 13: 89-102.

126. Ellgaard L, Molinari M, Helenius A (1999) Setting the standards: quality control in the secretory pathway. Science 286: 1882-1888.

127. Hosoi T, Hyoda K, Okuma Y, Nomura Y, Ozawa K (2007) Akt up- and down-regulation in response to endoplasmic reticulum stress. Brain Res 1152: 27-31.

128. Manning BD, Cantley LC (2007) AKT/PKB signaling: navigating downstream. Cell 129: 1261-1274.

129. Neary JT, Rathbone MP, Cattabeni F, Abbracchio MP, Burnstock G (1996) Trophic actions of extracellular nucleotides and nucleosides on glial and neuronal cells. Trends Neurosci 19: 13-18.

130. Franke H, Sauer C, Rudolph C, Krugel U, Hengstler JG, et al. (2009) P2 receptor-mediated stimulation of the PI3-K/Akt-pathway in vivo. Glia 57: 1031-1045.

131. Tabas I, Ron D (2011) Integrating the mechanisms of apoptosis induced by endoplasmic reticulum stress. Nat Cell Biol 13: 184-190.

132. Christen B, Hornemann S, Damberger FF, Wuthrich K (2012) Prion protein mPrP[F175A](121-231): structure and stability in solution. J Mol Biol 423: 496-502.

133. Nystrom S, Mishra R, Hornemann S, Aguzzi A, Nilsson KP, et al. (2012) Multiple substitutions of methionine 129 in human prion protein reveal its importance in the amyloid fibrillation pathway. J Biol Chem 287: 25975-25984.

134. Damberger FF, Christen B, Perez DR, Hornemann S, Wuthrich K (2011) Cellular prion protein conformation and function. Proc Natl Acad Sci U S A 108: 17308-17313.

135. Sigurdson CJ, Joshi-Barr S, Bett C, Winson O, Manco G, et al. (2011) Spongiform encephalopathy in transgenic mice expressing a point mutation in the beta2-alpha2 loop of the prion protein. J Neurosci 31: 13840-13847.

136. Sigurdson CJ, Nilsson KP, Hornemann S, Heikenwalder M, Manco G, et al. (2009) De novo generation of a transmissible spongiform encephalopathy by mouse transgenesis. Proc Natl Acad Sci U S A 106: 304-309.

137. Hornemann S, Christen B, von Schroetter C, Perez DR, Wuthrich K (2009) Prion protein library of recombinant constructs for structural biology. FEBS J 276: 2359-2367.

138. Kopito RR (1999) Biosynthesis and degradation of CFTR. Physiol Rev 79: S167-173.

139. Wennerstrand P, Dametto P, Hennig J, Klingstedt T, Skoglund K, et al. (2012) Structural Characteristics Determine the Cause of the Low Enzyme Activity of Two Thiopurine S-Methyltransferase Allelic Variants: A Biophysical Characterization of TPMT*2 and TPMT*5. Biochemistry.

140. Yoo BC, Krapfenbauer K, Cairns N, Belay G, Bajo M, et al. (2002) Overexpressed protein disulfide isomerase in brains of patients with sporadic Creutzfeldt-Jakob disease. Neurosci Lett 334: 196-200.

141. Wang X, Shi Q, Xu K, Gao C, Chen C, et al. (2011) Familial CJD associated PrP mutants within transmembrane region induced Ctm-PrP retention in ER and triggered apoptosis by ER stress in SH-SY5Y cells. PLoS One 6: e14602.

142. Hetz C, Russelakis-Carneiro M, Maundrell K, Castilla J, Soto C (2003) Caspase-12 and endoplasmic reticulum stress mediate neurotoxicity of pathological prion protein. EMBO J 22: 5435-5445.

143. Torres M, Castillo K, Armisen R, Stutzin A, Soto C, et al. (2010) Prion protein misfolding affects calcium homeostasis and sensitizes cells to endoplasmic reticulum stress. PLoS One 5: e15658.

144. Tang Y, Xiang W, Terry L, Kretzschmar HA, Windl O (2010) Transcriptional analysis implicates endoplasmic reticulum stress in bovine spongiform encephalopathy. PLoS One 5: e14207.

145. Wang SB, Shi Q, Xu Y, Xie WL, Zhang J, et al. (2012) Protein disulfide isomerase regulates endoplasmic reticulum stress and the apoptotic process during prion infection and PrP mutant-induced cytotoxicity. PLoS ONE 7: e38221.

146. Uchiyama K, Muramatsu N, Yano M, Usui T, Miyata H, et al. (2013) Prions disturb post-Golgi trafficking of membrane proteins. Nat Commun 4: 1846.

147. Senatore A, Restelli E, Chiesa R (2013) Synaptic Dysfunction in Prion Diseases: A Trafficking Problem? Int J Cell Biol 2013: 543803.

148. Credle JJ, Finer-Moore JS, Papa FR, Stroud RM, Walter P (2005) On the mechanism of sensing unfolded protein in the endoplasmic reticulum. Proc Natl Acad Sci U S A 102: 18773-18784.

149. Gardner BM, Walter P (2011) Unfolded proteins are Ire1-activating ligands that directly induce the unfolded protein response. Science 333: 1891-1894.

150. Moreno JA, Halliday M, Molloy C, Radford H, Verity N, et al. (2013) Oral treatment targeting the unfolded protein response prevents neurodegeneration and clinical disease in prion-infected mice. Sci Transl Med 5: 206ra138.

151. Colla E, Coune P, Liu Y, Pletnikova O, Troncoso JC, et al. (2012) Endoplasmic reticulum stress is important for the manifestations of alpha-synucleinopathy in vivo. J Neurosci 32: 3306-3320.

152. Hoozemans JJ, Scheper W (2012) Endoplasmic reticulum: the unfolded protein response is tangled in neurodegeneration. Int J Biochem Cell Biol 44: 1295-1298.

153. Unterberger U, Hoftberger R, Gelpi E, Flicker H, Budka H, et al. (2006) Endoplasmic reticulum stress features are prominent in Alzheimer disease but not in prion diseases in vivo. J Neuropathol Exp Neurol 65: 348-357.

154. Carnemolla A, Fossale E, Agostoni E, Michelazzi S, Calligaris R, et al. (2009) Rrs1 is involved in endoplasmic reticulum stress response in Huntington disease. J Biol Chem 284: 18167-18173.

155. Lajoie P, Snapp EL (2011) Changes in BiP availability reveal hypersensitivity to acute endoplasmic reticulum stress in cells expressing mutant huntingtin. J Cell Sci 124: 3332-3343.

156. Roussel BD, Kruppa AJ, Miranda E, Crowther DC, Lomas DA, et al. (2013) Endoplasmic reticulum dysfunction in neurological disease. Lancet Neurol 12: 105-118.

157. Halliday M, Mallucci GR (2014) Targeting the unfolded protein response in neurodegeneration: A new approach to therapy. Neuropharmacology 76 Pt A: 169-174.

158. Jucker M (2010) The benefits and limitations of animal models for translational research in neurodegenerative diseases. Nat Med 16: 1210-1214.

159. Rulicke T (2004) Pronuclear microinjection of mouse zygotes. Methods Mol Biol 254: 165-194.

160. Young R, Passet B, Vilotte M, Cribiu EP, Beringue V, et al. (2009) The prion or the related Shadoo protein is required for early mouse embryogenesis. FEBS Lett.

161. Watts JC, Stohr J, Bhardwaj S, Wille H, Oehler A, et al. (2011) Protease-Resistant Prions Selectively Decrease Shadoo Protein. PLoS Pathog 7: e1002382.

162. Westaway D, Genovesi S, Daude N, Brown R, Lau A, et al. (2011) Down-Regulation of Shadoo in Prion Infections Traces a Pre-Clinical Event Inversely Related to PrP Accumulation. PLoS Pathog 7: e1002391.

163. Daude N, Wohlgemuth S, Brown R, Pitstick R, Gapeshina H, et al. (2012) Knockout of the prion protein (PrP)-like Sprn gene does not produce embryonic lethality in combination with PrP(C)-deficiency. Proc Natl Acad Sci U S A 109: 9035-9040.

164. van Gaalen MM, Steckler T (2000) Behavioural analysis of four mouse strains in an anxiety test battery. Behav Brain Res 115: 95-106.

165. Karl T, Pabst R, von Horsten S (2003) Behavioral phenotyping of mice in pharmacological and toxicological research. Exp Toxicol Pathol 55: 69-83.

166. Barlow C, Hirotsune S, Paylor R, Liyanage M, Eckhaus M, et al. (1996) Atm-deficient mice: a paradigm of ataxia telangiectasia. Cell 86: 159-171.

167. Carter RJ, Lione LA, Humby T, Mangiarini L, Mahal A, et al. (1999) Characterization of progressive motor deficits in mice transgenic for the human Huntington's disease mutation. J Neurosci 19: 3248-3257.

ACKNOWLEDGMENTS

I believe the Ph.D. experience is not just research, but a phase of life where I could grow and mature on every single dimension of my life; previously unknown skills were brought out, both technical and social. I would like to thank all the people that made it possible and helped me throughout this challenging journey.

- Prof. Dr. Adriano Aguzzi for his constant support, brilliant ideas, and for keeping the motivation high. I am very thankful to him for all the opportunities I have been given, such as collaborations, supervising students, attending meetings, writing grants and reports, and participating at international meetings. All these made my Ph.D. an outstanding formative experience.
- Prof. Dr. Rudolf Aebersold, Prof. Dr. Mathias Heikenwalder and Prof. Dr. Peter Sonderegger for kindly agreeing to be part of my Ph.D Committee and for their inputs and support during these years.

Furthermore, I want to express my vivid gratitude to my collaborators:

- Dr. Tracy O'Connor for her constant supervision and support during these years, the critical comments and inputs, and for cheering me up with her amazing sarcasm.
- Dr. Asvin Lakkaraju for his incredible help and support with my projects during the past 6 months, a true motivator.
- Dr. Anna Maria Calella, who taught me everything I needed to know to work in the lab. Her patience and support were both formidable.
- Lukas Villiger for his contribution to the project during his Master's thesis and afterwards; his contributions have been significant, and not just project-wise, but for the pleasant discussions about work and life and for his friendship.
- Dr. Uli Hermmann for the countless discussions over our projects, as well as his technical help and for translating the summary. Further, his passion for research is a constant source of motivation and optimism.
- Dr. Claire Bridel and Dr. Thomas Rülicke for the generation of the FTgpi mice. Dr. Pawel Pelczar, , Dr. Donal McHugh, Dr. Arlind Adili, Cinzia Tiberi, Giovanni Colacicco and Monika Bieri for their contributions to my projects.

Very little would have been possible without the support of the technical team. My sincere appreciation goes to Delic Mirzet, Christine Sturzenegger and Victor Escalante for their huge help in the animal facility; Petra Schwarz, Ahmet Varol, and Rita Moos for their technical assistance; Livia Takacs and Karina Arroyo for the genotyping service.

I would like to thank those people, who other than being great scientists, became amazing friends who supported me and inspired me throughout my studies. Thanks to Dr. Tiziana Sonati, Badmavady Segarane, Dr. Mario Nuvolone, Dr. Jana Sponarova, Dr. Alexander Küffer, Dr. Alzbeta Trancikova, Mario Hermann, Dr. Gitta Seleznik, Dr. Agnes Lau, Dr. Zoë Van Helmond, Dr. Tory Johnson, Dr. Caihong Zhu and Li Bei, Dr. Henning Leske, Dr. Nike Krautler and Läufer Thorsten, for the unforgettable moments, parties, journeys, but also difficult moments we shared.
A big thank to every member of Adriano's group, because everyone contributed to my work and influenced me through valuable discussions and constructive criticisms.

I am deeply thankful to Dr. Zoë Van Helmond for correcting and revising this thesis, and for providing insightful inputs.

Last but not least, I would like to thank all my old friends back in Italy and the new ones I made in Zürich, who provided the social environment who made my life in these years simply marvellous. Special thanks go to my best friends Luca and Davide, who were always patient with me, and for the fun and laughs we had these years.

I dedicate this work to my mother, my father and my brother for their unconditional love and support, for their encouragements, and for the sacrifices they endured so that I could do this Ph.D and live such a great life.

PUBLICATIONS

Dametto P, Bridel C, Lakkaraju A, Villiger L, O'Connor T, Herrmann U, Pelczar P, Rülicke T, McHugh D, Adili A, Aguzzi A

Membrane tethering of the flexible tail of PrP triggers prion-like neurodegeneration (Submitted)

Dametto P, Tiberi C, Colacicco G, Aguzzi A

Overexpression of Shadoo in peripheral nerves does not rescue the polyneuropathy in Prnp knock-out mice.

(Manuscript in preparation)

Herrmann H, Sonati T, Falsig J, Reimann R, **Dametto P**, O'Connor T, Li B, Lau A, Hornemann S, Sorce S, Rehrauer H and Aguzzi A

Anti-PrP antibodies and prion infections trigger converging pathways of toxicity

(Manuscript in preparation)

Wennerstrand P, **Dametto P**, Hennig J, Klingstedt T, Skoglund K, Appell ML, Mårtensson LG, *Structural characteristics determine the cause of the low enzyme activity of two thiopurine S-methyltransferase allelic variants: a biophysical characterization of TPMT*2 and TPMT*5*. Biochemistry, 2012: 51(30):5912-20

Oliveira-Martins JB, Yusa S, Calella AM, Bridel C, Baumann F, **Dametto P**, Aguzzi A, *Unexpected tolerance of alpha-cleavage of the prion protein to sequence variations*. PLoS ONE 5, 2010: e9107